NASA CONTRACTOR REPORT

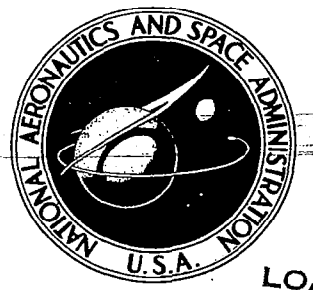

NASA CR-2114

ANALYTICAL AND EXPERIMENTAL INVESTIGATION OF CIRCULATION CONTROL BY MEANS OF A TURBULENT COANDA JET

by E. S. Levinsky and T. T. Yeh

Prepared by
AIR VEHICLE CORPORATION
San Diego, Calif.
for Ames Research Center

NATIONAL AERONAUTICS AND SPACE ADMINISTRATION • WASHINGTON, D. C. • SEPTEMBER 1972

1. Report No. NASA CR-2114	2. Government Accession No.	3. Recipient's Catalog No.
4. Title and Subtitle Analytical and Experimental Investigation of Circulation Control by Means of A Turbulent Coanda Jet		5. Report Date September 1972 6. Performing Organization Code
7. Author(s) E.S. Levinsky and T.T. Yeh		8. Performing Organization Report No. 10. Work Unit No.
9. Performing Organization Name and Address Air Vehicle Corporation San Diego, Ca.		11. Contract or Grant No. NAS 2-5359 13. Type of Report and Period Covered Contractor Report
12. Sponsoring Agency Name and Address National Aeronautics & Space Administration Washington, D.C.		14. Sponsoring Agency Code

15. Supplementary Notes

16. Abstract An analytical and experimental investigation of circulation control on a circular cylinder by means of tangential blowing (Coanda effect) is presented. The analytical method developed has also been used to estimate the blowing coefficients required for achieving potential flow on airfoils with flaps.

The analysis is presented for conditions for which the flow in the boundary layer ahead of the jet exit is turbulent. The turbulent boundary layer and the jet layer on the upper surface, and the turbulent boundary layer on the lower surface are computed by a multi-strip integral method. The region of integration is between the corresponding transition and separation points on each surface. Longitudinal curvature effects, which give rise to a radial pressure gradient across the jet layer and to an additional adverse tangential pressure gradient just upstream of the separation point, are included in the jet layer analysis in an approximate manner. The longitudinal curvature effect is found to have a pronounced influence on the separation of the jet layer.

The method has been programmed in FORTRAN IV. Values of the calculated surface pressure distribution, location of the separated region, and values of induced circulation and lift have been compared with wind tunnel test data. Significant parameters in the analysis effecting jet separation are the ratios of the maximum jet velocity in the fully merged jet layer just downstream of the jet exit to the average velocity in the jet slot, to the free stream velocity, and to the maximum jet velocity at the separation point. For the range of cases considered, the ratios of the jet slot thickness to the cylinder radius and to the boundary layer thickness were found to have only a negligible effect on jet separation, except for their influence on the ratio of the maximum jet velocity to the average jet velocity inside the slot.

In general, the analyses and the test data showed reasonable agreement with regard to pressure distribution, boundary- and jet-layer separation, and included circulation and lift. However, the predicted value of C_ℓ for a given lift coefficient was found to depend upon the ratio of the maximum jet velocity to the average jet velocity inside the slot, which was established empirically. Further improvement of the method, especially in regard to determining the shape of the initial jet profile and to evaluating the jet growth and velocity decay ahead of the separation point should result in better overall agreement and remove some of the empirical relations contained in the theory.

17. Key Words (Suggested by Author(s))	18. Distribution Statement
Coanda Jet	UNCLASSIFIED-UNLIMITED

19. Security Classif. (of this report)	20. Security Classif. (of this page)	21. No. of Pages	22. Price*
Unclassified	Unclassified	97	$3.00

* For sale by the National Technical Information Service, Springfield, Virginia 22151

CONTENTS

ANALYTICAL AND EXPERIMENTAL INVESTIGATION OF CIRCULATION CONTROL BY MEANS OF A TURBULENT COANDA JET

By E. S. Levinsky and T. T. Yeh
Air Vehicle Corporation

SUMMARY

An analytical and experimental investigation of circulation control on a circular cylinder by means of tangential blowing (Coanda effect) is presented. The analytical method developed has also been used to estimate the blowing coefficients required for achieving potential flow on airfoils with flaps.

The analysis is presented for conditions for which the flow in the boundary layer ahead of the jet exit is turbulent. The turbulent boundary layer and the jet layer on the upper surface, and the turbulent boundary layer on the lower surface are computed by a multi-strip integral method. The region of integration is between the corresponding transition and separation points on each surface. Longitudinal curvature effects, which give rise to a radial pressure gradient across the jet layer and to an additional adverse tangential pressure gradient just upstream of the separation point, are included in the jet layer analysis in an approximate manner. The longitudinal curvature effect is found to have a pronounced influence on the separation of the jet layer.

The method has been programmed in FORTRAN IV. Values of the calculated surface pressure distribution, location of the separated region, and values of induced circulation and lift have been compared with wind tunnel test data. Significant parameters in the analysis effecting jet separation are the ratios of the maximum jet velocity in the fully merged jet layer just downstream of the jet exit to the average velocity in the jet slot, to the free stream velocity, and to the maximum jet velocity at the separation point. For the range of cases considered, the ratios of the jet slot thickness to the cylinder radius and to the boundary layer thickness were found to have only a negligible effect on jet separation, except for their influence on the ratio of the maximum jet velocity to the average jet velocity inside the slot.

In general, the analyses and the test data showed reasonable agreement with regard to pressure distribution, boundary- and jet-layer separation, and induced circulation and lift. However, the predicted value of C_μ for a given lift coefficient was found to depend upon the ratio of the maximum jet velocity to the average jet velocity inside the slot, which was established empirically. Further improvement of the method, especially in regard to determining the shape of the initial jet profile and to evaluating the jet growth and velocity decay ahead of the separation point should result in better overall agreement and remove some of the empirical relations contained in the theory.

INTRODUCTION

Considerable research has been carried out in the past dealing with lift augmentation through circulation control by means of tangential blowing over an airfoil with a rounded trailing edge, e.g., references 1 through 3. The purpose of the present study is to develop an analytical method for predicting the circulation and lift induced by tangential blowing over a circular cylinder under conditions for which the boundary layer ahead of the jet exit is turbulent. Although the present method is directly applicable only to airfoils of cylindrical cross section, e.g., as proposed for circulation controlled rotors (refs. 1 and 2), the tangential blowing lift generating mechanism, which is due to the Coanda effect, will also occur on other airfoils with blunt trailing edges, e.g., a modified elliptical section (ref. 3). It is also demonstrated that the method can serve as a basis for predicting the lifting characteristics of STOL aircraft employing tangential blowing circulation control on wings and flaps with sharp trailing edges (leading and trailing edge blowing).

The physical explanation of the Coanda jet mechanism is well known. Thus, for either static or forward speed conditions, should the tangential jet try to separate from the curved surface, a small vortex would be formed between the inner boundary of the jet and the wall which would reduce the static pressure at the wall below that at the outer surface of the jet and cause the jet to bend along the surface. For an attached jet, the radial pressure difference is balanced by centrifugal force. Due to viscosity, the jet gradually loses momentum and the local radii of curvature of the streamlines increase with angular distance θ from the jet exit. Both effects contribute to a gradual decrease in the radial pressure difference across the jet and to an additional adverse pressure gradient along the surface. It is this self-induced adverse pressure gradient $\partial p/\partial\theta$ which eventually causes the jet to separate. The angle through which the jet is able to adhere to the surface is known to depend upon a number of parameters including the excess momentum in the jet layer (C_μ in coefficient form), the nature of the jet layer (laminar or turbulent), the incidence angle of the jet exit with respect to the free stream direction θ_e, and Reynolds number.

Considerable test data are available for turbulent Coanda jets under both static and forward speed conditions, e.g., Fekete (ref. 4), Newman (ref. 5), and references 1 through 3. Additional wind tunnel data under forward speed conditions are presented in the present report. Data for laminar flow conditions are less readily available, but have been obtained under static conditions by testing in oil (ref. 6).

A complete theoretical analysis of the Coanda jet effect, even for laminar flow conditions, has, to our knowledge, not been carried out. Thus, Glauert (ref. 7) treated the flow of a jet along a straight surface (termed "wall jet") under static external conditions and for both laminar and turbulent flow. However, because of the plane wall, the pressure in the jet was constant everywhere and no separation occurred. Bloom and Steiger (ref. 8) extended the laminar jet theory to conditions with external

flow, but did not include any self-induced pressure gradient effects. The laminar solution of Parks and Petersen (ref. 9), although entitled "Coanda Type Flow," is actually identical to the laminar wall-jet solution of Glauert. The laminar jet solutions by Wygnanski and Champagne (ref. 10) include effects of self-induced pressure gradients and are valid for surfaces on which the radius of curvature increases with θ in a manner such that the velocity profiles remain similar. Wei and Levinsky (ref. 6) treated the laminar jet over a cylinder under static outside flow conditions by a second-order boundary-layer theory which included the normal momentum equation and allowed for a pressure difference across the jet layer. To the order of the terms retained, the drop in wall shear and rise in surface pressure agreed with test results up to $\theta < 45^{\circ}$, but were found to be much less than observed experimentally for larger θ.

On the other hand, methods developed to date for a turbulent wall jet are all semi-empirical in that assumptions are required for the form of the turbulent shear stress, for the shape of the velocity profile, and for the separation criterion, e.g., Glauert (ref. 7), Gartshore and Newman (ref. 11) Kind (ref. 12), and Guitton (ref. 13).

Glauert developed separate solutions for the outer and inner portions of the wall jet under static outside flow conditions. The outer portion, beyond the maximum velocity point y_m, was assumed similar to a free jet with a constant eddy viscosity ϵ across the region, whereas the inner region was taken similar to a wall boundary layer with the shear at the wall $\tau(0)$ given by the Blasius formula

$$\tau(0) = 0.0235\, u^2 \left(\frac{\nu}{u\, y}\right)^{1/4} = \epsilon \rho \frac{\partial u}{\partial y}$$

The above equation implies that $u \sim y^{1/7}$ in order that τ be non zero at the wall. Solutions obtained for the outer and inner regions both contained undetermined constants which were determined by matching at the maximum velocity position. Although the Glauert results agree well with experimental data, no curvature effects are included and hence no separation is predicted by this analysis.

Gartshore and Newman treat the turbulent wall jet with (or without) outside flow by a multi-strip integral method in which the jet layer is divided into four regions. The velocity profile in the inner two regions (below $y = y_m$) is taken of the form

$$u/u_m = (y/y_m)^n$$

where u_m, y_m, and n are unknown functions of the polar angle θ. The velocity profile in the outer regions is taken of the form

$$u = u_1 + (u_m - u_1) \exp\left[- \ln 2 \left(\frac{y - y_m}{L} \right)^2 \right]$$

where u_1 is the outside potential flow velocity and L is a fourth unknown function of θ. Four ordinary differential equations are obtained which are readily integrated for the four unknown functions, provided, however, that expressions are available for the turbulent shear stress at the surface and at the boundary of each strip. Although the method of Gartshore and Newman does lead to a prediction of flow separation, when $n \geq 1/2$, such separation is due to adverse pressure gradient effects in the outside potential flow. Curvature effects, which can induce an additional adverse pressure gradient into the jet layer, are not included in their formulation, because of the neglect of the radial momentum equation. The procedure to be followed for the Coanda jet layer in the current paper is essentially an extension of the multi-strip integral method of Gartshore and Newman to include curvature and induced pressure gradient effects. We note also that Gartshore (ref. 14) has investigated limitations of the above method due to thick boundary layers upstream of the blowing slot.

Kind (ref. 12) used a single expression due originally to Spalding (ref. 15) which contains two unknown parameters for the velocity profile across the entire wall jet. The two differential equations needed to solve for the wall jet development are supplied by an equation for the conservation of angular momentum and by an entrainment equation. Empirical corrections are included for the effects of curvature on entrainment and on the mean pressure inside the layer. Kind also used an empirical criterion based on local pressure gradient to determine the separation point and thereby obtained good agreement with test results. It was decided to base the present formulation upon the procedure of Gartshore and Newman rather than that of Kind, because the former method was judged to be somewhat less dependent upon empirical correlations and could be more readily generalized to include curvature and induced pressure gradient effects.

Guitton (ref. 13) treated the turbulent jet flow over surfaces for which the radius of curvature was either proportional to the jet layer thickness or constant by perturbation methods wherein the plane jet flow is the zeroth order approximation and the expansion parameter is proportional to the ratio of the jet thickness to the radius of curvature. In the former case self-preserving similarity type solutions were obtained, somewhat in analogy with the results of reference 10 for laminar flow. In the case of a constant radius surface, assuming zero shear at the wall and constant angular momentum leads to expressions for the decay of the maximum velocity and the growth of the jet thickness which depend upon a single unknown constant which is determined empirically. Guitton notes that the perturbation method becomes invalid when the expansion parameter exceeds 0.07. Comparison with the test data of reference 4 for the maximum jet velocity and thickness shows fair agreement for small values of the expansion parameter, up to $\theta \sim 45^\circ$. No evidence of separation at larger angles of θ is predicted.

We note that none of the methods discussed so far is able to predict the rapid rise in surface pressure which occurs ahead of the jet separation point (e.g., figure 12). Failure of these methods was noted by Kind (ref. 16), who further pointed out that the rise in surface pressure could be predicted by determining the local radius of curvature of the jet streamlines and then integrating the equations of motion normal to the streamlines. Kind obtained the streamline radii of curvature and velocities from experimental data (ref. 4), and agreement with measured surface pressures was shown to be excellent.

Because of the expected strong coupling between the surface pressure distribution and separation of the Coanda jet, it appears that any method for calculating lift due to tangential blowing must be able to predict the surface pressure distribution with reasonable accuracy. The method to be presented in the present paper approximates the pressure distribution over the cylinder by assuming that the streamline radius of curvature is constant up to a distance of several jet thicknesses ahead of the separation point. Over this region the static pressure distribution outside of the jet layer is assumed to be given by potential flow theory with circulation. The static pressure on the surface is somewhat less than that outside of the jet layer because of centrifugal force effects. For a distance of several jet thicknesses ahead of the separation point the pressure difference across the jet layer is assumed to decrease linearly reaching zero at the separation point. Thus, the additional suction on the surface of the cylinder due to jet curvature is assumed to vanish at the separation point. This is in accordance with test data showing zero static pressure increase across the jet layer at separation (ref. 16). Turbulent shear values inside the jet layer will be based on the expressions of Gartshore and Newman (ref. 11), and alternatively, on wall jet measurements by Goradia and Colwell (ref. 23), neither of which include longitudinal curvature effects.

The overall flow model used in the present method, including the equations for the laminar boundary layer, turbulent boundary layer, and Coanda jet regions, is presented in the next section. Succeeding sections present sample calculations and comparisons with new and existing test data. A description of the wind tunnel model, test conditions and corrections; and a listing of the computer program are found in the Appendices.

LIST OF SYMBOLS

$A_{c_i}, B_{c_i}, \ldots, F_{c_i}$	coefficients for curvature effects defined in Appendix C
$A_i, B_i, \ldots, F_i$	coefficients defined in Appendix C
a_j	coefficients in eqs. (35) and (36)
$A_{p_i}, B_{p_i}, \ldots, F_{p_i}$	coefficients for induced pressure effects defined in Appendix C

AR	aspect ratio
b	cylinder span (exposed length of semispan model equals $b/2$)
C_D	drag coefficient
C_L	overall lift coefficient
C_ℓ	two-dimensional lift coefficient
c_p	local pressure coefficient normalized by q_∞
$\tilde{c}_p$	normalized pressure coefficient across jet layer, eq. (45)
C_μ	jet momentum coefficient [eq. (40)]
D	denominator in eq. (36)
f_o, f_1, f_2, f_{11}, ...	functions of η defined in ref. 22
H	shape factor δ^*/θ^*
K	empirical factor in eq. (34)
K_1, K_2, K_5, K_6	definite integrals defined in Appendix C
L	length in jet velocity profile, eq. (9)
L'	$[\pi/4 \ln 2]^{1/2} L$
N	number of thicknesses $y_m + L$ ahead of the separation point at which a linear adverse tangential pressure gradient is imposed; also, numerator in eq. (36)
n	exponent in jet velocity profile, eq. (9)
p	pressure
Δp_i	pressure difference across i'th jet layer zone, eqs. (22) and (23)
q	total velocity inside boundary layer; also, dynamic pressure
R	cylinder radius

$\mathcal{R}$	local streamline radius of curvature
r	radial distance from center of cylinder
Re	Reynolds number $R V_\infty / \nu$
Re_{θ^*}	momentum thickness Reynolds number $u_1 \theta^* / \nu$
t	jet slot exit thickness
u	tangential velocity component inside boundary layer
u_j	average velocity inside jet slot exit
u_{j_∞}	average jet velocity when expanded isentropically to free stream static pressure, eq. (41)
v	radial velocity component inside boundary layer
V_∞	remote free stream velocity
x	distance along cylinder surface
y	normal distance from surface
Γ	induced circulation
$\hat{\Gamma}$	$\Gamma / 4 \pi V_\infty R$
δ	turbulent boundary-layer thickness
δ^*	turbulent displacement thickness
δ^*_ℓ	laminar displacement thickness
ϵ	eddy viscosity; also, downwash angle at cylinder
η	normalized boundary-layer thickness in eqs. (35) and (36)
θ	polar angle measured clockwise from top of cylinder
$\Delta\theta$	angular distance from forward stagnation point
θ^*	turbulent momentum thickness

θ_e	jet exit incidence angle
θ^*_ℓ	laminar momentum thickness
μ	viscosity
ν	kinematic viscosity
ν_t	effective turbulent viscosity
ρ	mass density
τ	shear

Subscripts

e	jet exit value
i	summation index i = 1, ..., 4
j	summation index j = 1, 2, ...; also, average value at jet slot exit
L	lower
ℓ	laminar
m	at maximum velocity point y_m inside jet layer profile
m/2	at height of $y_m/2$ inside jet layer
sep	separation
stag	forward stagnation point
t	turbulent
U	upper
$y_m + L$	at height $y_m + L$ inside jet layer
o	wall value
1	potential theory value taken at surface
∞	remote free stream value

THEORY

Flow Model

We shall consider the two-dimensional incompressible flow past a circular cylinder with circulation generated by tangential blowing. The flow past such a cylinder may be described by the model shown in figure 1. The flow outside the viscous regions (boundary and jet layers and separated wake) is taken as a potential flow with circulation Γ for which the inviscid velocity at the surface $u_1(\theta)$ is

$$u_1 = 2 V_\infty (\cos \theta + \hat{\Gamma}) \tag{1}$$

where $\hat{\Gamma} = \Gamma / 4 \pi V_\infty R$, V_∞ is the remote free stream velocity, and R is the cylinder radius.

The viscous flow is split at the forward stagnation point into upper and lower surface boundary layers. The boundary layer along the lower surface is taken as laminar up to the lower transition point. The boundary layer is assumed to be fully turbulent between the transition point and the lower separation point (see figure 1). The surface pressure coefficient at the lower separation point is assumed to be given by potential flow theory. Thus, from equation (1),

$$c_p\left(\theta_{sep_L}\right) = 1 - 4\left[\cos\left(\theta_{sep_L}\right) + \hat{\Gamma}\right]^2 \tag{2}$$

Similarly, the upper surface boundary layer is assumed laminar up to the upper transition point, and turbulent from the transition point to the jet exit slot. At the jet exit θ_e the boundary layer is assumed to merge with the jet flow, and the resultant Coanda jet is taken as turbulent between the jet exit and the upper separation point. The surface pressure at the upper separation point $c_p\left(\theta_{sep_U}\right)$ is again assumed given by potential theory.

The wake region $\theta_{sep_U} \le \theta \le \theta_{sep_L}$ is taken to be at constant pressure in accordance with previous experimental data (refs. 1, 2, 4, 16), and as indicated by the present test results (see Appendix B). Thus, we require

$$c_p\left(\theta_{sep_U}\right) = c_p\left(\theta_{sep_L}\right) \tag{3}$$

Equation (3) is used in the present formulation to determine the point θ_{sep_U} for a given value of $\hat{\Gamma}$. Thus, from

equations (2) and (3) we obtain

$$\theta_{sep_U} = \cos^{-1}\left\{\frac{\left[1 - c_p\left(\theta_{sep_L}\right)\right]^{1/2}}{2} - \hat{\Gamma}\right\} \tag{4}$$

In the present method $\hat{\Gamma}$ is considered given. The values of θ_{sep_L} and $c_p\left(\theta_{sep_L}\right)$ are found by integrating the boundary layer equations along the lower surface of the cylinder from the forward stagnation point until the point at which the boundary layer separates. Conditions in the turbulent boundary layer just ahead of the jet exit are found by integrating the boundary-layer equations along the upper surface of the cylinder. Properties in the jet layer downstream of the jet exit are found by integrating the Coanda jet equations up to the upper separation point. Starting conditions for the Coanda jet equation are dependent upon the boundary-layer properties ahead of the jet exit slot and upon the thickness and the momentum of the jet issuing from the slot. The problem is to determine that particular value of jet momentum (or slot thickness) for which the Coanda jet layer just separates at the required position θ_{sep_U}. In general, this must be found a posteriori by trying several values of jet momentum.

Coanda Jet Equations

We consider first the equations of momentum and continuity for a two-dimensional, incompressible, turbulent flow in cylindrical coordinates (r, θ). For a steady mean flow over a cylinder of radius R, retention of terms of $0(1)$ and $0(\delta)$ in the tangential and normal momentum equations gives (see ref. 17):

$$\frac{\rho u}{R}\frac{\partial u}{\partial \theta} + \frac{\rho v r}{R}\frac{\partial u}{\partial r} + \frac{\rho u v}{R} = -\frac{1}{R}\frac{\partial p}{\partial \theta} + \frac{2\tau}{R} + \frac{r}{R}\frac{\partial \tau}{\partial r} \tag{5}$$

$$\frac{u}{q}\frac{\partial p}{\partial r} - \frac{v}{q}\frac{1}{r}\frac{\partial p}{\partial \theta} = \frac{\rho q^2}{\mathcal{R}} \tag{6}$$

$$\frac{\partial v}{\partial r} + \frac{1}{r}\frac{\partial u}{\partial \theta} + \frac{v}{r} = 0 \tag{7}$$

Here u and v are tangential and radial components, respectively, of the resultant velocity q; ρ is the density; p is the local static pressure; $\mathcal{R}$ is the local streamline radius of curvature, and τ is the total shear stress defined as

$$\tau = \mu\frac{\partial u}{\partial r} - \rho\langle u' v'\rangle \tag{8}$$

All unprimed quantities are time averaged values and primed quantities represent instantaneous values. The brackets $\langle\ \rangle$ indicate a time average. All viscous terms in the normal momentum equation, equation (6), have been omitted, since they are assumed of higher order.

Equations (5) to (8) will be solved for the velocity distribution in the Coanda jet layer using multi-strip integral methods. Thus, following reference 11, we assume a four-parameter velocity profile of the form

$$\left.\begin{aligned} u &= u_m\,(y/y_m)^n \qquad , \quad y \le y_m \\ u &= u_1 + (u_m - u_1)\,\exp\left[-\ell n\,2\left(\frac{y - y_m}{L}\right)^2\right] \\ & \qquad\qquad y \ge y_m \end{aligned}\right\} \tag{9}$$

where $y = r - R$ and u_1 is the local free stream velocity which is assumed given by equation (1). The four unknown parameters u_m, n, y_m, and L are unknown functions of θ and are to be determined.

The wall-jet layer is divided into four strips or zones as shown in figure 2. By first eliminating v from equation (5) through use of equation (7), and by substituting for u through equation (9), integration of the tangential momentum equation across each of the strips is readily carried out and may be shown to yield a system of four quasi-linear ordinary differential equations of the form

$$A_i \frac{du_1}{dx} + B_i \frac{du_m}{dx} + C_i \frac{dL}{dx} + D_i \frac{dy_m}{dx} + E_i \frac{dn}{dx} + F_i$$

$$= -\int_{y_{i_L}}^{y_{i_U}} \frac{uv}{R}\,dy - \int_{y_{i_L}}^{y_{i_U}} \left(\frac{\partial\left(\frac{p}{\rho}\right)}{\partial x} + u_1 \frac{du_1}{dx}\right) dy \tag{10}$$

$$i = 1,\ 2,\ 3,\ 4.$$

Following the convention of Gartshore and Newman, the subscripts 1, 2, 3, and 4 were chosen to correspond to integration across the strips $0 \to y_m$, $y_m \to y_m + L$, $y_m \to \infty$, and $y_m/2 \to y_m$, respectively. Here $dx = R\,d\theta$, and y_{i_L} and y_{i_U} represent the lower and upper integration limits for the i'th strip.

The coefficients A_i, B_i, ... E_i are identical to those given previously by Gartshore and Newman, since all inviscid longitudinal-curvature and self-induced pressure-gradient effects are included in the two terms on the right hand side of equation (10). The coefficients F_i contain differences of the order $\frac{\delta}{R}$ from the values given by Gartshore and Newman, due to the influence of longitudinal curvature on the viscous terms in equation (5). For completeness, the coefficients have been listed in Appendix C.

Shear stress relations. —We note that the coefficients F_i include values of the shear stress τ_o on the surface of the cyliner, τ_m at the maximum velocity point, $\tau_{m/2}$ at one-half the height of the maximum velocity point, and τ_L at a height $y_m + L$. For laminar flow, the shear stress at these locations may be expressed in terms of the viscosity μ and the velocity gradient, and hence the system of equations (8) through (10) form a closed set. For turbulent flow, on the other hand, the shear stress as given by equation (8) is dependent upon the mean value of the product of the instantaneous velocities and cannot be expressed in terms of the velocity gradient. Hence, closure of the system of equations must be accomplished by supplying auxiliary relations for the turbulent shear values.

Two sets of relations have been used in the present paper for approximating the turbulent shear stresses. The first set is based largely on expressions given in reference 11. The second set utilizes new expressions for τ_o and τ_m based on measurements given in reference 23.

According to reference 11, the wall shear is given by a modified Ludwig-Tillman law of the form

$$\frac{\tau_o}{\rho u_m^2} = 0.0128 \left(\frac{y_m u_m}{\nu} \right)^{-1/6} \left[\frac{n}{(n+1)(2n+1)} \right]^{(11n-1)/6} \tag{11}$$

The shear stress at the height $y_m/2$ from the surface is given by the expression

$$\frac{\tau_{m/2}}{\rho u_m^2} = \nu_t \left(\frac{\partial u}{\partial y} \right)_{y_{m/2}} = \frac{u_m \delta_m^*}{Re_{y_{m/2}}} \left(\frac{\partial u}{\partial y} \right)_{y_{m/2}} = \frac{2n^2}{2^n (n+1)} \left[Re_{y_{m/2}} \right]^{-1} \tag{12}$$

where $Re_{y_{m/2}} = \frac{\delta_m^* u_m}{\nu_t}$ was assumed constant and equal to 50 for the midpoint of the inner jet layer in accordance with previous boundary-layer measurements.

For the maximum velocity point Glauert (ref. 7) assumed that the shear stress $\tau_m = 0$, because $\left(\frac{\partial u}{\partial y}\right)_{y_m} = 0$. Newman, however, (ref. 5) points out that τ_m will not be zero even though the velocity gradient vanishes at this point, because the jet layer is asymmetrical about y_m. Gartshore and Newman related τ_m to the shear $\tau_{y_m + L}$ at the height $y_m + L$ through the expression

$$\tau_m = \tau_{y_m + L} \left[0.15 + 0.30 \, (y_m / L)^2\right] \tag{13}$$

Harris (ref. 19) expressed τ_m in terms of the wall shear through the relation

$$\tau_m = - \tau_o \left(1 - \frac{u_1}{u_m}\right)^2 \tag{14}$$

Both of the above equations for τ_m yield a negative value for τ_m, since, as will be shown below, $\tau_{y_m + L} \leq 0$.

The shear $\tau_{y_m + L}$ at the mid velocity point in the outer jet layer may be written

$$\tau_{y_m + L} / \rho u_m^2 = \left[\nu_t \frac{\partial u}{\partial y}\right]_{y_m + L} / u_m^2 = -\left(1 - \frac{u_1}{u_m}\right)^2 \frac{\ell n \, 2}{Re_{y_m + L}} \tag{15}$$

where equation (9) has been used to evaluate the velocity gradient at $y_m + L$. The Reynolds number $Re_{y_m + L} = \left(\frac{u_m - u_1}{\nu_t}\right) L$ was approximated equal to 50 for several of the sample calculations. Equations (11), (12), (13), and (15) constituted the first set of shear stress relations.

For the second set of shear stress relations, alternate expressions were used for τ_o and τ_m from reference 23 [eqs. (9) and (10) of ref. 23]. In addition, the Reynolds number $Re_{y_m + L}$ was approximated as

$$Re_{y_m + L} = 35 \left[1 + 295 \left(\frac{\partial u / \partial x}{\partial u / \partial y}\right)^2\right]$$

as discussed in reference 11.

None of the above expressions for the turbulent shear have been modified for effects of longitudinal curvature. Based on boundary-layer measurements, Tetervin (ref. 17) approximated the decrease in wall shear with longitudinal curvature by the polynomial expression

$$\frac{\tau_o}{(\tau_o)_{R=\infty}} = 1 - 0.338 \times 10^3 \left(\frac{\theta^*}{R}\right) + 0.0438 \times 10^6 \left(\frac{\theta^*}{R}\right)^2 \qquad (16)$$

$$0 \le \frac{\theta^*}{R} \le 0.004$$

However, since use of equation (16) by Tetervin failed to predict the observed behavior of δ^*/θ^* with x/R (ref. 17), it was decided to use the unmodified expressions for wall shear in the present study.

Curvature and induced pressure gradient terms.— The two integrals on the right hand side of equation (10) represent effects of curvature and induced pressure gradient, respectively, and vanish for the case of a flat surface for which $R = \infty$. It is these two terms which distinguish the flat wall jet from a Coanda jet flow over a curved surface, and lead to earlier separation for the latter.

In order to evaluate the curvature term [first term on the right hand side of equation (10)], it is convenient to first obtain v from the equation of continuity, equation (7). This gives, to lowest order in y/R

$$v(y) = -\int_o^y \frac{\partial u}{\partial x}\, dy$$

Substituting for u from equation (9) gives, when $y \le y_m$

$$v = -\frac{y_m u_m}{n+1}\left(\frac{y}{y_m}\right)^{n+1}\left[\frac{du_m/dx}{u_m} - n\,\frac{dy_m/dx}{y_m} + \left(\ell n\,\frac{y}{y_m} - \frac{1}{n+1}\right)\frac{dn}{dx}\right] \qquad (17)$$

and, when $y \ge y_m$,

$$v = -\frac{y_m u_m}{n+1}\left[\frac{du_m/dx}{u_m} - n\,\frac{dy_m/dx}{y_m} - \frac{dn/dx}{n+1}\right] - (y - y_m)\,\frac{du_1}{dx}$$

$$- (u_m - u_1)\,dy_m/dx + (u_m - u_1)\left[\frac{dy_m}{dx} + \left(\frac{y - y_m}{L}\right)\frac{dL}{dx}\right]\exp\left[-\left(\frac{y - y_m}{L}\right)^2 \ell n\, 2\right]$$

$$- \left[L(du_m/dx - du_1/dx) + (u_m - u_1)\,dL/dx\right]\int_o^{\frac{y-y_m}{L}} \exp\left[-\xi^2 \ell n\, 2\right] d\xi \qquad (18)$$

Making use of equations (9), (17), and (18), the curvature term may be expressed in the form

$$\int_{y_{i_L}}^{y_{i_U}} \frac{uv}{R}\, dy = A_{c_i} \frac{du_l}{dx} + B_{c_i} \frac{du_m}{dx} + C_{c_i} \frac{dL}{dx} + D_{c_i} \frac{dy_m}{dx} + E_{c_i} \frac{dn}{dx} + F_{c_i}$$

$$i = 1, 2, \ldots, 4 \qquad (19)$$

where the subscripts i refer to the same integration zones as for equation (10). In performing the integration, it was assumed that the integrals across the strip $y_m + L \leq y \leq \infty$ were small compared to the total integrals. Hence, the coefficients $A_{c_2} = A_{c_3}$, etc. This assumption is believed consistent with the assumptions to be made in evaluating the induced pressure terms, viz., that the static pressure has reached the outside potential value at $y = y_m + L$. The coefficients A_{c_i}, B_{c_i}, etc. are given in Appendix C.

The induced pressure gradient term is evaluated by use of the normal momentum equation. Equation (6) may be simplified by assuming that the radial velocity component is much less than the tangential component of velocity over the major portion of the jet layer for which the jet remains thin. This assumption should remain valid until the jet begins to thicken prior to separation. Thus, we approximate equation (6) by

$$\frac{\partial p}{\partial r} = \frac{\rho u^2}{R} \qquad (20)$$

for $\theta_e \leq \theta \leq \theta_{sep} - \dfrac{(y_m + L)\, N}{R}$

Here we have replaced the local streamline radius of curvature by R. The thickness $y_m + L$ varies with θ, and N refers to the number of thicknesses $y_m + L$ ahead of the separation point for which the simplified normal momentum equation will be used.

Using equation (20) and assuming that the static pressure $p_{y_m + L}$ at the height $y_m + L$ equals the outside static pressure p_1, the static pressure along the boundaries of the various zones in the jet layer becomes

$$\left.\begin{aligned} p_o &= p_1 - \Delta p_1 - \Delta p_2 \\ p_{m/2} &= p_1 - \Delta p_2 - \Delta p_4 \\ p_m &= p_1 - \Delta p_2 \\ p_{m+L} &= p_1 \end{aligned}\right\} \tag{21}$$

$$\text{where } \Delta p_i = \int_{y_{i_L}}^{y_{i_U}} \left(\frac{\partial p}{\partial r}\right) dy = \int_{y_{i_L}}^{y_{i_U}} \frac{\rho u^2}{R}\, dy \tag{22}$$

The pressure differences Δp_i are readily evaluated through use of equation (9), giving

$$\left.\begin{aligned} \Delta p_1 &= \frac{\rho u_m^2 y_m}{(2n+1)R} \\ \Delta p_2 &= \frac{\rho L}{R}\left(0.06\, u_1^2 + 0.26\, u_1 u_m + 0.68\, u_m^2\right) \\ \Delta p_3 &= \Delta p_2 \\ \Delta p_4 &= \frac{\rho u_m^2 y_m}{(2n+1)R}\left[1 - \left(\frac{1}{2}\right)^{2n+1}\right] \end{aligned}\right\} \tag{23}$$

The integrand $\frac{\partial p/\rho}{\partial x} + u_1 \frac{du_1}{dx}$ in the induced pressure gradient term may be readily evaluated by direct differentiation of equations (21). Using average values for p across each zone gives for i = 1

$$\int_0^{y_m} \left(\frac{\partial p}{\partial x} + \rho u_1 \frac{du_1}{dx} \right) dy = \rho u_1 \frac{du_1}{dx} y_m + \left[\frac{\partial p_o}{\partial x} + \frac{\partial p_{m/2}}{\partial x} \right] \frac{y_m}{4}$$

$$+ \left[\frac{\partial p_{m/2}}{\partial x} + \frac{\partial p_m}{\partial x} \right] \frac{y_m}{4}$$

$$= - y_m \frac{d}{dx} \left[\frac{\Delta p_1}{4} + \Delta p_2 + \frac{\Delta p_4}{2} \right] \tag{24}$$

Similarly, for $i = 2$ and $i = 3$,

$$\int_{y_m}^{y_m + L_o} \left(\frac{\partial p}{\partial x} + \rho u_1 \frac{du_1}{dx} \right) dy = \int_{y_m}^{\infty} \left(\frac{\partial p}{\partial x} + \rho u_1 \frac{du_1}{dx} \right) dy = - \frac{L}{2} \frac{d}{dx} \left(\Delta p_2 \right) \tag{25}$$

whereas, for $i = 4$,

$$\int_{y_{m/2}}^{y_m} \left(\frac{\partial p}{\partial x} + \rho u_1 \frac{du_1}{dx} \right) dy = - \frac{y_m}{2} \frac{d}{dx} \left[\Delta p_2 + \frac{\Delta p_4}{2} \right] \tag{26}$$

After carrying out the indicated differentiation through use of equations (23), the results may be grouped in the form

$$\int_{y_{i_L}}^{y_{i_U}} \left(\frac{\partial p/\rho}{\partial x} + u_1 \frac{du_1}{dx} \right) dy = A_{p_i} \frac{du_1}{dx} + B_{p_i} \frac{du_m}{dx} + C_{p_i} \frac{dL}{dx} + D_{p_i} \frac{dy_m}{dx}$$

$$+ E_{p_i} \frac{dn}{dx} + F_{p_i} \tag{27}$$

$$i = 1, 2, \ldots 4$$

where the coefficients A_{p_i}, B_{p_i}, etc., are again given in Appendix C.

The assumption of a thin jet layer breaks down near the separation point, as pointed out earlier, and the approximate form of the normal momentum equation given by equation (20) would not be expected to hold when the jet thickens. When the jet approaches the separation point the

streamline radii of curvature $\mathcal{R}$ in the full normal momentum equation, equation (6), tend to become very large as the jet straightens (see fig. 1). It is in this region that the radial pressure difference $p_1 - p_o$ across the jet drops rapidly to zero due to the loss in centrifugal force. This may be seen from the experimental pressure distributions, e.g., figures 10 to 14.

Because of the failure of equation (20) near the separation point, the induced pressure gradient term in equation (20) has been approximated by the linear expression

$$\int_{y_{i_L}}^{y_{i_U}} \left(\frac{\partial p/\rho}{\partial x} + u_1 \frac{du_1}{dx} \right) dy = \left(y_{i_U} - y_{i_L} \right) \left[\frac{\Delta p_i}{R(\theta_{sep} - \theta)} \right]_{\theta = \theta_{sep} - \frac{(y_m + L) N}{R}}$$

for the region $\theta_{sep} - \dfrac{(y_m + L)}{R} N < \theta \leq \theta_{sep}$. (28)

Equation (28) implies a linear decrease in the induced static pressure difference within the jet layer from its value Δp_i at $\theta = \theta_{sep} - \dfrac{(y_m + L)}{R} N$ to zero at $\theta = \theta_{sep}$. The additional pressure gradient thereby imposed, which will be on the order of

$$0 \left[(t/R)\ \rho u_j^2 / (y_m + L)\ N \right]_{\theta = \theta_{sep} - \frac{(y_m + L)\ N}{R}}$$

will increase the tendency of the jet layer to separate. Here u_j is the average jet velocity at the exit which is of thickness t. In order for the linear induced pressure gradient approximation to be valid, the jet momentum required for separation at θ_{sep} should prove relatively insensitive to N.

In accordance with the above approximation, the coefficients in equation (27) are taken as

$$A_{p_i} = B_{p_i} = \ldots = E_{p_i} = 0 \tag{29}$$

and

$$F_{p_i} = \left(y_{i_U} - y_{i_L} \right) \left[\frac{\Delta p_i}{(y_m + L)\ N} \right]_{\theta = \theta_{sep} - \frac{(y_m + L) N}{R}} \tag{30}$$

for the interval $\theta_{sep} - \dfrac{(y_m + L)}{R} N < \theta \leq \theta_{sep}$.

Starting conditions.— Equations (10) constitute a set of four parabolic differential equations with dependent variables u_m, L, y_m, and n, and independent variable $x = R\theta$. Initial conditions are required at the jet exit $\theta = \theta_e$.

By assuming an average velocity u_j for the jet at the exit of thickness t, conservation of momentum gives

$$u_j(u_j - u_1)\, t - u_1^2 \theta^* = \int_0^{y_m} u(u - u_1)\, dy + \int_{y_m}^{\infty} u(u - u_1)\, dy \tag{31}$$

The terms on the left hand side of equation (31) represent the net excess momentum in the jet and boundary layer at $\theta = \theta_e$. The terms on the right hand side represent the excess momentum in the fully merged jet layer with a velocity profile of the form given by equation (9). Transition to the jet layer velocity profile is assumed to occur in a negligible distance. Substituting equation (9) into equation (31) and carrying out the indicated integration then gives for the height y_m

$$\frac{y_m}{t} = \frac{1 - \frac{u_1}{u_j}\left(1 + \frac{\theta^*}{t}\,\frac{u_1}{u_j}\right)}{\frac{u_m}{u_j}\left[\frac{u_m/u_j}{2n+1} - \frac{u_1/u_j}{n+1}\right] + \frac{L'}{y_m}\left[\frac{u_m}{u_j} - \frac{u_1}{u_j}\right]\left[\frac{u_1}{u_j} + \frac{1}{\sqrt{2}}\left(\frac{u_m}{u_j} - \frac{u_1}{u_j}\right)\right]} \tag{32}$$

A second initial condition was obtained by taking the ratio

$$L'/y_m = \left[\frac{\pi}{4 \ell n\, 2}\right]^{1/2} L/y_m = 6 \tag{33}$$

which is in accordance with the measurements of Fekete (ref. 4) and the calculations of Glauert (ref. 7) for zero outside flow conditions. The sensitivity of the resulting Coanda jet development and separation to variations in the initial value of L'/y_m remains to be determined under conditions of forward speed.

The third initial condition is supplied by the starting value of the exponent $n(\theta_e)$. Values for $n(\theta_e)$ are expected to lie in the range $1/7 < n(\theta_e) < 1/5$. The results of the calculations may be shown to be insensitive to the value used for $n(\theta_e)$, since $n(\theta)$ has been found to

rapidly adjust to the same value downstream of θ_e over the above range of $n(\theta_e)$ (see figs. 6 and 7).

The fourth initial condition is the value $u_m(\theta_e)/u_j$. Use of the conservation of mass equation for determining $u_m(\theta_e)/u_j$ has been ruled out because of the entrainment of mass from the outside flow into the jet layer just downstream of the exit. Data by Fekete show that the maximum jet velocity $u_m(\theta_e)$ is somewhat less than the average velocity u_j and that the ratio $u_m(\theta_e)/u_j$ decreases with decreasing t/R. Dunham (ref. 1) also notes a significant influence of the parameter t/R on the effective jet momentum. From considerations of viscous mixing, it appears that $u_m(\theta_e)/u_j$ should vary inversely with the ratio δ/t, where δ is the boundary layer thickness ahead of the slot. On the other hand, the parameter which will be shown to have the major influence on the Coanda jet separation is the ratio $u_m(\theta_e)/u_l(\theta_e)$, or equivalently, $u_m(\theta_e)/V_\infty$. In order for the jet moment coefficient C_μ to be nearly independent of t for the same value of $u_m(\theta_e)/V_\infty$, we require $u_m(\theta_e)/u_j \sim t^{1/2}$. Hence, it seems reasonable to assume the variation

$$\frac{u_m(\theta_e)}{u_j} = K\left(\frac{t}{\delta}\right)^{1/2} \leq 1 \tag{34}$$

where the parameter K is to be found from experimental data.

Equations (32), (33), (34), together with an assumption for $n(\theta_e)$, constituted the usual set of starting conditions. An alternate set of starting conditions was also used which did not involve the empirical constant K. The alternate starting conditions ($\theta = \theta_e$) consisted of taking $y_m = L = t$, obtaining u_m/u_j from equation (32), and again assuming the initial value for n. We note that the alternate starting conditions seem preferable, since they do not contain the constant K. However, the ratio u_m/u_j may no longer vary with $t^{1/2}$, since equation (34) is no longer used, and C_μ will therefore be somewhat dependent upon t/R.

We remark that considerable uncertainty exists with respect to the initial values for the jet velocity parameters and, in fact, with regard to the adequacy of equation (9) in representing the jet velocity profile for thin jets (refs. 14,23). Measurements of the jet velocity profile near the exit would be of substantial aid in determining the starting jet parameters. On the other hand, a calculation of the initial mixing between the jet and the external flow by finite-difference methods, as reviewed in reference 20, could also serve to eliminate some of the empiricism in the starting parameters.

Separation condition.— The Coanda jet is assumed to separate when the exponent n for the inner velocity profile exceeds $1/2$ with $dn/d\theta > 0$. This separation condition, which was also used in reference 11, is based on an analogy with turbulent boundary-layer theory which, on the basis of the standard mixing length hypothesis, may be shown to yield zero shear stress at the wall when $n = 1/2$ (ref. 21). The condition $n = 1/2$ is equivalent to a value of the shape factor of the inner profile

$$H_m = \delta_m^*/\theta_m^* = 2n + 1 = 2$$

We note that expressions for wall shear from equation (11) or from equation (9) of reference 23 do not vanish when $n = 1/2$. These equations may be regarded as approximate when $n \sim 1/2$.

Boundary-Layer Theory

As discussed previously, a boundary-layer calculation is carried out along the lower surface to determine the lower surface separation point for a given $\hat{\Gamma}$. A boundary-layer calculation is also performed along the upper surface between the forward stagnation point and jet exit in order to evaluate the boundary-layer thicknesses δ and θ^* just ahead of the exit for initializing the Coanda jet calculation.

Laminar boundary layer.— The laminar boundary-layer calculation is initiated at the forward stagnation point $\theta_{stag} = \cos^{-1}(-\hat{\Gamma})$ and continued along both the upper and lower surfaces until the momentum thickness Reynolds number $Re_{\theta^*} = \dfrac{|u_1|\theta^*}{\nu} = 300$. Standard series expansion methods are used to calculate the laminar boundary-layer properties (e.g., ref. 22), and result in the expressions

$$\frac{\delta_\ell^*}{R} = \left(\frac{R V_\infty}{\nu}\right)^{-1/2} \left(\frac{du_1/d\theta}{V_\infty}\right)_{\theta_{stag}}^{-1/2} \left[\frac{(\eta - f_o)\Delta\theta + (\eta - f_1)a_1\Delta\theta^2 + (\eta - f_2)a_2\Delta\theta^3 + \ldots}{\Delta\theta + a_1\Delta\theta^2 + a_2\Delta\theta^3 + \ldots}\right]_{\lim \eta \to \infty} \tag{35}$$

and

$$\frac{\theta_\ell^*}{R} = \left(\frac{R V_\infty}{\nu}\right)^{-1/2} \left(\frac{du_1/d\theta}{V_\infty}\right)_{\theta_{stag}}^{-1/2} \left(\frac{N(\Delta\theta)}{D(\Delta\theta)}\right)_{\lim \eta \to \infty} \tag{36}$$

where

$$N = \left[f_o''(0) - (\eta - f_o)\right]\frac{\Delta\theta^2}{2} + a_1\left[f_1''(0) - 2(\eta - f_o) - (\eta - f_1)\right]\frac{\Delta\theta^3}{3}$$

$$+ a_1^2\left[f_1 - \int_o^\infty (f_1')^2 d\eta\right]\Delta\theta^4 + 2a_2\left[\frac{f_o + f_2}{2} - \int_o^\infty f_o' f_2' d\eta\right]\Delta\theta^4$$

$$+ 2a_1^2\left[\frac{f_{11}}{2} - \int_o^\infty f_{11}' f_o' d\eta\right]\Delta\theta^4 + \ldots$$

and

$$D = \Delta\theta^2 + 2a_1\Delta\theta^3 + (a_1^2 + 2a_2)\Delta\theta^4 + \ldots$$

Here, following the method in reference 22, u has been expanded in the series

$$u = \left[\frac{du_1}{d\theta}\right]_{\theta_{stag}}\left\{f_o'(\eta)\,\Delta\theta + a_1 f_1'(\eta)\Delta\theta^2 + \left[a_2 f_2'(\eta) + a_1^2 f_{11}'(\eta)\right]\Delta\theta^3 + \ldots\right\}$$

where

$$\eta = \left(\frac{y}{R}\right)\left[\frac{R V_\infty}{\nu}\left(\frac{du_1/d\theta}{V_\infty}\right)\right]^{1/2}_{\theta_{stag}}$$

$$a_j = \frac{1}{(j+1)!}\left[\frac{d^{(j+1)}u_1/d\theta^{(j+1)}}{du_1/d\theta}\right]_{\theta_{stag}}, \qquad j = 1, 2, \ldots$$

and the f functions are given in Table VI.1 of reference 22. The derivatives $d^{(j+1)}u_1/d\theta^{(j+1)}$ are readily evaluated from equation (1), and $\Delta\theta$ represents the angular distance from the forward stagnation point, viz., $\Delta\theta = \theta - \cos^{-1}(-\hat{\Gamma})$. For the upper surface $\Delta\theta \geq 0$, whereas on the lower surface $\Delta\theta \leq 0$.

The range of convergence of the laminar boundary-layer expansion is unknown, although the series expansion for the outer flow $u_1(\theta)$ is

readily found to be accurate to within 10% for $-\pi/2 \le \Delta\theta \le \pi/2$, when retaining terms up to and including a_2. Extension of the range of validity would require evaluation of additional odd-subscripted f functions beyond f_1, which has to our knowledge not been carried out.

Turbulent boundary layer.— The multi-strip integral representation of the turbulent boundary-layer equations is readily obtained from equations (10) by setting $u_m = u_1$ and $L = 0$. [Curvature and induced pressure gradient terms will be neglected in the boundary-layer approximation in accordance with the usual ordering procedures.] This gives, with y_m replaced by δ,

$$D_1 \frac{d\delta}{dx} + E_1 \frac{dn}{dx} = -\frac{\tau_o}{\rho} - (A_1 + B_1) \frac{du_1}{dx} \tag{37}$$

$$D_4 \frac{d\delta}{dx} + E_4 \frac{dn}{dx} = -\frac{\tau_{m/2}}{\rho} - (A_4 + B_4) \frac{du_1}{dx} \tag{38}$$

where the coefficients are given in Appendix C.

The unknowns in the turbulent boundary layer are the thickness δ and the exponent n. Initial conditions for δ and n are supplied by equating the turbulent and laminar momentum and displacement thicknesses at the transition points, viz.,

$$\left.\begin{aligned} \frac{\delta_t^*}{R} &= \left(\frac{\delta}{R}\right) \frac{n}{n+1} = \frac{\delta_\ell^*}{R} \\ \frac{\theta_t^*}{R} &= \left(\frac{\delta}{R}\right) \frac{n}{(n+1)(2n+1)} = \frac{\theta_\ell^*}{R} \end{aligned}\right\}_{\theta_{transition}} \tag{39}$$

where δ_ℓ^*/R and θ_ℓ^*/R are given by equations (35) and (36). The turbulent boundary-layer equations are integrated along the upper surface until $\theta = \theta_e$ and along the lower surface up to the lower separation point at which $n = 1/2$.

NUMERICAL SOLUTION AND SAMPLE CALCULATIONS

The system of equations described in the previous section representing the boundary and Coanda jet layers has been programmed for solution on the CDC 3600 digital computer in the FORTRAN IV language. The laminar boundary-layer properties are obtained algebraically, whereas the turbulent boundary and jet layers are obtained using a Runge-Kutta marching procedure. A listing of the computer programs and sample input and output are given in Appendix D.

Results of sample calculations for values $\hat{\Gamma} = 0,\ 0.25$, and 0.50, and based on the Reynolds number $Re = R V_\infty/\nu = 5 \times 10^5$ and $\theta_e = 0^o$ are presented below.

The laminar boundary-layer development according to equations (35) and (36) has been plotted in figure 3 for both upper and lower surfaces of the cylinder. Only minor differences due to $\hat{\Gamma}$ are noted for δ^*/R and θ^*/R, except for the location of the calculated transition point.

The turbulent boundary-layer development along the lower surface of the cylinder is shown in figure 4. Of special interest are the calculated separation points $(n = 1/2)$ at the values $\theta_{sep_L} = 135^o, 142^o$, and 150^o for $\hat{\Gamma} = 0,\ 0.25$, and 0.50, respectively. The turbulent boundary-layer development and corresponding separation points along the upper surface, without blowing, are shown in figure 5. Also indicated are the required upper-surface separation points θ_{sep_U} for satisfying the separation condition of equations (3) and (4). Tangential blowing is required along the upper surface to attain the required separation locations when $\hat{\Gamma} > 0$.

The development of the Coanda jet layer over the upper surface is shown in figures 6 through 9 for $\hat{\Gamma} = 0.50$. The required value of θ_{sep_U} is 97.5^o for this value of $\hat{\Gamma}$. The significant parameters in the theory for determining the jet strength are the ratios $u_m(\theta_e)/u_1(\theta_e)$ [or equivalently, $u_m(\theta_e)/V_\infty$] and t/R, and will be used in the following comparisons. These parameters may be used to evaluate the jet momentum coefficient C_μ defined herein as

$$C_\mu = \left(\frac{t}{R}\right)\left(\frac{u_j}{V_\infty}\right)\left(\frac{u_{j_\infty}}{V_\infty}\right) \tag{40}$$

which has been found to correlate the experimental data. Here the

ratio u_j/V_∞ is given in terms of $u_m(\theta_e)/V_\infty$, K, and t/δ through equation (34), and u_{j_∞} is the velocity attained by the jet when expanded isentropically to the remote free stream pressure. For incompressible flow, Bernoulli's law gives

$$\frac{u_{j_\infty}}{V_\infty} = \left[1 + \left(\frac{u_j}{V_\infty}\right)^2 \left(1 - 2\frac{t}{R}\right) - \left(\frac{u_1}{V_\infty}\right)^2\right]^{1/2}_{\theta_e} \tag{41}$$

We consider first the effect of $u_m(\theta_e)/V_\infty$ on the Coanda jet layer development for $t/R = 0.01$ and with curvature and induced pressure gradient terms omitted (fig. 6). In this case, although the tendency of the jet to separate is clearly delayed by increasing the jet velocity ratio $u_m(\theta_e)/V_\infty$, the results are seen to be physically unrealistic in that no separation occurs at $\theta_{sep_U} = 97.5^\circ$ for any value of $u_m(\theta_e)/V_\infty$.

On the other hand, with the curvature and induced pressure gradient terms included, separation is found to occur at $\theta = 97.5^\circ$ when $u_m(\theta_e)/V_\infty \simeq 4.4$. The results in figure 7 are for the values $N = 5$ and $K = 1$. This increased tendency of the jet to separate, at the larger values of $u_m(\theta_e)/V_\infty$, in contrast to the results in figure 6, is due to the additional pressure rise imposed ahead of the separation point, i.e., when $\theta_{sep} - \frac{(y_m + L)\,N}{R} \le \theta \le \theta_{sep}$, due to loss of centrifugal force as discussed previously.

The change Δn resulting from this additional pressure rise may be estimated by solving equations (10) for dn/dx with $i = 1$ and 4, and then isolating the contribution resulting from the induced pressure gradient term. The result is

$$\frac{dn}{dx} = \frac{-y_m(D_4 - D_1/2)\ \partial/\partial x\ (p/\rho + u_1^2/2)}{D_4 E_1 - E_4 D_1} \tag{42}$$

Evaluating the coefficients from Appendix C gives

$$\frac{dn}{dx} = \frac{(2^n - 1)}{2\,\ell n\,2}(2n+1)(n+1)\ \frac{t/R}{(u_m/u_j)^2}\ \frac{d\tilde{c}_p}{dx} \tag{43}$$

where $\tilde{c}_p = \left(\frac{R}{t}\right)\frac{p_1 - p_o}{1/2\,\rho u_j^2} \simeq 2$ is the normalized pressure coefficient for the difference in pressure across the jet layer. Taking an average value for the exponent $n \simeq 0.40$, using equation (34) to calculate $u_m(\theta_e)/u_j$, and evaluating u_m at θ_{sep_U} gives

$$\Delta n \simeq \frac{0.58}{K^2}\left(\frac{\delta}{R}\right)\left[\frac{u_m(\theta_e)}{u_m(\theta_{sep_U})}\right]^2 \Delta\tilde{c}_p \qquad (44)$$

Equation (44) clearly shows that the rise in the exponent n required for separation ($\Delta n \simeq 0.2$ to 0.3 for separation) is independent of the additional adverse pressure gradient ahead of the separation point, but depends on the pressure rise coefficient $\Delta\tilde{c}_p$ against which the jet layer must act.

We note that equation (44) is dependent upon the square of the ratio of the maximum jet velocity at the exit $u_m(\theta_e)$ to the maximum jet velocity at the separation point $u_m(\theta_{sep})$, and that Δn is therefore highly dependent upon the decay rate of u_m with θ. The higher the decay rate, the larger the value of Δn and the stronger the tendency of the Coanda jet layer to separate.

We note also that equation (44) is independent of the jet thickness ratio t/R, although this result depends on the use of equation (34) which is empirical. The factor K in equation (44) is also empirical, and relates $u_m(\theta_e)$ to the average velocity inside the jet slot u_j through equation (34). Since equation (44) is independent of N, as well as of t/R, we expect that the separation positions found as a function of $u_m(\theta_e)/V_\infty$ in figure 7 should be nearly independent of the parameters N and t/R. This is shown to be the case in figures 8 and 9, wherein N and t/R are varied over the range $3 \le N \le 10$ and $0.005 \le t/R \le 0.015$, respectively. Effects of the parameter K, which relate $u_m(\theta_e)/V_\infty$ to u_j/V_∞ and hence to C_μ, will be discussed in the following section.

The variation of n with θ, using the alternate starting conditions and the second set of shear relations, is shown in figures 10 and 11 for $\hat{\Gamma} = 0.29$ and 0.5, respectively. The calculations were performed for $t/R = 0.015$ and $N = 5$. The empirical factor K does not occur when the alternate starting conditions are used, as mentioned previously. However, some variation in the value of C_μ required for separation with t/R is to be expected when using the alternate starting conditions.

EVALUATION OF THEORY AND COMPARISON WITH TEST DATA

The methods presented in the previous sections have been evaluated by comparing with wind tunnel test data of tangential blowing over a cylinder obtained during the course of the current study. Model descriptions and test conditions are presented in Appendix B.

Pressure Data

The variation of local pressure coefficient c_p around the cylinder for zero tangential blowing is shown in figure 12 as a function of Reynolds number. Also included are the corresponding drag coefficients C_D. Both pressure and drag data clearly show a rapid change from laminar to turbulent separation when $Re \geq 1.8 \times 10^5$. All testing with tangential blowing was therefore carried out at Reynolds numbers exceeding this value. Also shown in figure 10 is the potential theory pressure distribution according to equation (1) with $\hat{\Gamma} = 0$. Agreement between potential theory and the turbulent data is surprisingly good on the windward surfaces, although the experimental data show a consistently more positive peak pressure coefficient (by $\Delta c_p \simeq 0.3$) and a more positive pressure over the unseparated portion of the leeward surfaces (by $\Delta c_p \simeq 0.5$). This discrepancy, which may be in part due to boundary-layer displacement effects and in part due to the large wake region, will be shown to decrease with increasing tangential blowing. As indicated in figure 12, the calculated values of θ_{sep} compare well with the data, although the calculated pressure coefficient $c_p(\theta_{sep})$ in the wake is more negative than the test results by $\Delta c_p \simeq 0.5$, due to the effects discussed above.

Test results on the effect of tangential blowing on pressure distribution with $\theta_e = 0^o$ are shown in figures 13 through 16 for several values of the momentum coefficient C_μ. The indicated values of $\hat{\Gamma}$, which were found by fitting equation (1) to the data outside of the separated region, are $\hat{\Gamma} = 0.06$, 0.29, 0.29, and 0.59 for values of $C_\mu = 0.05$, 0.28, 0.25 and 0.66, respectively. Figures 13 and 14 are for a slot thickness $t/R = 0.0057$, whereas figures 15 and 16 are for a slot thickness $t/R = 0.015$, The pressure distributions in figures 14 and 15 are found to be remarkably similar, although the thickness ratios vary by a factor of nearly 3, thus indicating the validity of C_μ as a correlating parameter for the experimental data.

The data show progressively improved agreement with potential theory as C_μ increases. It is of note that the surface pressure in the jet layer is more negative than the potential theory values outside the jet layer due to

centrifugal force effects, as previously assumed in the theory. The pressure difference across the jet layer $p_1 - p_o$ was given in coefficient form in equation (43) as

$$\tilde{c}_p(\theta) = \left(\frac{R}{t}\right)\left[\frac{p_1 - p_o}{1/2\,\rho\, u_j^2}\right] \simeq 2 \tag{45}$$

where the value 2 corresponds to a jet of constant thickness t and velocity u_j. Equation (45) may be expressed in terms of the usual pressure coefficient c_p as

$$\Delta c_p = \frac{p_1 - p_o}{\frac{1}{2}\rho V_\infty^2} = \left(\frac{u_j}{V_\infty}\right)^2 \left(\frac{t}{R}\right) \tilde{c}_p \simeq 2\, C_\mu \tag{46}$$

The variation of Δc_p with θ may be predicted by the theory, and calculated results for $t/R = 0.01$ are presented in figures 14 through 16 for $\hat{\Gamma} = 0.25$ and 0.59. Although the theory does not predict some of the irregularities in Δc_p observed in the measurements, both theory and test data exceed the value $2C_\mu$ over the major length of attached flow and then drop rapidly to zero just ahead of the separation point. This leads to the additional tendency of the jet to separate as assumed in the analysis.

The region over which Δc_p is assumed to linearly decrease to zero is also shown in the figures. The experimental data in figure 14 show a much more severe adverse pressure gradient and somewhat larger value of θ_{sep_U} than predicted by the theory. This may have been due in part to the narrow slot size ($t/R = 0.0057$) used for the test.

On the other hand, agreement between the theory and test results in figures 15 and 16 is somewhat closer in regard to the pressure distribution ahead of the separation point and in regard to predicted values of θ_{sep_U} and $c_{p_{sep}}$. Additional comparisons between test results and theory are clearly required to evaluate the accuracy of the theoretical model and the effects of such parameters as N, K, Re, etc. on pressure distribution and separation.

The effect of θ_e on pressure distribution and on $\hat{\Gamma}$ for the same value of C_μ is shown in figure 17. Increasing θ_e from 0° to 20° is seen to result in an increase in $\hat{\Gamma}$ from 0.59 to 0.67 at $C_\mu = 0.66$.

In general, increasing θ_e beyond 20° did not result in any increase in circulation or lift at constant C_μ, as will be shown in the following paragraph dealing with the force data.

Force Data

The force data in the form C_ℓ versus C_μ have been plotted in figure 18 for $\theta_e = 0^\circ$ for values of $t/R = 0.0057$, 0.010, and 0.015. The experimental data, which were obtained on a semispan model of exposed aspect ratio equal to 4, were corrected to correspond to two-dimensional values as explained in Appendix B. Using the basic initial conditions, the theoretical value of C_μ for a given $u_m(\theta_e)/V_\infty$ depends on the value of the parameter K, with $K = 0.7$ appearing to give the best fit with the data. Also shown in figure 18 are theoretical results using the alternate initial conditions and shear laws for $t/R = 0.015$ and 0.010. The latter method appears to somewhat underestimate the required C_μ value for the present experimental data.

In addition, figure 18 shows two-dimensional experimental data by Cheeseman and by Jones and Buckingham from reference 1. These data appear to correlate well with the corrected three-dimensional model data obtained from the current test program. All data show a rather abrupt decrease in slope C_ℓ versus C_μ for values of $C_\ell \geq 5$. This result may be due to sonic effects in the jet, since values of total to static pressure equal to 1.8 were required for the largest C_μ values plotted. Current test data for values of the jet pressure ratio exceeding 1.85 gave much lower values of C_ℓ at higher C_μ's, and have not been plotted.

The effect of θ_e on C_ℓ at constant C_μ is shown in figure 19. Although C_ℓ generally increases with increasing θ_e for $\theta_e \leq 20^\circ$, a maximum C_ℓ is reached near $\theta_e \simeq 20^\circ$, and C_ℓ is found to decrease for θ_e somewhat beyond this value. Corresponding theoretical calculations of the effect of θ_e on C_ℓ have as yet not been carried out.

Velocity Profile Data

The wall jet layer calculations have also been compared with velocity profile survey data taken inside a wall jet over a flat surface with an outside flow of adverse pressure gradient (ref. 23). The comparison was made for the test case corresponding to an initial value $u_j/u_1(0) = 1.62$. As indicated in figure 20, the assumed starting profile, which was given by equation (9), did not match the velocity minimum in the outer region of the wall jet. As shown also in figure 20, the predicted decay in u_m was somewhat less than measured, possibly due to the velocity minimum in the starting profile. The more rapid experimental decay in u_m could also account for the larger experimental values of C_μ required for producing a given $\hat{\Gamma}$. This is in accordance with the previous discussion relating

equation (44) wherein it was shown that the higher the decay rate of u_m with θ, the larger the value $\Delta n(\theta)$ and the more likely the Coanda jet to separate.

CONCLUSIONS AND RECOMMENDATIONS

A theory and computer program have been developed for predicting the circulation and lift induced by tangential blowing over a circular cylinder under conditions of turbulent separation. The theory has been evaluated by comparison with test data of pressure distribution, separation position, and induced circulation (or lift) for several values of the ratio of the jet-slot thickness to cylinder radius and jet velocity to free stream velocity. The induced pressure difference across the jet layer due to centrifugal force effects has been included in the theory, and was found to have a pronounced effect on the jet separation.

The predicted value of C_μ required to achieve a given lift coefficient was found to be highly dependent upon the ratio of the maximum velocity u_m in the fully developed jet layer profile just downstream of the exit θ_e to the average jet velocity inside the slot u_j. This ratio was estimated from equation (34) by either of two methods, one of which involved an empirical constant K and was found to give good agreement with pressure and force data with $K = 0.7$. The alternative method, which did not involve any empirical constant, underpredicted the blowing requirements for achieving a given C_L. An improved analytic procedure for determining $u_m(\theta_e)/u_j$ and a more general velocity profile employing a velocity minimum appear necessary in order to obtain improved agreement.

The tendency of the jet layer to separate was also found to be highly dependent upon the maximum velocity u_m in the jet layer at the separation point θ_{sep_U} as indicated by equation (44). Measurements of the initial Coanda jet velocity profile and of the decay in maximum velocity from the jet exit to the separation indicate a somewhat faster decay rate in u_m than predicted by the theory. This faster decay rate may be due to the velocity minimum in the initial jet velocity profile, and if generally true, could explain the lower C_μ values predicted by the theory. Additional velocity profile data are required to verify this effect.

Air Vehicle Corporation
San Diego, California
February 29, 1972

APPENDIX A

TANGENTIAL BLOWING BLC ON AN AIRFOIL

The method developed for estimating the jet momentum coefficient C_μ required to achieve a given nondimensional circulation $\hat{\Gamma}$ on a circular cylinder may be applied, with only minor modification, to tangential blowing over an airfoil with a flap. In the case of an airfoil, the outside pressure distribution may be again assumed given by potential theory after the critical value of C_μ has been reached. Because of the sharp trailing edge, the critical C_μ value is taken as that value of the jet momentum coefficient which moves the jet layer separation point to the trailing edge. Thus, the upper flow is assumed decoupled from that on the lower surface. Curvature effects, which cause an additional pressure rise Δp, are included in the calculation over the rounded flap knee. The corresponding change in the exponent n is again given by equation (44) where R now refers to the radius of the flap knee. The pressure rise Δp is assumed to occur linearly over a distance of five jet layer thicknesses just beyond the end of the flap knee, in much the same manner as assumed at the separation point with the circular cylinder.

Calculations were made for the flapped airfoil of reference 24 with flap deflection angles of 20° and 60°. The corresponding upper surface measured velocity u_1/V_∞ versus normalized distance s/c from the stagnation point are shown in figure 21 along with the locations of the jet exit and flap knee regions. The potential theory velocity distributions were very close to the measured distributions shown in figure 21 at the critical C_μ values of 0.027 and 0.067. The second peak in u_1 near the leading edge with $\delta_f = 60^\circ$ was due to a nose flap deflection in this case. By carrying out calculations with successively increasing amounts of blowing, the variations n versus s/c shown in figures 22 and 23 were obtained. The alternate initial conditions and shear relations were used for the computations. Calculated values of C_μ needed to move the separation point to the trailing edge are seen to be $C_\mu \sim 0.018$ and $C_\mu \sim 0.047$ for $\delta_f = 20^\circ$ and 60°, respectively. A graphical comparison between theory and experiment is given in figure 24, wherein it is again evident that the theory underpredicts the amount of blowing required for attached flow. Results from a previous investigation (ref. 25) on another flapped airfoil are also included in figure 24 for comparison.

APPENDIX B

WIND TUNNEL TEST PROGRAM

A supporting wind-tunnel program was carried out with the aid of the NASA Technical Monitor (Mr. Victor Corsiglia) in the 7 × 10 ft. low speed wind tunnel at the U.S. Army Aeronautical Research Laboratory, Ames Research Center. Purpose of the test program was to provide pressure and force data with tangential blowing to help evaluate the analytical procedures developed herein.

Model Geometry

A semispan model consisting of a circular cylinder mounted vertically in the tunnel and attached to a balance beneath the tunnel floor was tested. The general arrangement was as shown in figure 25, and consisted of an outer cylinder of 6-inch diameter with an inner pipe of 2.5-inch diameter. The height (exposed semispan) of the cylinder above a circular boundary-layer splitter plate was 24.8 in. Compressed air was supplied through the inner pipe and entered the plenum region between the concentric cylinders through a large number of 0.1-in. diameter holes (approximately 300 in number). The holes were drilled through the side of the inner pipe opposite the jet slot (see fig. 25), and were spaced to provide flow uniformity in the plenum region.

The jet exit slot in the outer cylinder was 24-in. long. The jet slot thickness t could be varied from 0.015 in. to 0.045 in. by sliding the slot leading edge circumferentially as shown in figure 25. The slot geometry was contoured so that the jet incidence angle to the surface of the cylinder would not exceed 10° with the largest slot opening.

Total head tubes were mounted at three spanwise stations along the slot to measure the average total pressure at the jet exit and to check total pressure uniformity. Static pressure taps were spaced circumferentially at intervals of approximately 10° around the outer cylinder at a spanwise station of 6 in. (25% of the semispan) from the inboard end of the slot.

Test Procedures and Conditions

Data without blowing were run at nominal q values from 5 psf to 75 psf whereas data with blowing were run at nominal q values of 25 psf and 50 psf. For each slot thickness $t = 0.015$, 0.030, and 0.045 and for a given jet total pressure the slot incidence θ_e was varied from approximately 0° to 30° by rotating the tunnel floor.

Data Reduction and Corrections

Two component (side force and drag) force data were obtained from the mechanical scale system, whereas pressure data were obtained from Scanivalve digital readouts for each run. Only a limited amount of the experimental data has been presented in the present report.

The jet velocity at the exit was found by measuring the ratio of the jet total pressure to the static pressure at the slot exit (25% span location). This procedure was favored over the use of available flow meter data, which together with a knowledge of the slot thickness will yield the average jet velocity over the entire span. The latter approach was not used, because it was judged to be more sensitive to inaccuracies in jet slot thickness and did not give the local jet velocity at the 25% semispan location for correlating with the pressure and force data.

Because of the finite aspect ratio (AR = 8 based on full lift carryover at the splitter plate) a downwash angle ϵ, which increased with increasing C_L, was produced by the trailing vortices. The experimental pressure distribution data plotted in figures 13 through 17 were shifted by the amount

$$\Delta\theta^{\circ} = \epsilon \simeq \frac{1.25\, C_L}{\pi\, AR}\, 57.3$$

for comparison with the theoretical results to correct for this effect.

The average lift coefficient across the cylinder C_L, as measured by the balance, was converted to a two-dimensional lift coefficient C_ℓ at the 25%-semispan station (corresponding to the location of the pressure data), for comparison with the two-dimensional theoretical results. Using the Kutta-Joukowski law

$$C_\ell = \frac{\rho\, V_\infty\, \Gamma\, b}{(1/2\, \rho\, V_\infty^2)\, 2R\, b} = 4\pi\hat{\Gamma}$$

where Γ is the value at the 25%-semispan position. The empirical relation $C_L \simeq 10.5\,\hat{\Gamma}$ was found from the experimental data giving

$$C_\ell \simeq \frac{4\pi}{10.5}\, C_L$$

APPENDIX C

COEFFICIENTS, COANDA JET THEORY

Integration of the tangential momentum equation across each of four strips (see fig. 2) of the jet layer results in a system of quasi linear ordinary differential equations of the form given by equation 10. The coefficients for each strip are as follows:

$$A_1 = -u_1 y_m$$

$$B_1 = \frac{u_m y_m}{(2n+1)(n+1)}$$

$$C_1 = 0$$

$$D_1 = -\frac{n u_m^2}{(2n+1)(n+1)}$$

$$E_1 = u_m^2 y_m \left[\frac{1}{(n+1)^2} - \frac{2}{(2n+1)^2}\right]$$

$$F_1 = \frac{\tau_o}{\rho} - \left(1 + \frac{y_m}{R}\right)\frac{\tau_m}{\rho} - \frac{y_m}{2R}\left(\frac{\tau_m}{\rho} + \frac{\tau_o}{\rho}\right)$$

$$A_2 = (u_m - u_1) L\left(\frac{5}{2} K_1 - 2K_2 - \frac{1}{2}\right) - u_1 K_1 L$$

$$B_2 = (u_m - u_1)\left[\frac{y_m}{2(n+1)} + L\left(2K_2 - \frac{K_1}{2}\right)\right] + u_1 L K_1$$

$$C_2 = (u_m - u_1)^2\left(K_2 - \frac{K_1}{2}\right) + u_1 (u_m - u_1)\left(K_1 - \frac{1}{2}\right)$$

$$D_2 = \frac{(u_m - u_1)}{2(n+1)} u_m$$

$$E_2 = - \frac{(u_m - u_1)\, u_m}{2(n+1)^2}\, y_m$$

$$F_2 = \frac{\tau_m}{\rho}\left(1 + \frac{y_m}{R}\right) - \frac{\tau_{m+L}}{\rho}\left(1 + \frac{y_{m+L}}{R}\right) - \frac{(\tau_m + \tau_L)}{2\rho}\,\frac{L}{R}$$

$$A_3 = 2(u_m - u_1)\, L' \left(1 - \frac{1}{\sqrt{2}}\right) - u_1\, L'$$

$$B_3 = (u_m - u_1)\left(\sqrt{2}\, L' + \frac{y_m}{n+1}\right) + u_1\, L'$$

$$C_3 = (u_m - u_1)\left[\frac{\pi}{4 \ell n\, 2}\right]^{1/2}\left(u_1 + \frac{u_m - u_1}{\sqrt{2}}\right)$$

$$D_3 = \frac{u_m (u_m - u_1)}{n+1}$$

$$E_3 = - \frac{(u_m - u_1)\, u_m\, y_m}{(n+1)^2}$$

$$F_3 = \frac{\tau_m}{\rho}\left(1 + \frac{y_m}{R}\right) - \frac{L}{2R}\left(\frac{\tau_m + 2\,\tau_L}{\rho}\right)$$

$$A_4 = - u_1\, y_m / 2$$

$$B_4 = u_m\, y_m \left[\frac{1 - \left(\frac{1}{2}\right)^{2n+1}}{(2n+1)(n+1)}\right]$$

$$C_4 = 0$$

$$D_4 = - u_m^2\, n \left[\frac{1 - \left(\frac{1}{2}\right)^{2n+1}}{(2n+1)(n+1)}\right]$$

$$E_4 = \frac{u_m^2 y_m}{(n+1)(2n+1)} \left\{ \frac{\left[1 - \left(\frac{1}{2}\right)^{2n+1}\right](2n^2 - 1)}{(2n+1)(n+1)} + \left(\frac{1}{2}\right)^{2n+1} \ell n\, 2 \right\}$$

$$F_4 = \frac{\tau_{m/2} - \tau_m}{\rho} + \frac{y_m}{R}\left(\frac{\tau_{m/2} - 2\tau_m}{2\rho}\right) - \frac{y_m}{4R}\left(\frac{\tau_{m/2} + \tau_m}{\rho}\right)$$

Here, we have used

$$K_1 = \int_0^1 \exp\left(-\ell n\, 2\, \xi^2\right) d\xi = 0.8101$$

$$K_2 = \int_0^1 \xi \exp\left(-2\, \ell n\, 2\, \xi^2\right) d\xi = 0.6805$$

and $$L' = \left[\frac{\pi}{4\, \ell n\, 2}\right]^{1/2} L$$

Numerical values of the integrals K_3 and K_4 used in reference 11 have been obtained and the results incorporated into the coefficients.

Evaluation of the curvature terms in equations (10) results in an expression of the form given by equations (19), where the coefficients are as follows:

$$A_{c_1} = C_{c_1} = F_{c_1} = 0$$

$$B_{c_1} = -\frac{y_m^2 u_m}{2R(n+1)^2}$$

$$D_{c_1} = \frac{y_m u_m^2 n}{2R(n+1)^2}$$

$$E_{c_1} = \frac{3 y_m^2 u_m^2}{4R(n+1)^3}$$

$$A_{c_2} = A_{c_3} = -\frac{L^2}{R}\left[u_1\left(\frac{1}{2} - K_5\right) + (u_m - u_1)\left(\frac{1}{4\ell n 2} - K_6\right)\right]$$

$$B_{c_2} = B_{c_3} = -\frac{L}{R}\left[\frac{u_1 y_m}{n+1} + L u_1 K_5 + \frac{y_m (u_m - u_1) K_1}{n+1} + L K_6 (u_m - u_1)\right]$$

$$C_{c_2} = C_{c_3} = \frac{L}{R}\left[u_1 (u_m - u_1)\left(\frac{1}{4\ell n 2} - K_5\right) + (u_m - u_1)^2 \left(\frac{3}{16\ell n 2} - K_6\right)\right]$$

$$D_{c_2} = D_{c_3} = \frac{L}{R}\left\{\frac{n}{n+1} u_m \left[u_1 + (u_m - u_1) K_1\right] - (u_m - u_1)\left[u_1 + (u_m - u_1) K_1\right]\right.$$

$$\left. + (u_m - u_1)\left[u_1 K_1 + (u_m - u_1) K_2\right]\right\}$$

$$E_{c_2} = E_{c_3} = \frac{L}{R}\frac{u_m y_m}{(n+1)^2}\left[u_1 + K_1 (u_m - u_1)\right]$$

$$F_{c_2} = F_{c_3} = 0$$

$$A_{c_4} = C_{c_4} = F_{c_4} = 0$$

$$B_{c_4} = -\frac{y_m^2 u_m}{R(n+1)^2}\left[\frac{1 - \left(\frac{1}{2}\right)^{2n+2}}{2}\right]$$

$$D_{c_4} = \frac{y_m u_m^2 n}{R(n+1)^2}\left[\frac{1 - \left(\frac{1}{2}\right)^{2n+2}}{2}\right]$$

$$E_{c_4} = \frac{y_m^2 u_m^2}{R(n+1)^2}\left[\frac{1-\left(\frac{1}{2}\right)^{2n+2}}{2}\right]\left[\frac{\frac{3}{2}}{n+1} - \frac{\left(\frac{1}{2}\right)^{2n+2}\ell n\, 2}{1-\left(\frac{1}{2}\right)^{2n+2}}\right]$$

where $K_5 = \int_0^1 \int_0^{\xi} \exp\left(-\xi_1^2 \ell n\, 2\right) d\xi_1\, d\xi = K_1 - \frac{1}{4\,\ell n\, 2}$

and $K_6 = \int_0^1 \exp\left(-\xi^2 \ell n\, 2\right) \int_0^{\xi} \exp\left(-\xi_1^2 \ell n\, 2\right) d\xi_1\, d\xi = \frac{\pi}{8\,\ell n\, 2}\left[\operatorname{erf}\sqrt{\ell n\, 2}\right]^2$

The induced pressure gradient term in equation (10) may be expressed in the form of equations (27), where the coefficients are as follows:

$$A_{p_1} = -y_m\left(\frac{\Delta p_2}{\rho}\right)\left[\frac{0.12\,u_1 + 0.26\,u_m}{0.06\,u_1^2 + 0.26\,u_1 u_m + 0.68\,u_m^2}\right]$$

$$B_{p_1} = -y_m\left\{\frac{(\Delta p_1/\rho)}{2u_m} + (\Delta p_2/\rho)\left[\frac{0.26\,u_1 + 1.36\,u_m}{0.06\,u_1^2 + 0.26\,u_1 u_m + 0.68\,u_m^2}\right] + \frac{(\Delta p_4/\rho)}{u_m}\right\}$$

$$C_{p_1} = -\frac{y_m}{L}\left(\frac{\Delta p_2}{\rho}\right)$$

$$D_{p_1} = -\frac{1}{4}\left(\frac{\Delta p_1}{\rho}\right) - \frac{1}{2}\left(\frac{\Delta p_4}{\rho}\right)$$

$$E_{p_1} = y_m \left\{ \frac{1}{2} \left(\frac{\Delta p_1}{\rho} \right) \left(\ell n\, 2 + \frac{1}{2n+1} \right) + \left(\frac{\Delta p_4}{\rho} \right) \left[\frac{1}{2n+1} - \left(\frac{2^{2n}+1}{2^{2n+1}-1} \right) \ell n\, 2 \right] \right\}$$

$$F_{p_1} = 0$$

$$A_{p_2} = A_{p_3} = -\frac{L}{2} \left(\frac{\Delta p_2}{\rho} \right) \left[\frac{0.12\, u_1 + 0.26\, u_m}{0.06\, u_1^2 + 0.26\, u_1 u_m + 0.68\, u_m^2} \right]$$

$$B_{p_2} = B_{p_3} = -\frac{L}{2} \left(\frac{\Delta p_2}{\rho} \right) \left[\frac{0.26\, u_1 + 1.36\, u_m}{0.06\, u_1^2 + 0.26\, u_1 u_m + 0.68\, u_m^2} \right]$$

$$C_{p_2} = C_{p_3} = -\frac{1}{2} \left(\frac{\Delta p_2}{\rho} \right)$$

$$D_{p_2} = D_{p_3} = E_{p_2} = E_{p_3} = F_{p_2} = F_{p_3} = 0$$

$$A_{p_4} = -\frac{y_m}{2} \left(\frac{\Delta p_2}{\rho} \right) \left[\frac{0.12\, u_1 + 0.26\, u_m}{0.06\, u_1^2 + 0.26\, u_1 u_m + 0.68\, u_m^2} \right]$$

$$B_{p_4} = -\frac{y_m}{2} \left\{ \left(\frac{\Delta p_2}{\rho} \right) \left[\frac{0.26\, u_1 + 1.36\, u_m}{0.06\, u_1^2 + 0.26\, u_1 u_m + 0.68\, u_m^2} \right] + \frac{1}{u_m} \left(\frac{\Delta p_4}{\rho} \right) \right\}$$

$$C_{p_4} = -\frac{y_m}{2L} \left(\frac{\Delta p_2}{\rho} \right)$$

$$D_{p_4} = -\frac{1}{4} \left(\frac{\Delta p_4}{\rho} \right)$$

$$E_{p_4} = \frac{y_m}{2} \left(\frac{\Delta p_4}{\rho} \right) \left[\frac{1}{2n+1} - \frac{\ell n\, 2}{\left(2^{2n+1} - 1 \right)} \right]$$

$$F_{p_4} = 0$$

APPENDIX D

COMPUTER PROGRAMS

Two computer programs entitled TURBUL and COANDA have been developed for calculating the boundary-layer and jet-layer characteristics, respectively. Each program utilizes format-free inlist features, so that initial data may be punched in a specified, but very flexible, manner.

Program TURBUL

Program TURBUL calculates the laminar and turbulent boundary layers on the lower and upper surfaces of the cylinder, and must be used first to supply starting data for Program COANDA. Major subroutines of Program TURBUL are: (i) LAMINAR, (ii) TURBLRU, (iii) TURBLRL, (iv) DY2DX02, and (v) RKLDEQ, and have been listed on pages 46 through 52. Subroutine LAMINAR calculates the laminar boundary-layer characteristics and transition points on both lower and upper surfaces. Subroutines TURBLRU and TURBLRL calculate the turbulent boundary-layer characteristics on the upper and lower surfaces, respectively, up to the separation points, and indicate conditions at the jet exit and the desired upper-surface separation point. Subroutine DY2DX02 solves the two simultaneous differential equations of the turbulent boundary-layer theory, equations (37) and (38), utilizing the Runge-Kutta-Gill method contained in subroutine RKLDEQ.

Recognized symbols and default values for the various input parameters are listed in Table I.

Program COANDA

Program COANDA calculates the jet layer development from the position of the jet exit to either the desired separation point or to the angular position at which $n \geq 1/2$. Major subroutines of Program COANDA are (i) DY4DX09, (ii) RKLDEQ, (iii) NWMATINV, (iv) XYPLOT, (v) RANGE, and (vi) AMPF, and have been listed on pages 53 through 68. Subroutine DY4DX09 solves the four simultaneous jet layer differential equations, equations (10), utilizing the Runge-Kutta-Gill method, subroutine RKLDEQ. Matrix inversion is accomplished by subroutine NWMATINV. The remaining three subroutines are used for plotting purposes.

Recognized symbols and default values for the various input parameters to Program COANDA are listed in Table II.

TABLE I

RECOGNIZED SYMBOLS, PROGRAM TURBUL

Program Symbol	Normal Designation	Default Value	Definition
GAMA	$\hat{\Gamma}$	0	normalized circulation
RVINF	$R\,V_\infty/\nu$	0	free stream Reynolds number Re
RC	$\lvert u_1 \rvert \theta_\ell / \nu$	300	momentum thickness Reynolds number at transition $Re_{\theta *}$
RT2	$\lvert u_1 \rvert \delta^* / \nu_t$	50	effective turbulent Reynolds number
DALM	$\Delta \theta_\ell$	0	laminar step size (deg)
DATB	$\Delta \theta_t$	0	turbulent step size (deg)

TABLE II

RECOGNIZED SYMBOLS, PROGRAM COANDA

Program Symbol	Normal Designation	Default Value	Definition
KCURV	–	3	a control integer which designates the following options
			= 1 , no curvature or induced pressure gradient effects included
			= 2 , assume radius of curvature $\mathcal{R}$ = R (constant)
			= 3 , assume radius of curvature $\mathcal{R}$ = R up to a distance $N(y_m + L)$ ahead of the separation point
			≥ 4 , input error
WR	t/R	0	ratio of exit slot width to cylinder radius
RJ	$R\,u_j/\nu$	Re/V_∞	jet Reynolds number. Needs be given only if $V_\infty = 0$.
RVINF	$R\,V_\infty/\nu$	0	free stream Reynolds number Re
GAMA	$\hat{\Gamma}$	0	normalized circulation
BLYM	$\delta(\theta_e)$	$\dfrac{\delta^*\left(\frac{\delta^*}{\theta^*}+1\right)}{\left(\frac{\delta^*}{\theta^*}-1\right)}$	turbulent boundary layer thickness at jet exit. [Either δ, or δ^* and θ^*, must be given.]

TABLE II (Continued)

BLN	$n(\theta_e)$	$\frac{1}{2}\left(\frac{\delta^*}{\theta^*} - 1\right)$	turbulent boundary layer exponent n at jet exit. [Either n, or δ^* and θ^*, must be given.]
DELTAS	δ^*	$\frac{n\,\delta}{n+1}$	turbulent displacement thickness at jet exit
THETAST	θ^*	$\frac{n\,\delta}{(n+1)\,(2n+1)}$	turbulent momentum thickness at jet exit
SMN	n	0.185	starting value for n, Coanda jet layer
BIGN	N	5	number of jet layer thickness ahead of separation point at which additional tangential pressure gradient is imposed
YMDY1	$y_m / y_m + L$	0.14	ratio of initial jet layer thicknesses
RT1	$[(u_m - u_1)\,L/\nu_t]_{y_m + L}$	50	effective turbulent Reynolds number evaluated at $y = y_m + L$
RT2	$[u_m\,\delta^*/\nu_t]_{y_m/2}$	50	effective turbulent Reynolds number evaluated at $y = y_m/2$
UJDVINF	u_j / V_∞	$1/V_\infty$	velocity ratio to be specified only if VINF is not given
VINF	V_∞ / u_j	1/ UJDVINF	to be specified only if U JDVINF is not given
CUM	K	1	empirical constant used to calculate $u_m(\theta_e)$ from equation (34)

TABLE II (Continued)

THETAO	θ_e	0	jet exit location (deg)
THETASP	θ_{sep}	0	desired separation point (must always be given)
ISTEP	–	–	number of step sizes used in the integration ($1 \leq$ ISTEP ≤ 9)
DANGLE(10)	$\Delta\theta$	–	integration step sizes (degs)
THETAE(10)	–	–	angular positions for changing step sizes

```
      PROGRAM TURBUL
      TYPE REAL N
      DIMENSION Y(2)
      COMMON /AAA/ GAMA,RVINF,RC,RT2
      NAMELIST /INPUT / GAMA,RVINF,DALM,DATB,RC,RT2
      RC=300.
      CALL INLIST(INPUT)
      DEGREE=180./3.1416
      DALM=DALM/DEGREE  $  DATB=DATB/DEGREE
      CALL LAMINAR(STAGN2,-DALM,THETAT,Y)
      CALL TURBLRL(THETAT,STAGN2,DATB,Y,U1)
      X=U1/2.-GAMA
      IF(X)1,2,3
    1 ANGLEND=3.1416-ACOS(X)
      GO TO 4
    2 ANGLEND=1.5708
      GO TO 4
    3 ANGLEND=ACOS(X)
    4 IF(ANGLEND .GT. STAGN2) ANGLEND=STAGN2
      THETASP=ANGLEND*DEGREE
      PRINT 70, THETASP, U1
   70 FORMAT(///10X,'THE EXPECTED WALL JET SEPERATION WILL BE AT THETA='
     *F8.3, ' DEGREES',/20X,'WHERE U1=',F11.3,/1H1)
      IF(GAMA .GT. 0.51) DALM=DALM*GAMA/0.5
      CALL LAMINAR(STAGN2,DALM,THETAT,Y)
      CALL TURBLRU(THETAT,THETASP,DATB,Y)
      END

      SUBROUTINE LAMINAR(STAGN2,DALM,THETAT,Y)
      INPUT ANGLES ARE IN RADIAN
     THE CIRCURATION GAMA=GAMA/(4*3.1416*R*V(INFINITY))
     THE FREE STREAM REYNOLDS NUMBER RV=R*V(INFINITY)/NU
     THE BOUNDARY LAYER REYNOLDS NUMBER RC=U1*THETA*)/NU
     THE LENGTH SCALE=R IS THE RADIUS OF THE CYLINDER
     THE VELOCITY SCALE V(INFINITY) IS THE FREE STREAM VELOCITY
      COMMON /AAA/ GAMA,RV    ,RC,RT2
      DIMENSION Y(2)
      DEGREE=180./3.1416
```

```
      DANGLE=DALM
      STAGN2=3.1416-ACOS(GAMA)   $   STAGN2A=STAGN2*DEGREE
      TRTGAMA=2.*SQRT(1.-GAMA**2)
      A1=GAMA/TRTGAMA   $   A2=-1./6.
      RVGAMA=(RV*TRTGAMA)**(-0.5)
      IF (DANGLE)1,2,2
    1 STAGN1=-STAGN2+6.2832
      PRINT 71
   71 FORMAT(///)
      PRINT 3   $   GO TO 5
    2 STAGN1=-STAGN2   $   PRINT 4
    3 FORMAT(10X,'THE LAMINAR BOUNDARY LAYER ON THE LOWER SURFACE',/)
    4 FORMAT(10X,'THE LAMINAR BOUNDARY LAYER ON THE UPPER SURFACE',/)
    5 STAGN1A=STAGN1*DEGREE
      PRINT 6 ,RV,RC,GAMA,A1,A2,STAGN1A,STAGN2A
    6 FORMAT(10X,'THE FREE STREAM REYNOLDS NUMBER RV=',E11.4,10X,'THE TR
     *ANSITION REYNOLDS NUMBER RC=',E11.4//10X,'THE CIRCULATION GAMA=',
     *F7.4,15X,'THE CONSTANTS A1=',E11.4,3X,'A2=',E11.4//10X,'THE UPSTRE
     *AM STAGNATION POINT THETA(STAG1)=',F10.2,' DEGREES',/10X,'THE DOWN
     *STREAM STAGNATION POINT THETA(STAG2)=',F10.2,' DEGREES',//)
      PRINT 8
    8 FORMAT(5X,'THETA(DEGREE)',' DTHETA(RADIAN)',11X,'U1/V',7X,'DELTA*/
     *R',7X, 'THETA*/R',' U1*(THETA*)/NU',/)
      DT=0.0   $   C1=0.0813*A1   $   C2=0.3398*A1
      C3=0.0713*A1**2-0.0443   $   C4=A1**2+2.*A2
      TA1=2.*A1   $   NDT=0
    9 DT2=DT*DT   $   UDT=1.+A1*DT+A2*DT2
      DELTA=RVGAMA*(0.6479+C1*DT+0.01897*DT2)/UDT
      THETA=RVGAMA*(0.2925+C2*DT+C3*DT2)/(1.+TA1*DT+C4*DT2)
      U1=TRTGAMA*DT*UDT
      R=U1*THETA*RV
      IF(R .LT. 0.) R=-R
```

```
      ANGLE=STAGN1+DT   $  ANGLEC=ANGLE*DEGREE
      PRINT 10,ANGLEC,DT,U1,DELTA,THETA,R
   10 FORMAT(F15.2,3X,5E15.4)
      IF(NDT .EQ. 1) GO TO 23
      IF(R .GE. RC) GO TO 20
      IF((ANGLE-STAGN2)*DALM .GE. 0.) GO TO 21
      R1=R   $   DT=DT+DANGLE   $   GO TO 9
   20 DT=DT-DANGLE*(R-RC)/(R-R1)
      NDT=1   $   GO TO 9
   21 PRINT 22
   22 FORMAT(10X,'THE BOUNDARY LAYER REYNOLDS NUMBER DOES NOT REACH THE
     * TRANSITION REYNOLDS NUMBER  BEFORE THE ANGLE THETA  IS GREATER TH
     *AN THE DOWNSTREAM STAGNATION POINT')
   23 THETAT=ANGLE
      PRINT 24
   24 FORMAT(//10X,'THE DATA AT THE TRANSITION POINT FROM LAMINAR TO TUR
     *BULENT BOUNDARY LAYER',/)
      PRINT 8
      PRINT 10,ANGLEC,DT,U1,DELTA,THETA,R
      Y(2)=0.5*(DELTA/THETA-1.)
      Y(1)=DELTA*(Y(2)+1.)/Y(2)
      PRINT 70,U1,Y
   70 FORMAT(//10X,'THE STARTING VALUES FOR THIS TURBULENT BOUNDARY LAYE
     *R ARE',/15X,'U1=',E11.4,5X,'YM=',E11.4,5X,'N=',E11.4,////10X,
     *10('*****',3X)////)
      RETURN
      END

      SUBROUTINE TURBLRU(UPHI0,UPHIEND,DPHI,Y)
C     INPUT ANGLES ARE IN RADIAN
      DIMENSION Y(2),DY(2)
      COMMON /AAA/ GAMA,RVINF,RC,RT2
      DEGREE=180./3.1416
      PRINT 1
    1 FORMAT(10X,'THE TURBULENCE BOUNDARY LAYER ON THE UPPER SURFACE'//)
     *'//10X,'RV=',E11.3,10X,'GAMA=',F7.4,//)
      PHI=0.0              $  NT=0    $  UPHI=UPHI0+PHI
      U1=2.*(COSF(UPHI)+GAMA)
```

```
      DU1=-2.*SINF(UPHI)
      DDPHI=DPHI/8.
      PHIEND=UPHI0+2.*DPHI-0.00001
      ND=1
      PRINT 4
      GO TO 11
   10 CALL DY2DX02(       Y(1),Y(2),U1,DU1,DY)
  100 S=RKLDEQ(2,Y,DY, PHI,DDPHI,NT)
      IF(S-1.0) 999,8,11
    8 GO TO (9,10,9)NT
    9 UPHI=UPHI0+PHI
      U1=2.*(COSF(UPHI)+GAMA)
      DU1=-2.*SINF(UPHI)
      GO TO 10
   11 CALL DY2DX02(       Y(1),Y(2),U1,DU1,DY)
      UPHI1=UPHI*DEGREF        $  PHI1=PHI*DEGREE




      PRINT 12,  UPHI1,PHI1,Y,U1,DY,DU1
   12 FORMAT(8E14.3)
    4 FORMAT(/3X'PHI(DEGREE)',6X,'PHI-PHI0',12X,'YM',13X,'N',12X,'U1',
     *11X,'DYM',12X,'DN',11X,'DU1'/)
      IF(ND .EQ. 1  .OR.  DU1 .GE.  0.0) GO TO 2
      IF( U1  .LT. 0.0  .OR.  Y(2) .GE. 0.5) GO TO  999
    2 IF(UPHI  .LT.  PHIEND) GO TO 100
      IF(ND .EQ. 2) GO TO 999
      ND=2  $  DDPHI=DPHI
      PHIEND=UPHIEND
      PRINT 70  $  GO TO 100
   70 FORMAT(/15X,8('*****',3X),/)
  999 RETURN
      END
```

```
      SUBROUTINE TURBLRL(LPHI0,LPHIEND,DPHI,Y,U1)
C     INPUT ANGLES ARE IN RADIAN
      TYPE REAL         LPHIEND,LPHI,LPHI0,LPHI1,N1,N2
      DIMENSION Y(2),DY(2)
      COMMON /AAA/ GAMA,RVINF,RC,RT2
      DEGREE=180./3.1416
      PRINT 1
    1 FORMAT(10X,'THE TURBULENCE BOUNDARY LAYER ON THE LOWER SURFACE'//)
      PHI=0.0             $  NT=0    $  LPHI=LPHI0-PHI
      U1=-2.*(COSF(LPHI)+GAMA)
      DU1=-2.*SINF(LPHI)
      PRINT 4
    4 FORMAT(/3X'PHI(DEGREE)',6X,'PHI0-PHI',12X,'YM',13X,'N',11X,'-U1',
     *11X,'DYM',12X,'DN',11X,'-DU1',/)
      DDPHI=DPHI/8.
      PHIEND=LPHI0-2.*DPHI+0.00001
      ND=1
      GO TO 11
   10 CALL DY2DX02(       Y(1),Y(2),U1,DU1,DY)
  100 S=RKLDFQ(2,Y,DY, PHI,DDPHI,NT)
      IF(S-1.0) 999,8,11
    8 GO TO (9,10,9)NT
    9 LPHI=LPHI0-PHI
      U1=-2.*(COSF(LPHI)+GAMA)
      DU1=-2.*SINF(LPHI)
      GO TO 10
   11 CALL DY2DX02(       Y(1),Y(2),U1,DU1,DY)
      LPHI1=LPHI*DEGREE      $  PHI1=PHI*DEGREE
      PRINT 12,  LPHI1,PHI1,Y,U1 ,DY,DU1
   12 FORMAT(8E14.3)
      IF(ND .EQ. 1  .OR.  DU1 .GE.  0.0) GO TO 2
      IF(U1 .LE. 0.0) GO TO 20
      IF(Y(2)-0.5) 3,20,5
    3 U11=U1   $  N1=Y(2)
    2 IF(LPHI  .GT.  PHIEND)GO TO 100
      IF(ND .EQ. 2) GO TO 20
      ND=2   $  DDPHI=DPHI
      PHIEND=LPHIEND
      PRINT 70  $  GO TO 100
```

```
   70 FORMAT(/15X,8('*****',3X),/)
    5 U12=U1   $  N2=Y(2)
      B=(N2-0.5)/(N2-N1)
      U1=U12-B*(U12-U11)
      PHI1=PHI1-DPHI*DEGREE*B
      LPHI1=LPHI0*DEGREE-PHI1
   20 PRINT 71, LPHI1,  PHI1, U1
   71 FORMAT(///10X,'THE LOWER TURBULENT FLOW SEPERATES AT',/10X,
     *'PHI=',F9.3,' DEGREES',6X,'PHI0-PHI=',F9.3,' DEGREES',6X,'WHERE -U
     *1=',F11.3,)
  999 RETURN
      END

      SUBROUTINE DY2DX02(   YM,N,U1,DU1,DY)
C    THE DIMENSIONLESS VELOCITY AND LENGTH ARE PROPERLY NORMALIZED BY THE
C      CHARACTERISTIC VELOCITY AND LENGTHE SCALES.  E.G. V(INFINITY), RADIUS OF
C      CYLINDER(R).
      COMMON /AAA/ GAMA,RV   ,RC,RT2
      TYPE REAL N,NP1, K ,N2
      DIMENSION DY(2)
      DATA K,RT2/0.6931,50./
      NP1=1./(N+1.)   $  TNP1=1./(2.*N+1.)
      SNP1=NP1**2   $  STNP1=TNP1**2
      TN2=NP1*TNP1   $  U12=U1**2
      N2=N*N   $  U12N=U12*N   $  U1YM=U1*YM   $  U12YM=U12*YM
      U1YMDU1=U1YM*DU1
      T0=0.01285*U12*(RV*U1YM)**(-0.16666667)*(N*TN2)**((11.*N-1.)*
     *0.16666667)
      T2=U12*N2*NP1/(2.**(N-1.)*RT2)
      W=(1.-0.5**(1./TNP1))*TN2
      D1=-U12N*TN2   $  E1=U12YM*(SNP1-2.*STNP1)
      D4=-U12N*W   $  E4=U12YM*(W*(2.*N2-1.)*TN2+K*(TN2-W))
      G1=-T0+U1YMDU1*(1.-TN2)
      G4=-T2+U1YMDU1*(0.5-W)
      DETERM=D1*E4-D4*E1
      DY(1)=(G1*E4-G4*E1)/DETERM
      DY(2)=(D1*G4-D4*G1)/DETERM
      RETURN
      END
```

```
      FUNCTION RKLDEQ(N,Y,F,X,H,NT)
C     D2 UCSD RKLDEQ        F 63
      DIMENSION  Y(10),F(10),Q(10)
      NT=NT+1
      GO TO (1,2,3,4),NT
    1 DO 11 J=1,N
   11 Q(J)=0.
      A=0.5
      X=X+0.5*H
      GO TO 5
    2 A=0.29289321881
      GO TO 5
    3 A=1.7071067812
      X=X+0.5*H
      GO TO 5
    4 DO 41 I=1,N
   41 Y(I)=Y(I)+H*F(I)/6.-Q(I)/3.
      NT=0
      RKLDEQ=2.
      GO TO 6
    5 DO 51 L=1,N
      Y(L)=Y(L)+A*(H*F(L)-Q(L))
   51 Q(L)=2.*A*H*F(L)+(1.-3.*A)*Q(L)
      RKLDEQ=1.
    6 CONTINUE
      RETURN
      END
$EXECUTE,A=UTILITY

  GAMA=0.25,  RVINF=5.0E5,  DALM=5.0,  DATB=4.0  END
```

```
      PROGRAM COANDA
      COMMON /1/ PRES1(6),PRES2(6),PRES4(6),CURVA1(5),CURVA2(5),
     *CURVA4(5) ,   B1,B2,B3,B4,A1DU1,A2DU1,A3DU1,A4DU1
      COMMON / CONST / KCURV, RJ    ,RT1,RT2
      COMMON / DPRESS / PPM2,PM2M,PMLO
      COMMON / YDY / Y(5),DY(5)
      TYPE REAL L0,N
      DIMENSION X(500),UM(500),YM(500),L0(500),N(500),Y1(500),U1(500),
     *DANGLE(10),THETAE(10)
      NAMELIST / DATA1/ KCURV, WR, RJ,RVINF,GAMA   ,BLYM,BLN,DELTAS,
     *THETAST,SMN,BIGN,YMDY1 ,RT1,RT2,UJDVINF,VINF  ,CUM
      NAMELIST / DATA2/ THETA0,THETASP,ISTEP,DANGLE,THETAE
      VINF=-100.
      RT1=RT2=50.
      KCURV=3
      BIGN=5.
      YMDY1=0.14
      SMN=0.185
      CUM=1.
      CALL INLIST (DATA1)
      CALL INLIST (DATA2)
      PRINT 71
   71 FORMAT(///)
      WP0=WR
      IF( ABSF(VINF) .LE. 1.E-5) 1,3
    1 U1(1)=Y(5)=DY(5)=0.0
      MVINF=1  $  PRINT 72
   72 FORMAT(15X'****  FOR THE STATIC CASE  *****'//)
      GO TO 38
    3 IF(UJDVINF .LE. 0. ) 36,37
   36 UJDVINF=1./VINF
      GO TO 4
   37 IF( VINF .LE. -10.)VINF=1./UJDVINF
    4 V=VINF
      MVINF=2
   38 GO TO (49,50,51,998) KCURV
  998 PRINT 80  $  GO TO 999
   80 FORMAT(///10X,'*****  THE ERROR INPUT IN THE CONSTANT KCURV ****')
```

```
   49 PRINT 52        $      GO TO 56
   52 FORMAT(10X,'KCURV=1,  THIS IS FOR A CYLINDER WITHOUT CONSIDER THE
     *CURVATURE EFFECTS'//)
   50 PRINT 53              $       GO TO 56
   53 FORMAT(10X'KCURV=2,  THIS IS FOR A CYLINDER WITH CONSTANT CURVATUR
     *E  R=1'//)
   51 PRINT 54
   54 FORMAT(10X,'KCURV=3,  THIS IS FOR A CYLINDER WITH CURVATURES'//)
   56 TWR0=2./WR0
      IF( RVINF  .GT. 10.)  RJ=RVINF/V
      DEGREE=180./3.1416
      THETA01=THETA0
      THETAS1=THETASP
      N(1)=SMN
      THETA0=THETA01/DEGREE
      THETAS=THETAS1/DEGREE
      ISTEP=ISTEP+1
      DO 63 IS=2,ISTEP
      DANGLE(ISTEP+2-IS)=DANGLE(ISTEP+1-IS)/DEGREE
   63 THETAF(ISTEP+2-IS)=THETAF(ISTEP+1-IS)/DEGREE
      DANGLE(1)=0.2*DANGLE(2)
      THETAF(1)=THETA0+10.*DANGLE(1)-0.0001
      THETA=THETA0
      GO TO (32,33) MVINF
   33 TV=2.*V
      Y(5)=U1(1)=TV*(COSF(THETA)+GAMA)
      DY(5)=-TV*SINF(THETA)
      CMU=WR0/V*SQRT(1-(U1(1)/V)**2+(1.-2.*WR0)/(V*V))
      PRINT 73, RVINF, GAMA, V,UJDVINF,CMU
   73 FORMAT(10X,'THE FREE STREAM REYNOLDS NUMBER RVINF=VINF*R0/NU=',
     *E11.4/ 10X,'THE CIRCULATION GAMA=',E11.4/ 10X,'THE FREE STREAM VEL
     *OCITY VINF/UJ=', E11.4,15X,'UJ/VINF=',E11.4/10X, 'THE JET MOMENTUM
     * CMU=', E11.4//)
   32 PRINT  79, RJ,WR0, THETA01, BIGN
   79 FORMAT(10X,'THE WALL JET REYNOLDS NUMBER RJ=UJ*R0/NU=',F11.4, //
     *10X,'RATIO OF SLOT WIDTH TO RADIUS OF CYLINDER W/R=',E11.4 //
     *,10X,'JET STARTS AT THETA=',F7.2,' DEGREES',
     *                              //10X,'IMPOSED INDUCED PRESSURE GRAD
```

```
     *IENT EFFECTS START AT YM+LO .GE. (THETAS(SEP)-THETA)/BIGN',/
     *15X,'WHERE BIGN=',E11.4,///)
      IF(BLYM*BLN .LT. 1.E-20) 47,48
   48 DELTAS=BLYM*BLN/(BLN+1.)
      THETAST=DELTAS/(2.*BLN+1.)
      GO TO 44
   47 BLN=0.5*(DELTAS/THETAST-1.)
      BLYM=DELTAS*(BLN+1.)/BLN
   44 PRINT 77, BLYM, BLN
      PRINT 78, U1(1), DELTAS, THETAST
   77 FORMAT(10X,'THE BOUNDARY LAYER PARAMETERS',/15X,'YM=',E11.4,10X
     *,'N=',E11.4,//)
   78 FORMAT(10X,'U1=',E11.4,10X,'DELTA(STAR)=',E11.4,10X,'THETA(STAR)='
     *,E11.4,///)
      UM(1)=SQRTF(WR0/BLYM)*CUM
      IF(UM(1)  .GT. 1.) UM(1)=1.
      C0=YMDY1/(1.-YMDY1)
      C1=SQRTF(3.1416/4./ALOG(2.))
      C3=(1.-U1(1))*WR0-THETAST*U1(1)**2
      C6=C0/(2.*N(1)+1.)+C1/SQRTF(2.)
      C6=C6*UM(1)**2
      C7=(-C0/(N(1)+1.)+C1*(1.-SQRTF(2.)))*U1(1)
      C7=C7*UM(1)
      C8=-C1*U1(1)**2*(1.-1./SQRTF(2.))
      L0(1)=C3/(C6+C7+C8)
      YM(1)=C0*L0(1)
      PHIS1=THETAS1-THETA01
      PRINT 75, THETAS1, PHIS1
   75 FORMAT(/10X,'THE EXPECTED SEPERATION AT  THETA=',F8.3,' DEGREES',
     *10X,'PHI=',F8.3,' DEGREES',///)
      NSTEP=0
      Y1(1)=L0(1)+YM(1)
      I=1   $  NT=0      $   NN=1
      Y(1)=UM(1)  $  Y(2)=L0(1)  $  Y(3)=YM(1)  $  Y(4)=N(1)
   31 NSTEP=NSTEP+1
      DA=DANGLE(NSTEP)
      THET=THETAE(NSTEP)
      IF ( THET   .GT. THETAS ) THET  =THETAS
```

```
      GO TO 5
   40 IF( KCURV .EQ. 4 ) 60,61
   60 PRES1(6)=DPDX1*Y(3)
      PRES2(6)=DPDX2*Y(2)
      PRES4(6)=DPDX4*Y(3)
   61 CALL DY4DX09
  100 S=RKLDEQ( 4    ,Y,DY,THETA,DA     ,NT)
      IF(Y(1) .LE. 0. .OR. Y(2) .LE. 0..OR. Y(3) .LE. 0.
     * .OR. Y(4) .LE. 0.) GO TO 26
      IF(S-1.0)999, 8,11
   26  PRINT 27 , Y          $  GO TO 20
   27 FORMAT(10X, 'TERMINATED THIS LOOP BECAUSE NEGATIVE VALUE OF UM, YM
     * , N OR L0'/ 10X,'UM=',F11.4, 5X,'L0=',E11.4,5X,'YM=',F11.4, 5X,
     *' N=',E11.4, 5X,'U1=',E11.4)
    8 GO TO (40,35) MVINF
   35 GO TO (9,40,9) NT
    9 Y(5)=TV*(COSF(THETA)+GAMA)
      DY(5)=-TV*SINF(THETA)
      GO TO 40
   11 I=I+1
      UM(I)=Y(1)   $  L0(I)=Y(2)   $  YM(I)=Y(3)   $  N(I)=Y(4)
      U1(I)=Y(5)   $  Y1(I)=Y(2)+Y(3)
    5 X(I)=THETA
      IF ( KCURV .EQ. 4) 62,64
   62 PRES1(6)=DPDX1*Y(3)
      PRES2(6)=DPDX2*Y(2)
      PRES4(6)=DPDX4*Y(3)
   64 CALL DY4DX09
      THETA1=THETA*DEGREE
      PHI1=THETA1-THETA01
      PRINT 12,I    ,PHI1,THETA1
   12 FORMAT(/2X'INTEGRATING POSITION I=',I4,                10X,'PHI=',
     *F8.3,' DEGREES',10X,'THETA=',F8.3,' DEGREES',/)
      GO TO (6,45,45,46) KCURV
   46 PRINT 74, PRES1(6),PRES2(6),PRES4(6)
   74 FORMAT(9X,'THE IMPOSED INDUCED PRESSURE GRADIENT EFFECTS ARE'/
     *10X,'FP1=',F11.4,12X,'FP2=FP3=',E11.4, 8X,'FP4=',F11.4/)
      GO TO 25
```

```
   45 P1=P2=P4=0.
      C1=C2=C4=0.0
      DO 30 K=1,5
      P1=P1+PRES1(K)*DY(K)
      P2=P2+PRES2(K)*DY(K)
      P4=P4+PRES4(K)*DY(K)
      C1=C1+CURVA1(K)*DY(K)
      C2=C2+CURVA2(K)*DY(K)
   30 C4=C4+CURVA4(K)*DY(K)
      PRINT  23, P1,P2,P4
   23 FORMAT ( 9X,'THE PRESSURE GRADIENT EFFECTS'/10X,'P1=',E11.4,13X,
     *'P2=P3=', E11.4,10X,'P4=',E11.4/)
      PRINT 24, C1,C2,C4
   24 FORMAT( 9X'THE CURVATURE EFFECTS'/10X,'C1=',E11.4,13X,'C2=C3=',
     *,E11.4,10X,'C4=',E11.4/)
      DPM=PML0*TWR0
      DPM2=DPM+PM2M*TWR0
      DP0=DPM2+P0M2*TWR0
      PRINT 21, DPM,DPM2,DP0
   21 FORMAT( 9X,'THE PRESSURE DIFFERENCES ARE',/
     *       ,10X,'DPM=',E11.4,12X,'DPM2=',E11.4,11X,'DP0=',E11.4,/)
   25 B1DUM=B1*DY(1)
      B2DUM=B2*DY(1)
      B3DUM=B3*DY(1)
      B4DUM=B4*DY(1)
      PRINT 22,B1DUM,B2DUM,B3DUM,B4DUM
   22 FORMAT (9X,'THE MAIN BDUDX TERMS'/10X,'B1DUM=' E11.4,10X,'B2DUM=',
     *E11.4,10X,'B3DUM=',E11.4,10X,'B4DUM=',E11.4,)
      PRINT 76, A1DU1,A2DU1,A3DU1,A4DU1
   76 FORMAT(10X,'A1DU1=',E11.4,10X,'A2DU1=',E11.4,10X,'A3DU1=',E11.4,
     *10X,'A4DU1=',E11.4,/)
    6 PRINT 34, DY
   34 FORMAT (9X,'DUM=',F11.4,2X,'DL0=',F11.4,2X,'DYM=',F11.4,2X,
     *' DN=',E11.4,2X,'DU1=',E11.4)
      PRINT 7, Y,Y1(I)
    7 FORMAT(9X,'UM=',F11.4,3X,'L0=',E11.4,3X,'YM=',E11.4,3X,' N=',
     *E11.4,3X,'U1=',E11.4,3X,'Y1=',F11.4//)
      IF(KCURV .NE. 3) GO TO 65
```

```
      IF(Y1(I)*BIGN  .LT. THETAS-THETA) GO TO 65
      KCURV=4
      DX=1./(THETAS-THETA)
         DPDX1=(PML0+0.75*PM2M+0.25*P0M2)*DX
         DPDX2=0.5*PML0*DX
         DPDX4=(PML0+0.5*PM2M)*DX
      PRINT 70, DPDX1, DPDX2, DPDX4      $  DPDX4=0.5*DPDX4
   70 FORMAT(/9X,11('*****',3X),/
     *         9X,'BEYOND THIS POINT THE CONSTANT IMPOSED PRESSURE GRADIE
     *NT EFFECTS ARE',/10X,'DPDX1=',E11.4,10X,'DPDX2=DPDX3=',E11.4,
     *10X,'DPDX4=',E11.4,/9X,11('*****',3X),///)
   65 GO TO (200,201) NN
  200 IF( N(I) .GT. 0.3) 202, 203
  202 NN=2     $  DA=0.5*DA
  201 IF (N(I) .GT. 0.55 ) GO TO 20
  203 IF(THETA-THET  )100,13,13
   13 IF(NSTEP .LT.  ISTEP)  31, 20
   20 DO 19 K=1,I
   19 X(K)=X(K)*DEGREE
      CALL XYPLOT(X,UM,1,I,50,X(I),X(1),0.0,0.0)
      PRINT 14
      CALL XYPLOT(X,L0,1,I,50,X(I),X(1),0.0,0.0)
      PRINT 15
      CALL XYPLOT(X,YM,1,I,50,X(I),X(1),0.0,0.0)
      PRINT 16
      CALL XYPLOT(X, N,1,I,50,X(I),X(1),0.0,0.0)
      PRINT 17
      IF(V .LE. 0.00001) GO TO 999
      CALL XYPLOT(X,U1,1,I,50,X(I),X(1),0.0,0.0)
      PRINT 18
   14 FORMAT (10X,'UM .VS. THETA(DEGREES)')
   15 FORMAT (10X,'L0 .VS. THETA(DEGREES)')
   16 FORMAT (10X,'YM .VS. THETA(DEGREES)')
   17 FORMAT (10X,' N .VS. THETA(DEGREES)')
   18 FORMAT (10X,'U1 .VS. THETA(DEGREES)')
  999 END
```

```
      SUBROUTINE NWMATINV(A,B,INDEX,NMAX,N,M,DETERM)                    NWMV   1
      DIMENSION A(NMAX,1),B(NMAX,1),INDEX(1)                            NWMV   2
      EQUIVALENCE(IROW,JROW,IR),(ICOLUM,JCOLUM,IC)                      NWMV   3
      EQUIVALENCE(AMAX,T,SWAP,IAMAX),(PIVOT,TEMP,ITEMP)                 NWMV   4
      DATA (MINUS=600000000000000B)                                     NWMV   5
C**   INITIALIZATION.
      DETERM=1.0                                                        NWMV   6
      DO 20 J=1,N                                                       NWMV   7
   20 INDEX(J)=MINUS                                                    NWMV   8
      DO 550 I=1,N                                                      NWMV   9
C**   SEARCH FOR ELEMENT OF LARGEST MAGNITUDE.
      AMAX=0.0                                                          NWMV  10
      DO 105 J1=1,N                                                     NWMV  11
      IF(-INDEX(J1)) 105,105,60                                         NWMV  12
   60 DO 100 K1=1,N                                                     NWMV  13
      IF(-INDEX(K1)) 100,100,80                                         NWMV  14
   80 TEMP=A(K1,J1)                                                     NWMV  15
      IF(TEMP)83,100,82                                                 NWMV  16
   82 TEMP=-TEMP                                                        NWMV  17
   83 IF(-ITEMP-IAMAX) 100,100,84                                       NWMV  18
   84 AMAX=-TEMP                                                        NWMV  19
      IR=K1                                                             NWMV  20
      IC=J1                                                             NWMV  21
  100 CONTINUE                                                          NWMV  22
  105 CONTINUE                                                          NWMV  23
      IF(AMAX)120,115                                                   NWMV  24
  115 DETERM=0                                                          NWMV  25
      RETURN                                                            NWMV  26
  120 IROW=IR                                                           NWMV  27
      ICOLUM=IC                                                         NWMV  28
      INDEX(ICOLUM)=INDEX(ICOLUM).AND..NOT.MINUS                        NWMV  29
      IF(.NOT.(IROW-ICOLUM))260,140                                     NWMV  30
  140 DETERM=-DETERM                                                    NWMV  31
C**   EXCHANGE ROWS.
      DO 200 L=1,N                                                      NWMV  32
      SWAP=A(IROW,L)                                                    NWMV  33
      A(IROW,L)=A(ICOLUM,L)                                             NWMV  34
  200 A(ICOLUM,L)=SWAP                                                  NWMV  35
      IF(.NOT.M)260,210                                                 NWMV  36
```

```
  210 DO 250 L=1, M                                                    NWMV  37
      SWAP=B(IROW,L)                                                   NWMV  38
      B(IROW,L)=B(ICOLUM,L)                                            NWMV  39
  250 B(ICOLUM,L)=SWAP                                                 NWMV  40
C**   SAVE PIVOT INFORMATION, DO DETERMINANT,
  260 INDEX(I)=IROW*100000000B+ICOLUM+INDEX(I)                         NWMV  41
      PIVOT   =A(ICOLUM,ICOLUM)                                        NWMV  42
      DETERM=DETERM*PIVOT                                              NWMV  43
C**   REDUCE LEADING COEF TO 1,
      A(ICOLUM,ICOLUM)=1.0                                             NWMV  44
      DO 350 L=1,N                                                     NWMV  45
  350 A(ICOLUM,L)=A(ICOLUM,L)/PIVOT                                    NWMV  46
      IF(,NOT,M)380,360                                                NWMV  47
  360 DO 370 L=1,M                                                     NWMV  48
  370 B(ICOLUM,L)=B(ICOLUM,L)/PIVOT                                    NWMV  49
C**   SUBSTITUTE FOR NTH VARIABLE,
  380 DO 550 L1=1,N                                                    NWMV  50
      IF(,NOT,(L1-ICOLUM)) 550,400                                     NWMV  51
  400 T=A(L1,ICOLUM)                                                   NWMV  52
      A(L1,ICOLUM)=0.0                                                 NWMV  53
      DO 450 L=1,N                                                     NWMV  54
  450 A(L1,L)=A(L1,L)-A(ICOLUM,L)*T                                    NWMV  55
      IF(,NOT,M)550,460                                                NWMV  56
  460 DO 500 L=1,M                                                     NWMV  57
  500 B(L1,L)=B(L1,L)-B(ICOLUM,L)*T                                    NWMV  58
  550 CONTINUE                                                         NWMV  59
C**   UNDO ROW EXCHANGES,
      L=N                                                              NWMV  60
      DO 710 L2=1,N                                                    NWMV  61
      JROW=INDEX(L)/100000000B                                         NWMV  62
      JROW=JROW.AND,77777B                                             NWMV  63
      JCOLUM=INDEX(L).AND,77777B                                       NWMV  64
      IF(,NOT,(JROW-JCOLUM))710,630                                    NWMV  65
  630 DO 705 K=1,N                                                     NWMV  66
      SWAP=A(K,JROW)                                                   NWMV  67
      A(K,JROW)=A(K,JCOLUM)                                            NWMV  68
  705 A(K,JCOLUM)=SWAP                                                 NWMV  69
  710 L=L-1                                                            NWMV  70
  740 RETURN                                                           NWMV  71
      END                                                              NWMV  72
```

```
      SUBROUTINE DY4DX09
      COMMON / CONST / KCURV, RJ    ,RT1,RT2
      COMMON / YDY / UM, L0, YM, N, U1, DY(5)
      COMMON / DPRESS / P0M2,PM2M,PML0
      COMMON /1/ BP1,CP1,DP1,EP1,AP1,FP1,BP2,CP2,DP2,EP2,AP2,FP2,
     *BP4,CP4,DP4,EP4,AP4,FP4,  BC1,CC1,DC1,EC1,AC1, BC2,CC2,DC2,FC2,AC2
     *, BC4,CC4,DC4,EC4,AC4,     B1,B2,B3,B4
     *,A1DU1,A2DU1,A3DU1,A4DU1
      DIMENSION              A(5,5),B(5,5),INDEX(5)
      TYPE REAL L0,N,K,K1,K2,K3,K4,NP1,N2,K5,K6
      DATA K,K1,K2,K3,K4/0.6931,0.8101,0.6805,1.0645,0.7526/,CK1,CK2,CK3
     * , CK4, CK5,TK4/0.95595,0.3101,0.27545,0.16425,0.6238,1.5052/
     *,K5,K6,CK6,CK7,CK8,CK9,CK10/0.4485,0.3264,0.0515,0.0351,0.1221,
     *0.0870,0.0554/
      NP1=1./(N+1.)   $   TNP1=1./(2.*N+1.)
      SNP1=NP1**2   $   STNP1=TNP1**2
      TN2=NP1*TNP1   $   UM2=UM**2
      U0=UM-U1   $   U02=U0**2
      N2=N*N   $   UM2N=UM2*N     $   UYM=UM*YM     $   UM2YM=UM2*YM
      U1L0=U1*L0   $    U0L0=U0*L0   $   U0YMNP1=U0*YM*NP1   $   U1U0=U1*U0
      U1UM=U1*UM   $   U12=U1**2    $   YMU1=YM*U1

      CN1=0.5**(1./TNP1)
      T0=0.01285*UM2*(RJ*UYM  )**(-0.16666667)*(N*TN2)**((1.*N-1.)
     **0.16666667)
      T1=-K*U02/RT1
      TM=T1*(0.15+0.30*(YM/L0)**2)
      T2=UM2*N2  *NP1/(2**(N-1.)*RT2)
      W=(1.-CN1)*TN2
      A1DU1=-YMU1*DY(5)
      A2DU1=(U0L0*CK4-U1L0*K1)*DY(5)
      A3DU1=(U0L0*CK5-U1L0*K3)*DY(5)
      A4DU1=0.5*A1DU1
      B1=UYM*TN2
      B2=K1*U1L0+CK1*U0L0+0.5*U0YMNP1
      B3=K3*U1L0+TK4*U0L0+U0YMNP1
      B4= JYM*W
      A(1,1)=B1                    $   A(1,2)=0.0
```

```
      AP4=0.5*AP1
      BP4=-0.5*(YCU32+YMPM2M/UM)
      CP4=0.5*CP1
      DP4=-0.25*PM2M
      EP4=0.5*YCNTN
      CP2=-0.5*PML0
      PML0L0=CP2*L0
      AP2=PML0L0*CU1/CU2
      BP2=PML0L0*CU3/CU2
      A(1,1)=A(1,1)+BP1
      A(1,2)=A(1,2)+CP1
      A(1,3)=A(1,3)+DP1
      A(1,4)=A(1,4)+EP1
      A(4,1)=A(4,1)+BP4
      A(4,2)=A(4,2)+CP4
      A(4,3)=A(4,3)+DP4
      A(4,4)=A(4,4)+EP4
      A(3,1)=A(3,1)+BP2
      A(3,2)=A(3,2)+CP2
      A(2,1)=A(2,1)+BP2
      A(2,2)=A(2,2)+CP2
      B(1,1)=B(1,1)     -AP1*DY(5)
      FPDU12=-AP2*DY(5)
      B(2,1)=B(2,1)+FPDU12
      B(3,1)=B(3,1)+FPDU12
      B(4,1)=B(4,1)     -AP4*DY(5)
    3 CUX=UM2YM*SNP1
      CU5=CUX*YM   *(0.5-0.25*CN1)
      CU4=CUX*YM   *0.25*CN1
      BC4=-CU5/UM
      DC4=CU5*N/YM
      EC4=CU5*(1.5*NP1-K/(2./CN1-1.))
      BC1=-CU4/UM+BC4
      DC1=CU4*N/YM+DC4
      EC1=CU4*(1.5*NP1+K)+EC4
      AC2= -L0    *(CK6*U1L0+CK7*U0L0)
      BC2= -L0    *(YM*NP1*(U1+U0*K1)+K5*U1L0+K6*U0L0)
      CC2= -L0    *(CK9*U1U0+CK10*U02)
```

```
      A(1,3)=-UM2N*TN2
      A(1,4)=UM2YM *(SNP1-2.*STNP1)
      A(4,1)=B4                    $     A(4,2)=0.0
      A(4,3)=-UM2N*W
      A(4,4)=UM2YM*(W*(2.*N2-1.)*TN2+K*(TN2-W))
      A(3,1)=B3
      A(3,2)=K3*U1U0+K4*U02
      A(3,3)=U0*UM*NP1
      A(3,4)=-A(3,3)*YM*NP1
      A(2,1)=B2
      A(2,2)=CK2*U1U0+CK3*U02
      A(2,3)=0.5*A(3,3)
      A(2,4)=0.5*A(3,4)
      B(1,1)=TM-T0-A1DU1
      B(2,1)=T1-TM-A2DU1
      B(3,1)=-TM-A3DU1
      B(4,1)=TM-T2-A4DU1
      GO TO (10,2,2,4)KCURV
    4 B(1,1)=B(1,1)-FP1
      B(2,1)=B(2,1)-FP2
      B(3,1)=B(3,1)-FP2
      B(4,1)=B(4,1)-FP4
      GO TO 3
   10 IF(KCURV .EQ. 1) 1,9
    2 CU1=0.12*U1+0.26*UM
      CU2=0.06*U12+0.26*U1UM+K2*UM2
      CU3=0.26*U1+1.36*UM
      PML0=L0      *CU2
      PM2M=UM2YM       *(1.-CN1)*TNP1
      P0M2=UM2YM       *CN1*TNP1
      YMPML0=YM*PML0   $   YMPM2M=YM*PM2M   $   YMP0M2=YM*P0M2
      YCU32=YMPML0*CU3/CU2
      AP1=-YMPML0*CU1/CU2
      BP1=-YCU32-(1.5*YMPM2M+0.5*YMP0M2)/UM
      CP1=-YMPML0/L0
      DP1=-0.75*PM2M-0.25*P0M2
      YCNTN=YMPM2M*(TNP1-K/(1./CN1-1.))
      EP1=1.5*YCNTN+0.5*(K+TNP1)*YMP0M2
```

```
      U1K1U0=U1+K1*U0
      DC2= L0    *(U1K1U0*(U1-NP1*UM)+U1U0*K1+K2*U02)
      EC2= L0    *UYM*SNP1*U1K1U0
      A(1,1)=A(1,1)     +BC1
      A(1,3)=A(1,3)     +DC1
      A(1,4)=A(1,4)     +EC1
      A(4,1)=A(4,1)     +BC4
      A(4,3)=A(4,3)     +DC4
      A(4,4)=A(4,4)     +EC4
      A(3,1)=A(3,1)     +BC2
      A(3,2)=A(3,2)     +CC2
      A(3,3)=A(3,3)+DC2
      A(3,4)=A(3,4)+EC2
      A(2,1)=A(2,1)     +BC2
      A(2,2)=A(2,2)     +CC2
      A(2,3)=A(2,3)+DC2
      A(2,4)=A(2,4)+EC2
      FPDU12=-AC2*DY(5)
      B(2,1)=B(2,1)+FPDU12
      B(3,1)=B(3,1)+FPDU12
    1 B(1,1)=B(1,1)+YM*(0.5*T0+1.5*TM)
      B(2,1)=B(2,1)-YM*(TM-T1)+L0*(0.5*TM+1.5*T1)
      B(3,1)=B(3,1)-YM*TM+L0*(0.5*TM+T1)
      B(4,1)=B(4,1)-YM*(0.25*T2-1.25*TM)
    9 CALL NWMATINV(A,B,INDEX,5,   4,1,DETERM)
      DO 11 II=1,4
   11 DY(II)=B(II,1)
      RETURN
      END
```

```
      FUNCTION RKLDEQ(N,Y,F,X,H,NT)
      D2 UCSD RKLDEQ        F 63

      DIMENSION  Y(10),F(10),Q(10)
      NT=NT+1
      GO TO (1,2,3,4),NT
    1 DO 11 J=1,N
   11 Q(J)=0.
      A=0.5
      X=X+0.5*H
      GO TO 5
    2 A=0.29289321881
      GO TO 5
    3 A=1.7071067812
      X=X+0.5*H
      GO TO 5
    4 DO 41 I=1,N
   41 Y(I)=Y(I)+H*F(I)/6.-Q(I)/3.
      NT=0
      RKLDEQ=2.
      GO TO 6
    5 DO 51 L=1,N
      Y(L)=Y(L)+A*(H*F(L)-Q(L))
   51 Q(L)=2.*A*H*F(L)+(1.-3.*A)*Q(L)
      RKLDEQ=1.
    6 CONTINUE
      RETURN
      END
```

```
      SUBROUTINE XYPLOT(X,Y,JI,KI,IYMAX,XXL,XXS,YYL,YYS)
      J7 UCSD XY PLOT  ,,MODIFIED ON AUG. 12,1970  BY YEH                    F 63
      THIS PROGRAM PLOTS X IN A 0-100 FIELD VS. Y IN A 0-IYMAX FIELD.
      X AND Y VALUES ARE ROUNDED (NOT TRUNCATED) TO NEAREST INTEGERS.
      ACTUAL VALUES OF X AND Y ARE PRINTED ON ABSCISSA AND ORDINATE.
      Y VALUES ARE PRINTED IN DESCENDING OR ASCENDING ORDER FOR LYAXIS
      EQUAL TO 1 OR EQUAL TO 2
      DIMENSION X(1),Y(1),IX(1025),IY(1025),IFX(101),ZX(11)              XYPLT  2
      IF (IYMAX .LT. 0) 30,31
   30 IYMAX=-IYMAX
      LYAXIS=2  $  GO TO 32
   31 LYAXIS=1
   32 XL=XXL  $  XS=XXS  $  YL=YYL  $  YS=YYS
      IF (  XXL  .LE.  XXS )       CALL RANGE(X,JI,KI,XL,XS)
      IF (  YYL  .LE.  YYS )       CALL RANGE(Y,JI,KI,YL,YS)
      IF(XL .LE. XS .OR. YL .LE. YS) GO TO 33
      XSCALE=(XL-XS)*.01                                                 XYPLT  3
      YSCALE=(YL-YS)/FLOATF(IYMAX)                                       XYPLT  4
      J=0                                                                XYPLT  5
      DO 105 I=JI,KI                                                     XYPLT  6
      IF (XL-X(I))105,101,101                                            XYPLT  7
  101 IF (X(I)-XS)105,102,102                                            XYPLT  8
  102 IF (YL-Y(I))105,103,103                                            XYPLT  9
  103 IF (Y(I)-YS)105,104,104                                            XYPLT 10
  104 J=J+1                                                              XYPLT 11
      IX(J)=(X(I)-XS)/XSCALE+0.5                                         XYPLT 12
      IY(J)=(Y(I)-YS)/YSCALE+0.5                                         XYPLT 13
  105 CONTINUE                                                           XYPLT 14
      JMAX=J                                                             XYPLT 15
      AT THIS POINT (X(I)-XS) AND (Y(I)-YS) VALUES HAVE BEEN ROUNDED TO
      NEAREST INTEGERS IN ARRAY FIELDS OF 0 TO 100 AND 0 TO IYMAX.
      DATA ARE SCREENED TO EXCLUDE VALUES OUTSIDE OF X AND Y LIMITS.
    1 FORMAT(1H1)                                                        XYPLT 16
    2 FORMAT(15H  Y VALUES.     ,20(5HI....),1HI)                        XYPLT 17
    4 FORMAT(1H E10.3,4X,  101A1)                                        XYPLT 18
    6 FORMAT(15X,20(5HI....),1HI)                                        XYPLT 19
```

```
    7 FORMAT(7H X=10**,I3,1H*,10(F7.3,3X),F7.3)                          XYPLT 20
    8 FORMAT(/8H YSCALE=E10.3,4X7HXSCALE=E10.3)                          XYPLT 21
      PRINT 1                                                            XYPLT 22
      DO 5 K=1,11                                                        XYPLT 23
    5 ZX(K)=10.*FLOATF(K-1)*XSCALE+XS                                    XYPLT 24
      CALL AMPF(ZX,IA)                                                   XYPLT 25
      GO TO (9,11) LYAXIS                                                XYPLT 26
    9 LL=IYMAX       $  PRINT 2  $  GO TO 13                           XYPLT 27
   10 LL=LL-1              $  GO TO 13                                  XYPLT 28
   11 LL=0       $  PRINT 7,IA,(ZX(K),K=1,11)                          XYPLT 29
      PRINT 2  $  GO TO 13                                               XYPLT 30
   12 LL=LL+1                                                            XYPLT 31
   13 DO 14 I=2,100                                                      XYPLT 32
   14 IFX(I)=(1H )                                                       XYPLT 33
      IFX(1)=1HI                                                         XYPLT 34
      IFX(101)=1HI                                                       XYPLT 35
      DO 16 J=1,JMAX                                                     XYPLT 36
      IF (IY(J)-LL)16,15,16                                              XYPLT 37
   15 II=IX(J)+1          $  IFX(II)=(1H*)                              XYPLT 38
   16 CONTINUE                                                           XYPLT 39
      ZY=FLOATF(LL)*YSCALE+YS                                            XYPLT 40
      PRINT 4,ZY,IFX                                                     XYPLT 41
      GO TO (17,18) LYAXIS                                               XYPLT 42
   17 IF (LL)19,19,10                                                    XYPLT 43
   18 IF (LL-IYMAX)12,20,20                                              XYPLT 44
   19 PRINT 6       $  PRINT 7,IA,(ZX(K),K=1,11)  $  GO TO 21           XYPLT 45
   20 PRINT 6                                                            XYPLT 46
   21 PRINT 8,YSCALE,XSCALE        $  GO TO 40                           XYPLT 47
      NOTE THAT WHEN SCREEN IS APPLIED, I AND J MAY NOT REPRESENT SAME
      ARRAY ELEMENTS OF X AND Y.
   33 PRINT 34,XL,XS,YL,YS
   34 FORMAT(10X,'THE PLOT ROUTINE WAS BY-PASS, SINCE',/10X'XL=',F11.4,
     *5X,'XS=',F11.4,10X,'YL=',F11.4,5X,'YS=',F11.4,/)
   40 RETURN                                                             XYPLT 48
      END                                                                XYPLT 49
```

```
      SUBROUTINE RANGE(X,JI,KI,XL,XS)                                   XYPLT 52
      DIMENSION X(1)                                                    XYPLT 53
      XL=XS=X(JI)                                                       XYPLT 54
      J2=JI+1                                                           XYPLT 55
      DO 4 I=J2,KI                                                      XYPLT 56
      IF (X(I) .GT. XL) 2,3                                             XYPLT 57
    2 XL=X(I) $   GO TO 4                                               XYPLT 58
    3 IF (X(I) .LT. XS)  XS=X(I)                                        XYPLT 59
    4 CONTINUE                                                          XYPLT 60
      RETURN                                                            XYPLT 61
      END                                                               XYPLT 62

      SUBROUTINE AMPF (X,I)
      DIMENSION X(1)
      A=X(11)
      IF (-X(1) .GT. A ) A=-X(1)
      I=ALOG10(A)
      AA=10.**(-I)
      DO 1 K=1,11
    1 X(K)=X(K)*AA
      RETURN
      END
$EXECUTE,A=UTILITY

GAMA=0.29, BLYM=0.0118,  BLN=0.185       VINF=0.255
CUM=0.7    VINF=0.180


WR=0.01 ,RVINF=5.0E5,              END
THETA0=0.0,  THETASP=76.5,  ISTEP=2,  DANGLE=2., 1., THETAE=60., 77.,  END
```

REFERENCES

1. Dunham, J.: "Experiments Towards a Circulation-Controlled Lifting Rotor. Part I - Wind Tunnel Tests." The Aeronautical Journal, Royal Aeronautical Society, Vol. 74, No. 709, Jan. 1970, pp. 91-103.

2. Gallaher, W.H.; Tyler, S.P.; and Harvey, M.T.: "Wind Tunnel Investigation of a Circulation Controlled Airfoil Rotor Concept," General Dynamics/Convair Rept. GDC-DCD-68-009, Dec. 1968.

3. Williams, R.M., and Rogers, E.O.: "Design Considerations of Circulation Controlled Rotors," Paper 603, 28th Annual Forum of the American Helicopter Society, Washington D.C., May 1972.

4. Fekete, G.I.: "Coanda Flow of a Two-Dimensional Wall Jet on the Outside of a Circular Cylinder," McGill U. Mech. Engr. R. L. Rept. No. 63-11, Aug. 1963.

5. Newman, B.G.: "Deflexion of Plane Jets by Adjacent Boundaries - Coanda Effect," in Boundary Layer and Flow Control, Vol. I, Pergamon Press, N.Y., 1961, pp. 232-264.

6. Wei, M.H.Y., and Levinsky, E.S.: "Laminar Coanda Jet Flow Around a Circular Cylinder," Air Vehicle Corporation Rept. No. 362, May 1970.

7. Glauert, M.B.: "The Wall Jet," Jour. Fluid Mech., Aug. 1956, pp. 161-177.

8. Bloom, M.H., and Steiger, M.H.: "Perturbed Boundary-Layer Solutions Applied to the Wall Jet and Blasius Profile," Developments in Mechanics - Vol. I, Plenum Press, N.Y., 1961, pp. 588-602.

9. Parks, E.K., and Petersen, R.E.: "Analysis of a Coanda-Type Flow." AIAA, Vol. 6, No. 1., Jan. 1968.

10. Wygnanski, I.J., and Champagne, F.H.: "The Laminar Wall Jet Over a Curved Surface," J. Fluid Mech. (1968), Vol. 31, Part 3, pp. 459-465.

11. Gartshore, I.S., and Newman, B.G.: "The Turbulent Wall Jet in an Arbitrary Pressure Gradient," The Aeronautical Quarterly, Vol. XX, Part 1, Feb. 1969, pp. 25-56.

12. Kind, R.J.: "A Calculation Method for Circulation Control by Tangential Blowing Around a Bluff Trailing Edge," Aeronautical Quarterly, Vol. XIX, Part 3, Aug. 1968, pp. 205-223.

13. Guitton, D. E.: "Corrigendum and Addendum to MERL Rept. 64-7, entitled 'Two-Dimensional Turbulent Wall Jets Over Curved Surfaces,' " McGill U. MERL T.N. 67-1, Feb. 1967.

14. Gartshore, I. S.: "Predictions of the Blowing Required to Suppress Separation from High Lift Aerofoils," AIAA Paper 70-872, July 1970.

15. Spalding, D. B.: "A Unified Theory of Friction, Heat Transfer and Mass Transfer in the Turbulent Boundary Layer and Wall Jet," ARC 25 925, 1964.

16. Kind, R. J.: "Calculation of the Normal-Stress Distribution in a Curved Wall Jet," West Va. U. Aerospace Engr. TR-18, Aug. 1969.

17. Tetervin, N.: "An Exploratory Theoretical Investigation of the Effect of Longitudinal Surface Curvature on the Turbulent Boundary Layer," Naval Ordnance Lab. Rept. 69-22, Feb. 1969.

18. Schlichting, H.: Boundary Layer Theory, McGraw-Hill, 1960.

19. Harris, G. L.: "The Turbulent Wall Jet on Plane and Curved Surfaces Beneath an External Stream," von Karman Institute for Fluid Dynamics, TN 27, Aug. 1965.

20. Beckwith, I. E., and Bushnell, D. M.: "Calculation by a Finite-Difference Method of Supersonic Turbulent Boundary Layers with Tangential Slot Injection," Langley Research Center, NASA TN D-6221, April 1971.

21. Stratford, B. S.: "The Prediction of Separation of the Turbulent Boundary Layer," Jour. of Fluid Mech., Vol. 5 (1959), pp. 1-16.

22. Rosenhead, L.: Laminar Boundary Layers, Oxford U. Press, 1963.

23. Goradia, S. H., and Colwell, G. T.: "Parametric Study of a Two-Dimensional Turbulent Wall Jet in a Moving Stream with Arbitrary Pressure Gradient," AIAA Journal, Nov. 1971.

24. Lawford, J. A., and Foster, D. N.: "Low-Speed Wind-Tunnel Tests of a Wing Section with Plain Leading- and Trailing-Edge Flaps Having Boundary-Layer Control by Blowing," British R&M 3639, 1970.

25. Thomas, F.: "Investigations into Increasing the Lift of Wings by Boundary-Layer Control Through Blowing," RAE Library Translation No. 1267, Nov. 1967.

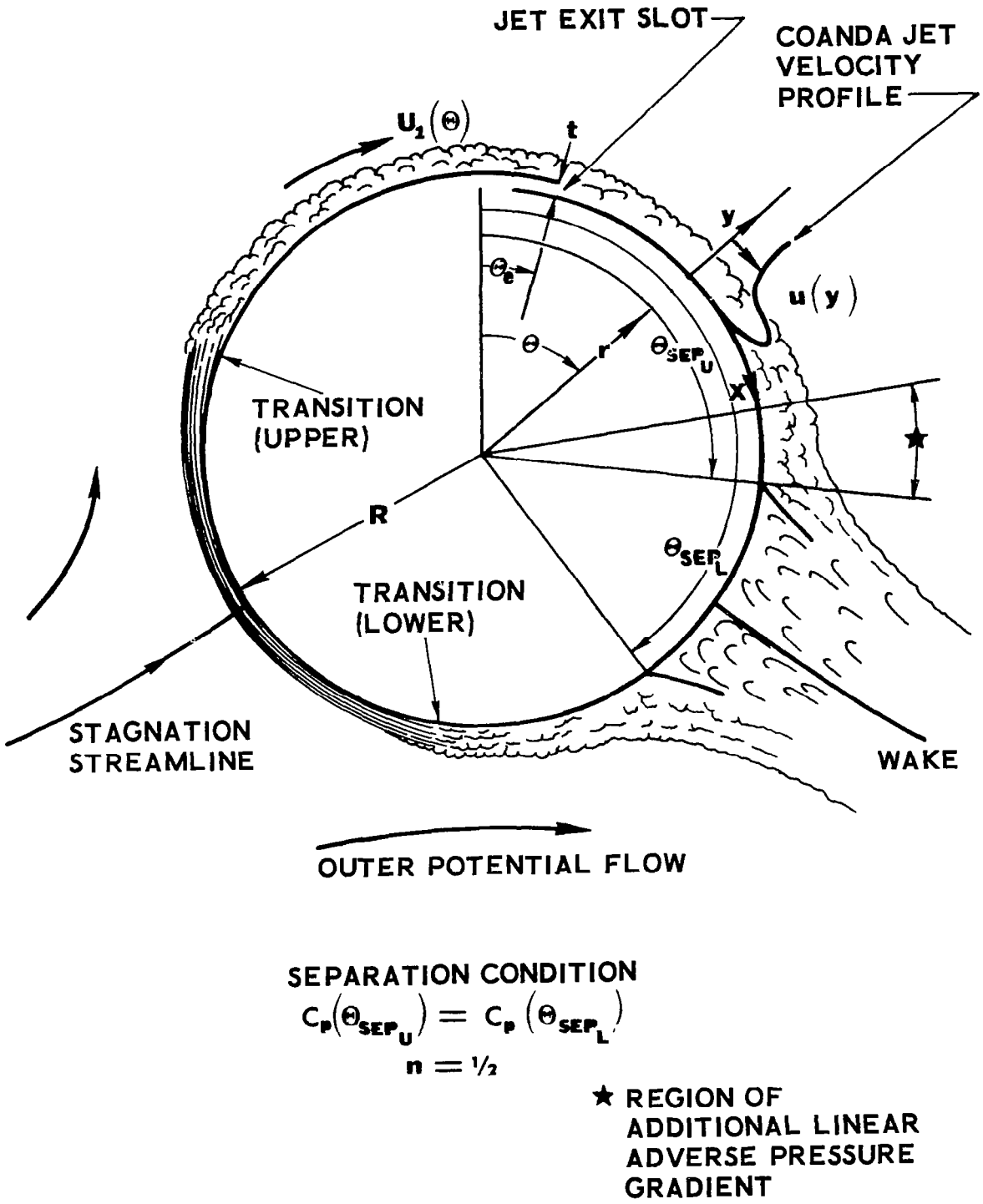

Figure 1.-Coordinate system, tangential blowing over a circular cylinder.

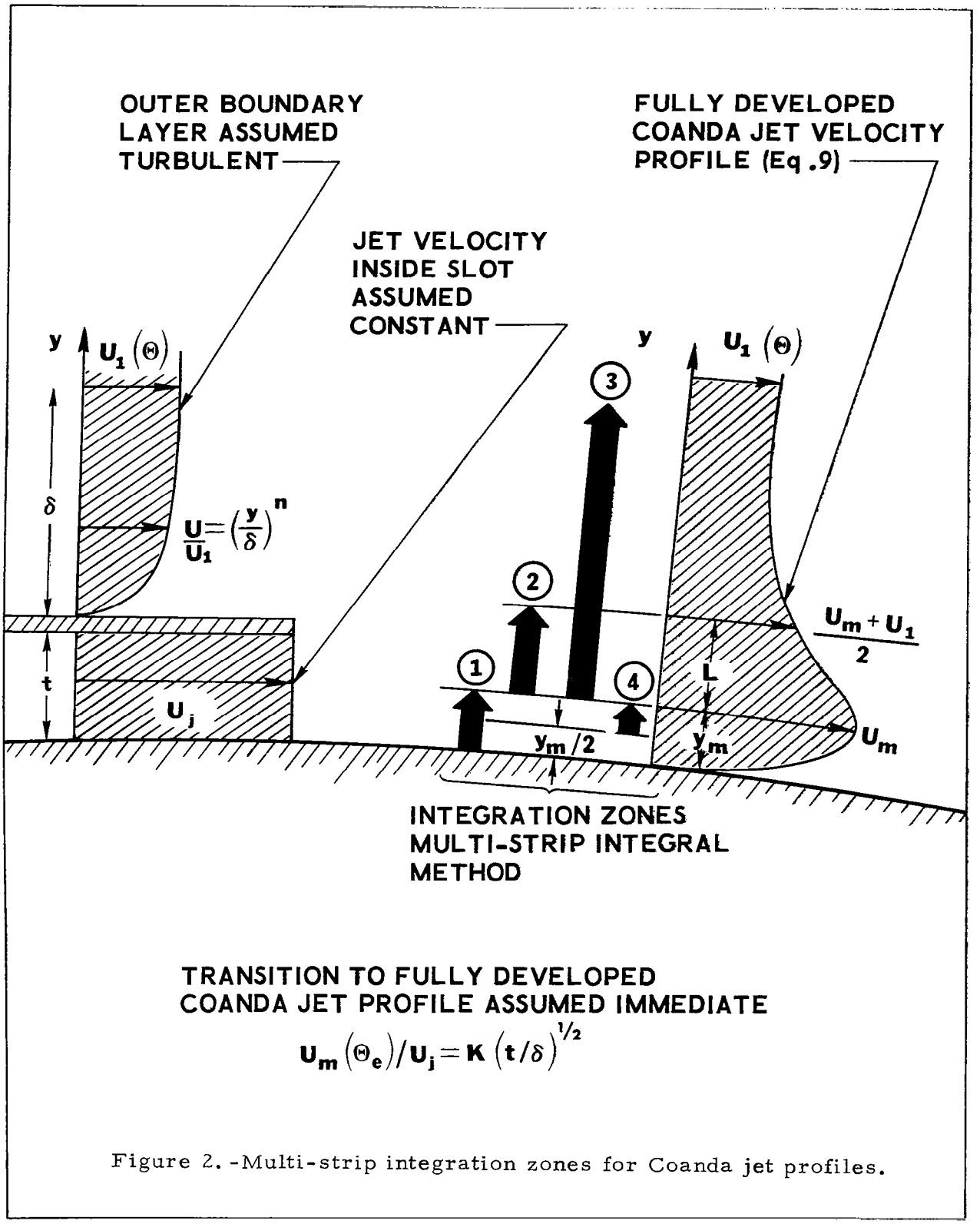

Figure 2. -Multi-strip integration zones for Coanda jet profiles.

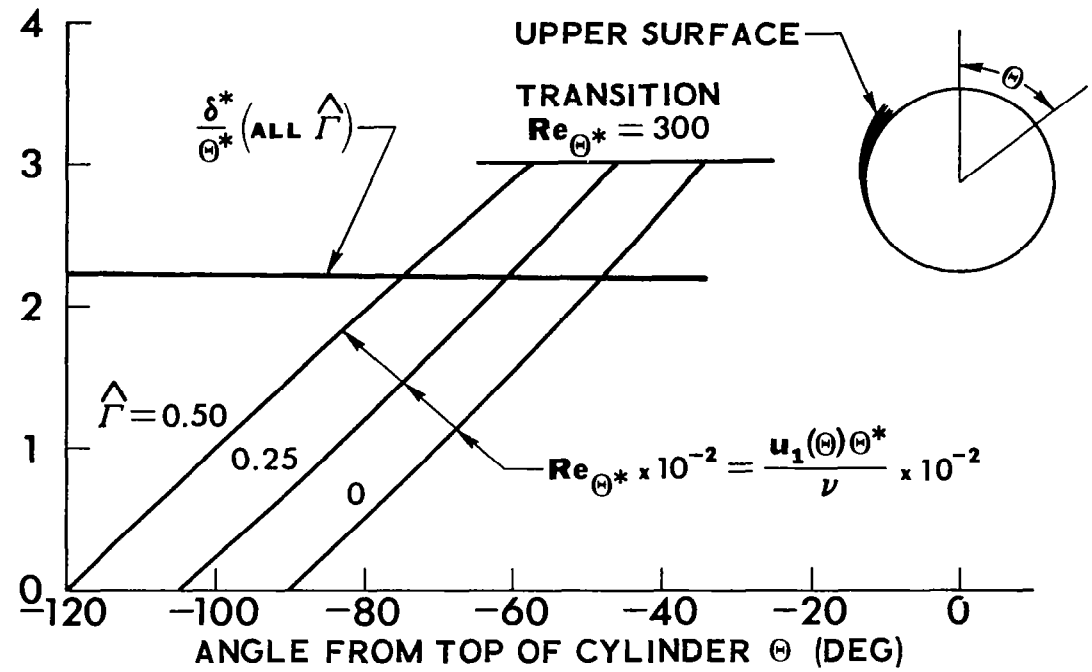

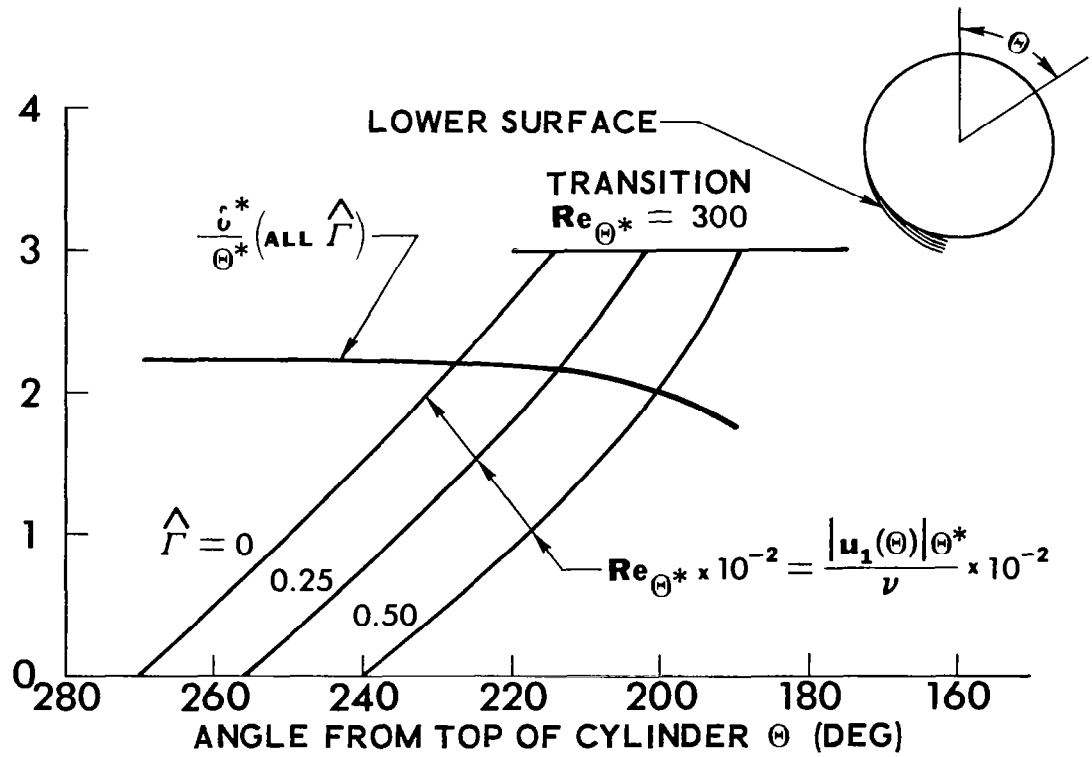

Figure 3.-Calculated laminar boundary-layer characteristics.

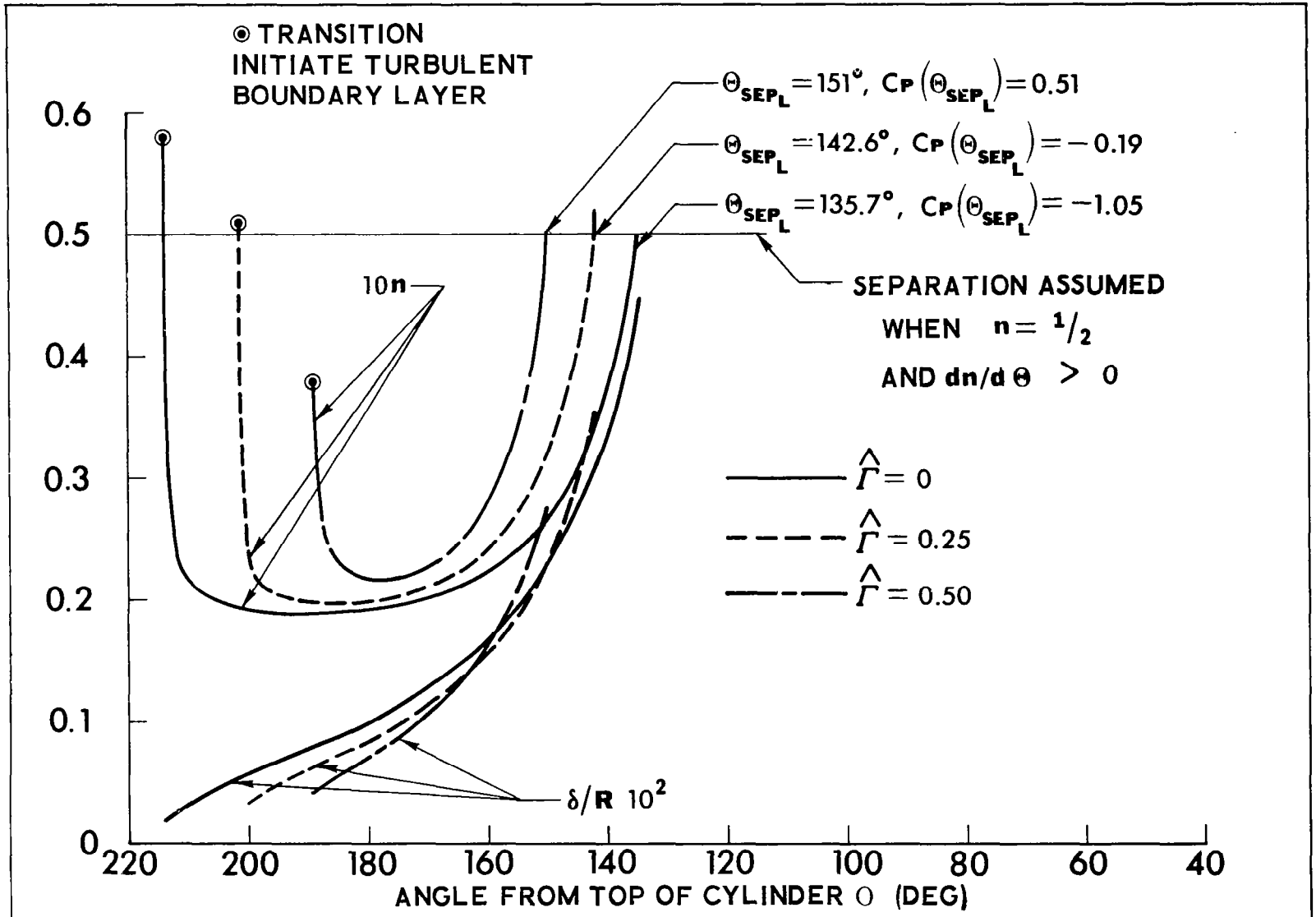

Figure 4. -Calculated lower surface turbulent boundary-layer characteristics.

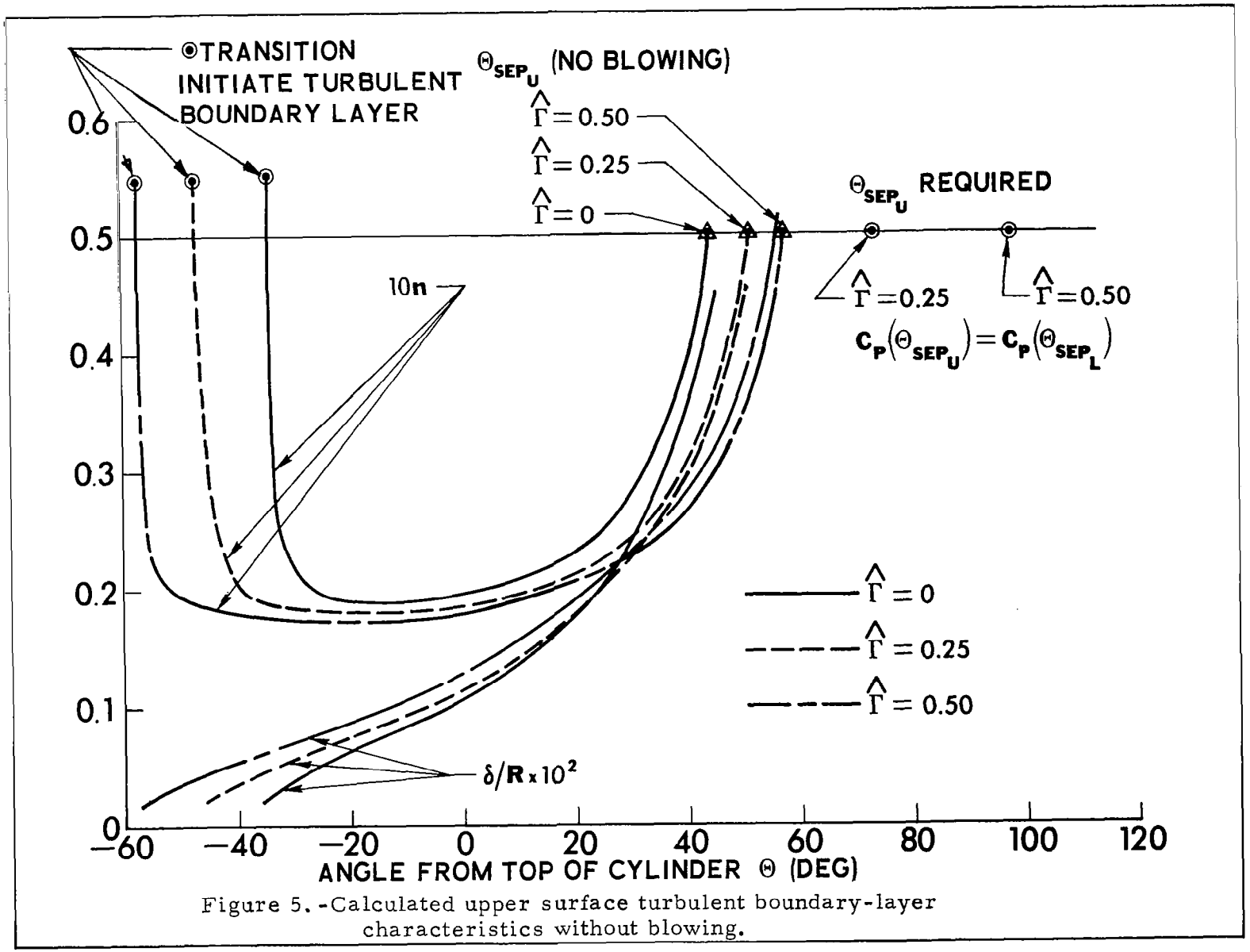

Figure 5.-Calculated upper surface turbulent boundary-layer characteristics without blowing.

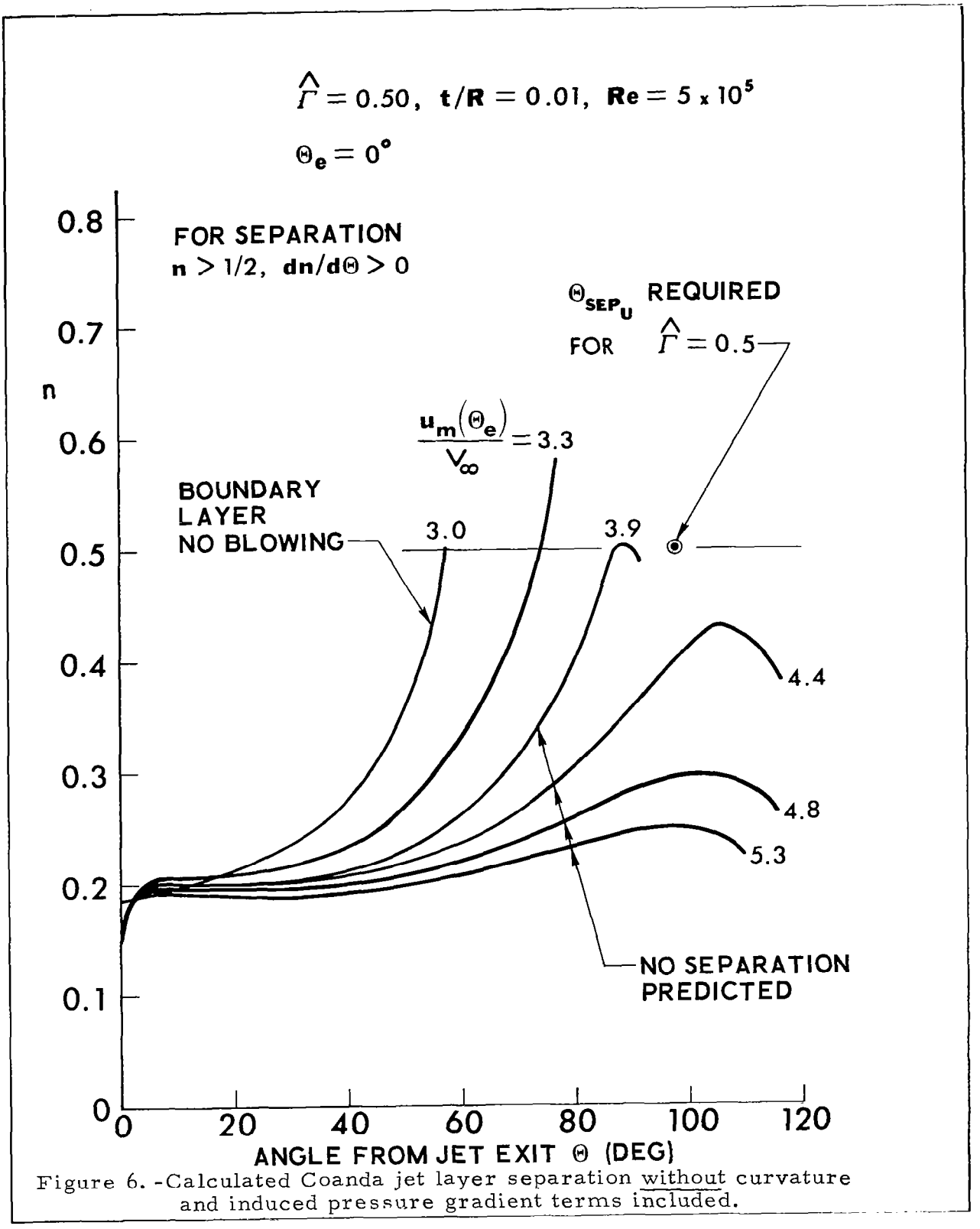

Figure 6. -Calculated Coanda jet layer separation without curvature and induced pressure gradient terms included.

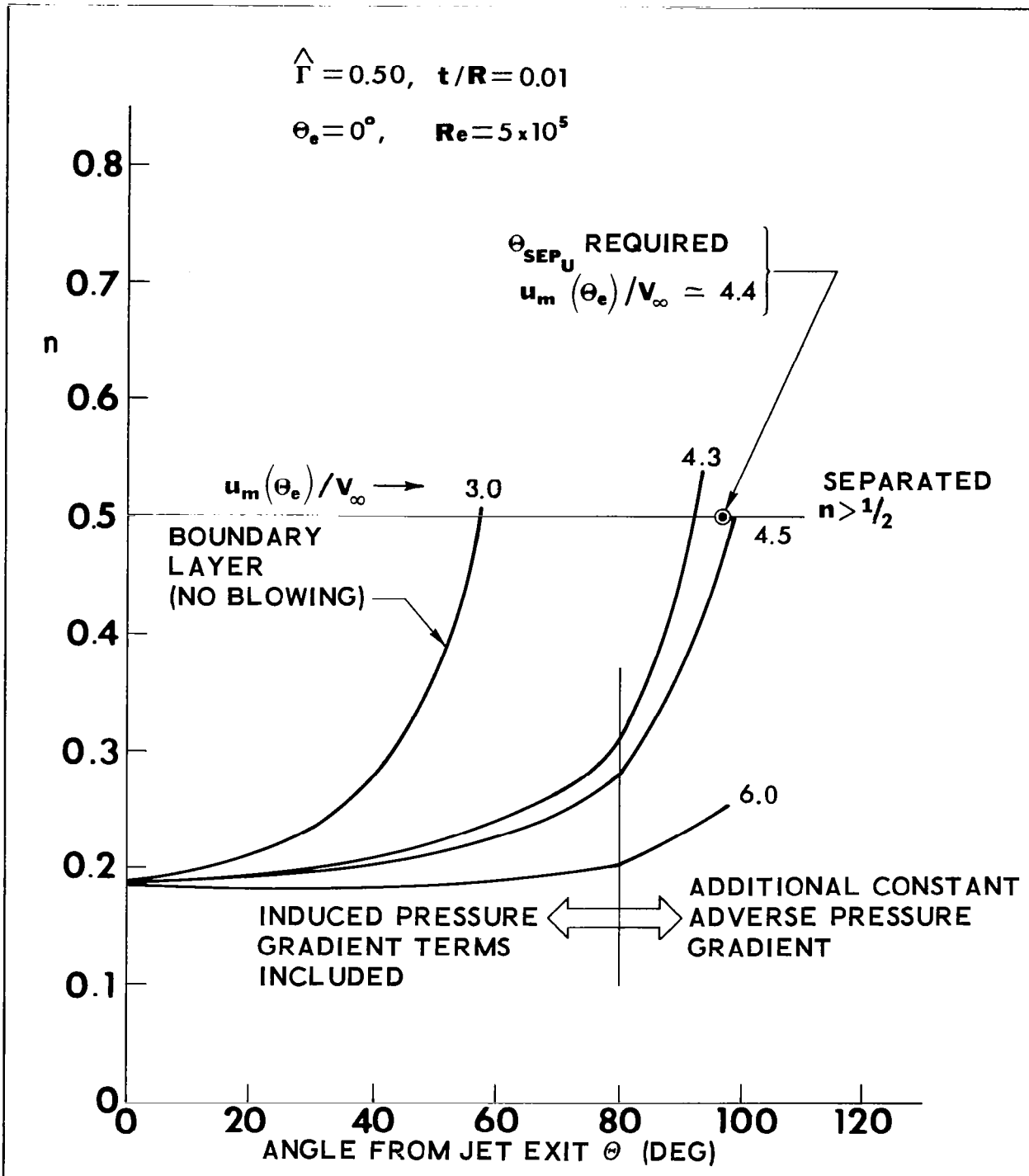

Figure 7. -Calculated Coanda jet layer separation including curvature and induced pressure gradient terms, $\overline{N = 5}$, $K = 1$.

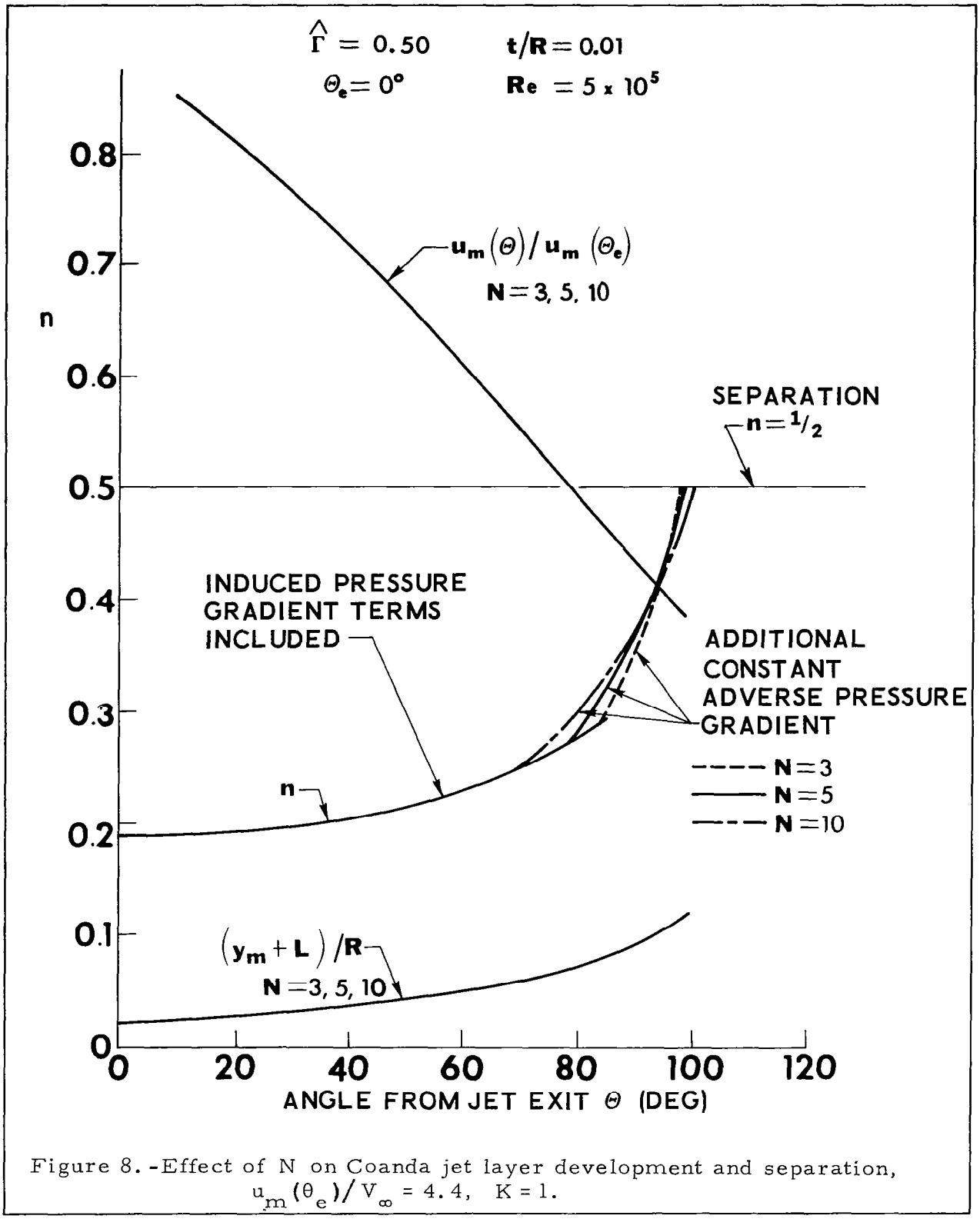

Figure 8.-Effect of N on Coanda jet layer development and separation, $u_m(\theta_e)/V_\infty = 4.4$, K = 1.

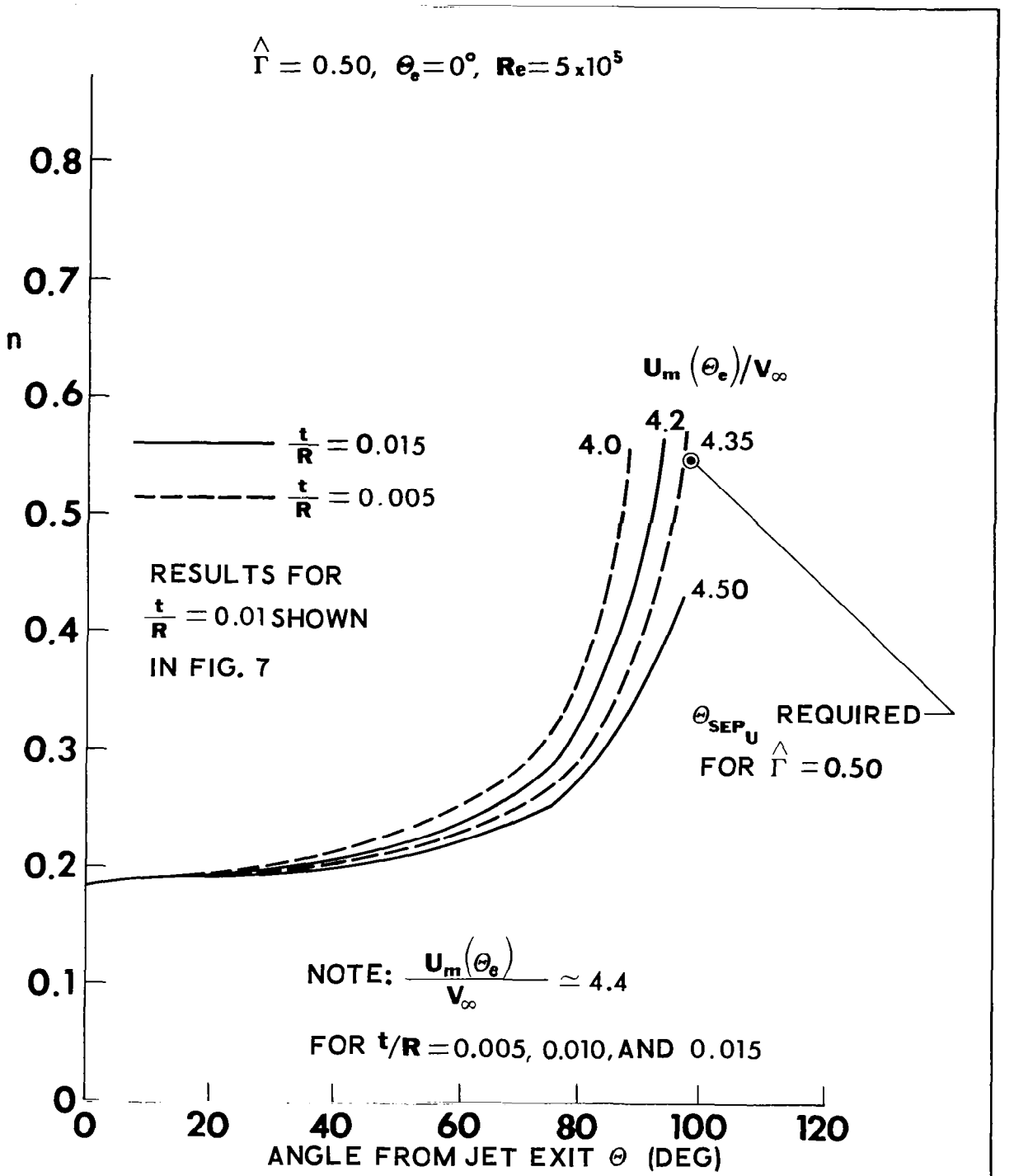

Figure 9. -Effect of t/R on Coanda jet layer development and separation, N = 5, K = 1.

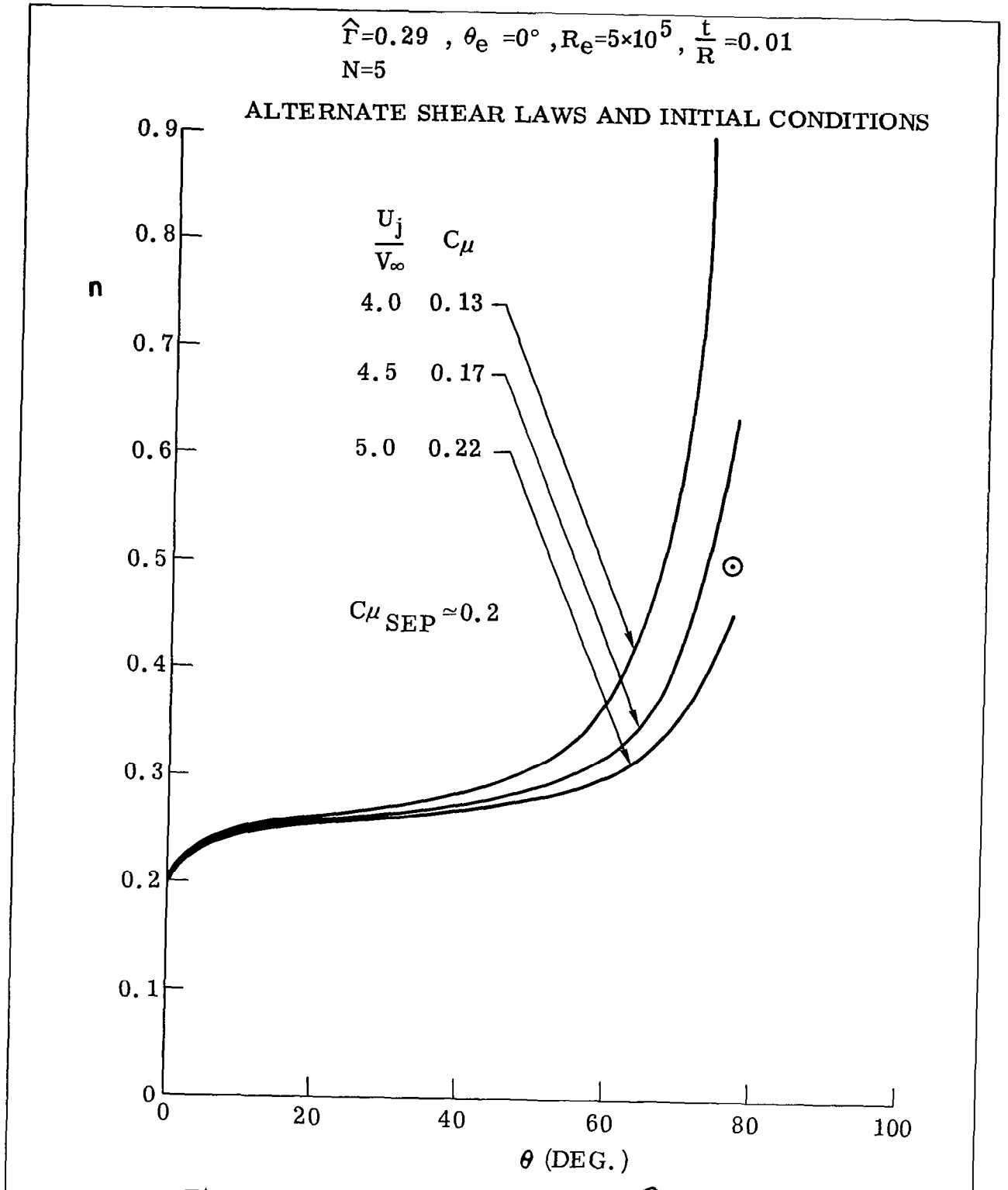

Figure 10. - Variation of n with θ , $\hat{\Gamma}$ = 0.29.

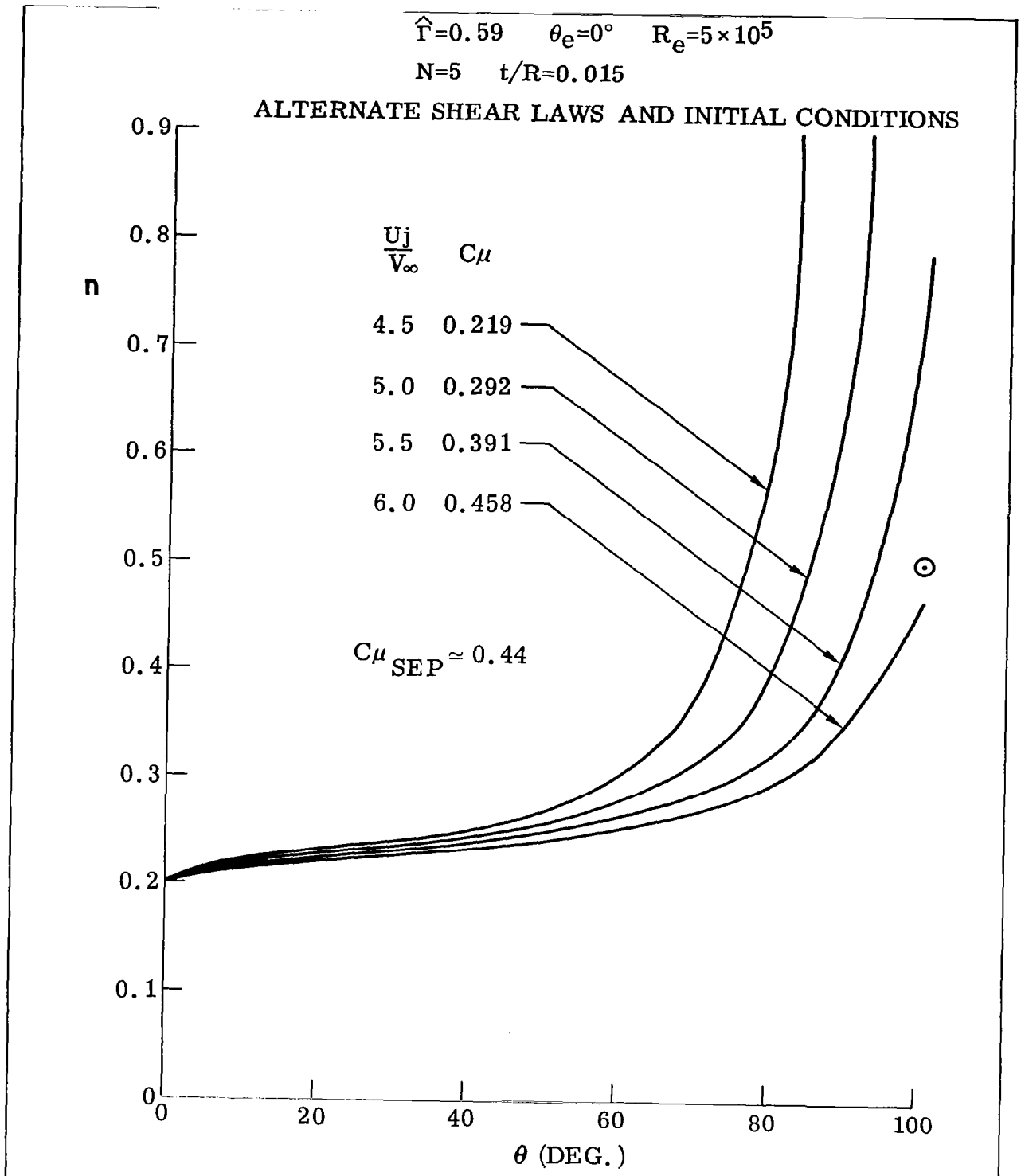

Figure 11. - Variation of n with θ , $\hat{\Gamma}$ = 0.59.

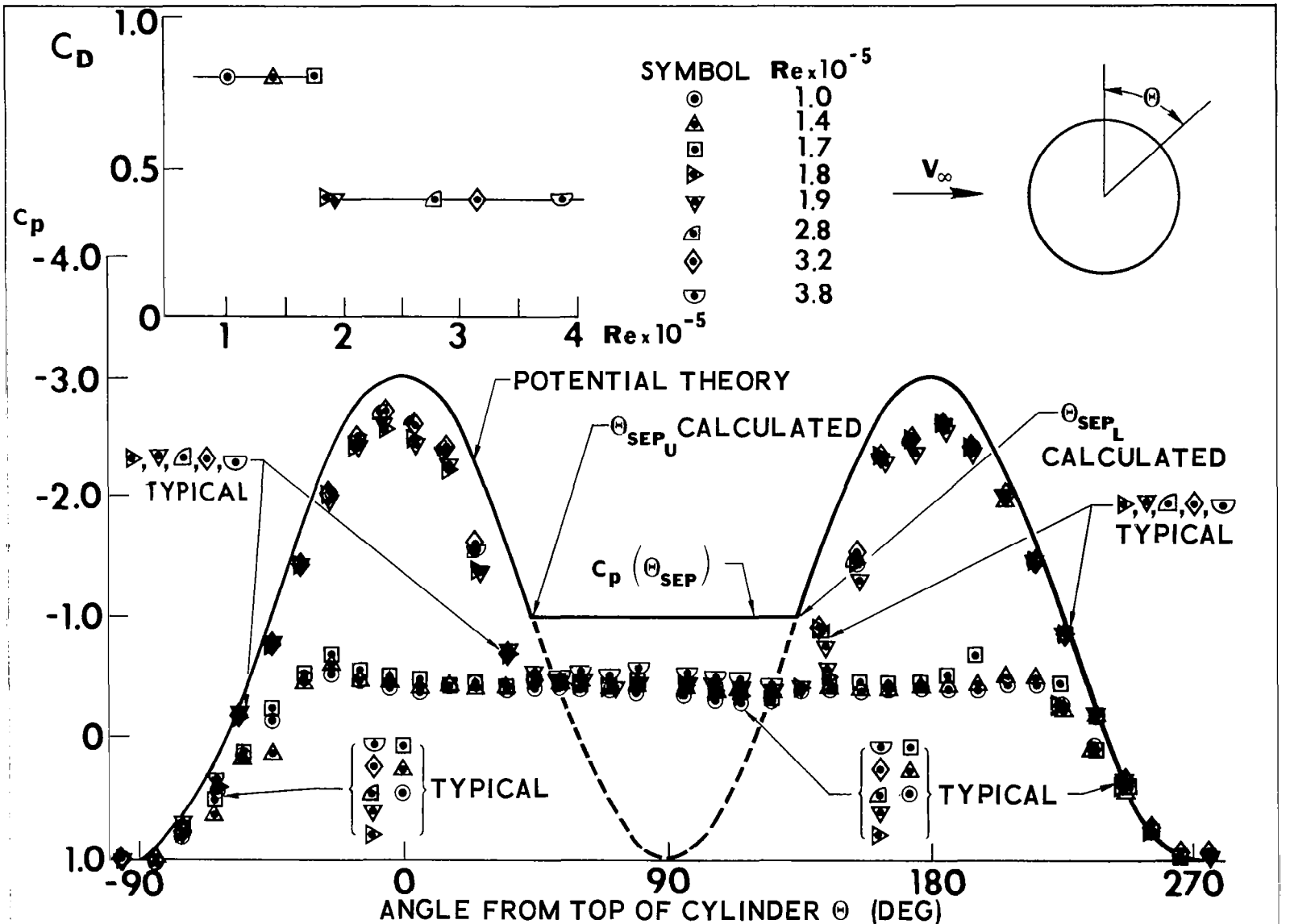

Figure 12. -Effect of Reynolds number on measured pressure distribution without blowing.

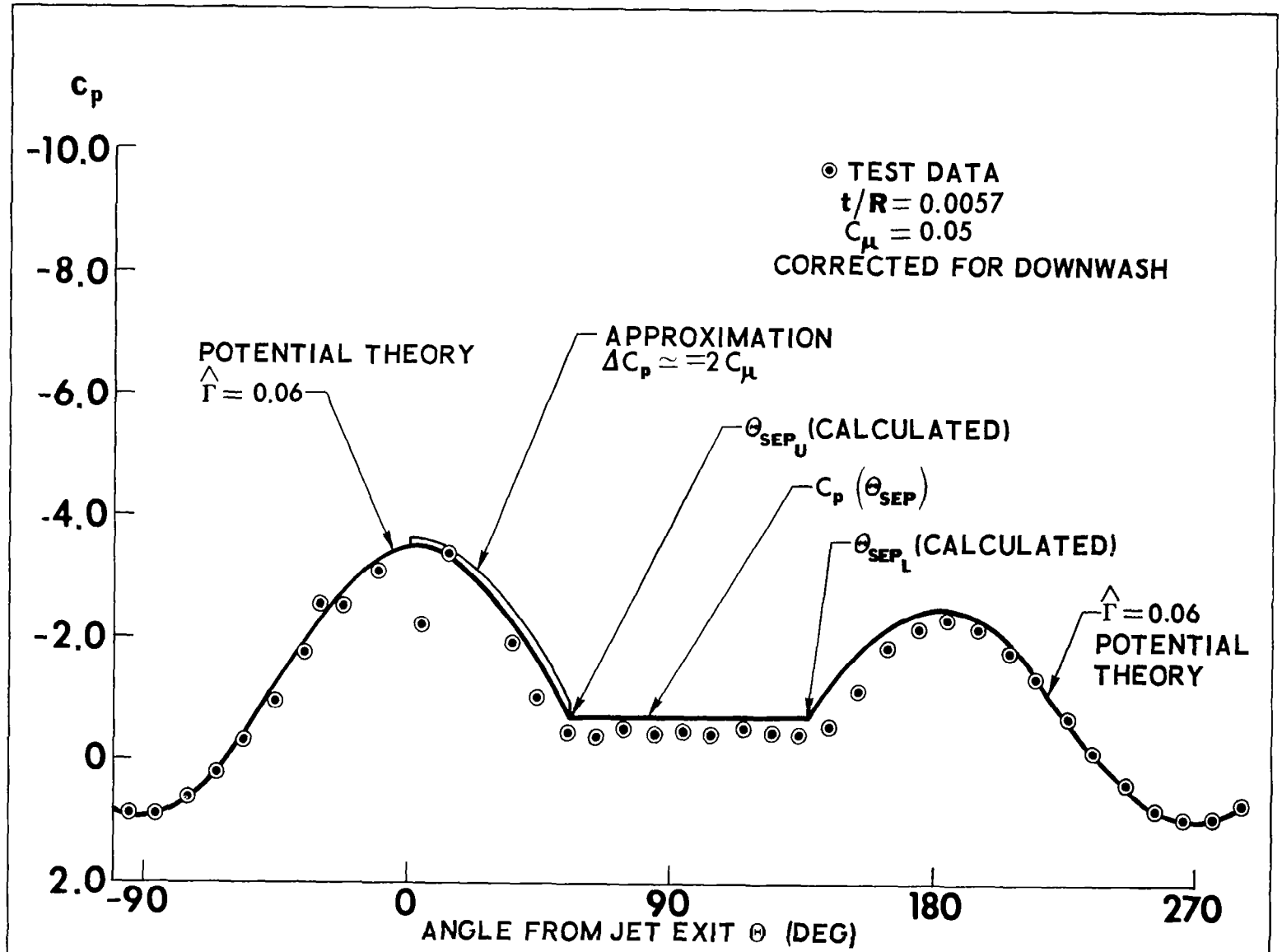

Figure 13. - Effect of tangential blowing on pressure distribution, $t/R = 0.0057$ and $C_\mu = 0.05$; and comparison with $\hat{\Gamma} = 0.06$ theory.

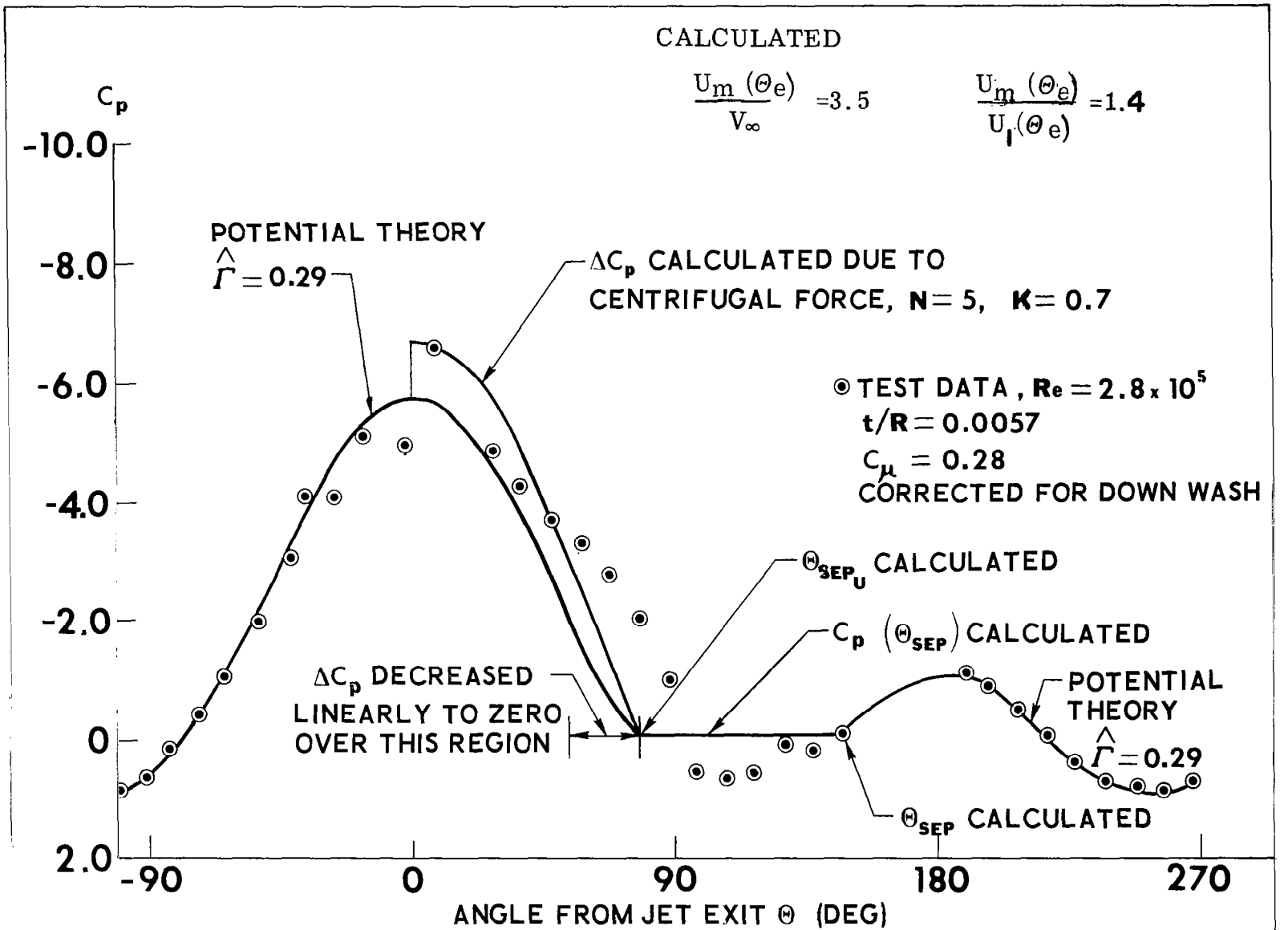

Figure 14 .-Effect of tangential blowing on pressure distribution, t/R=0.0057 and C_μ=0.28; and comparison with $\hat{\Gamma}$=0.29 theory.

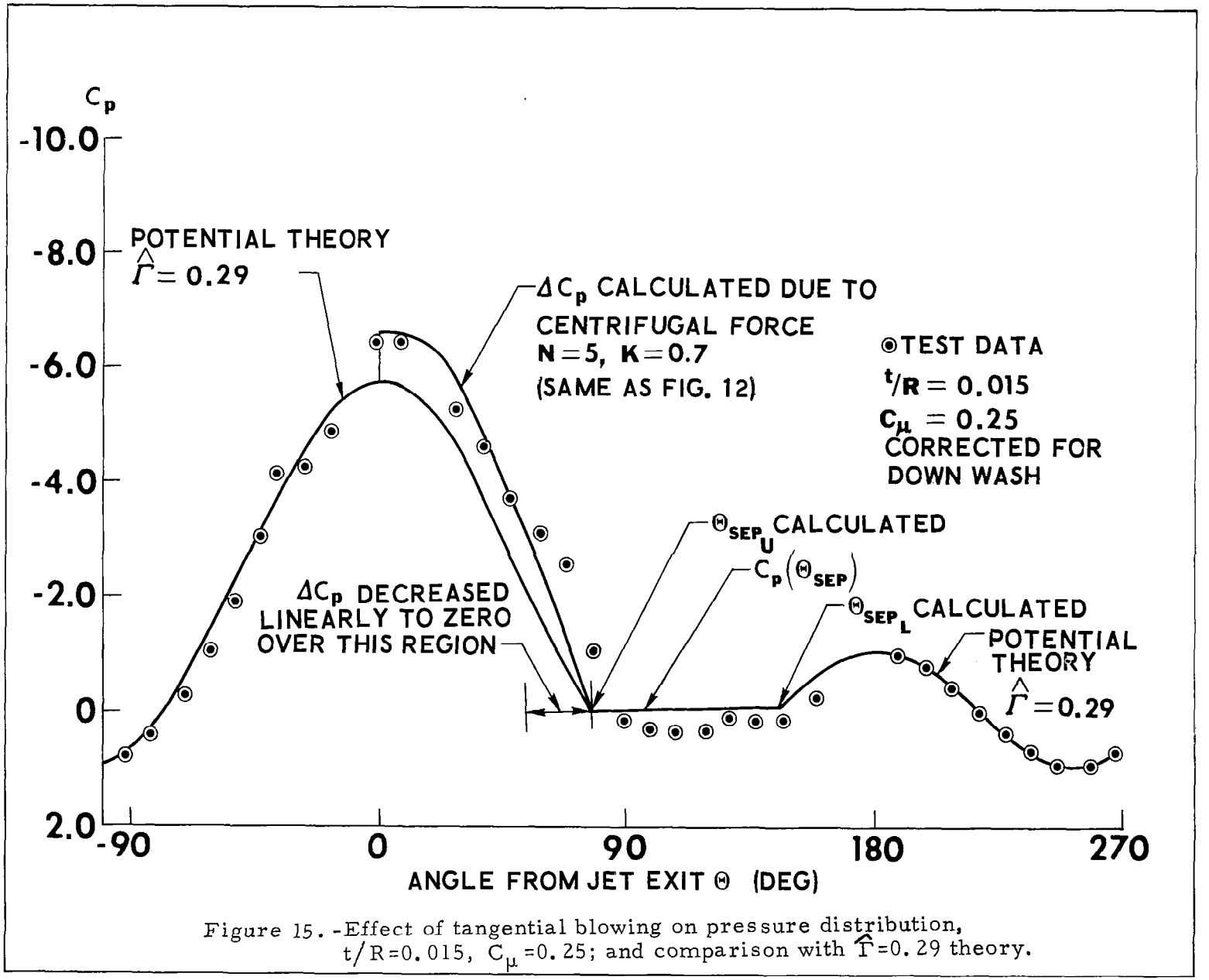

Figure 15. -Effect of tangential blowing on pressure distribution, $t/R = 0.015$, $C_\mu = 0.25$; and comparison with $\hat{\Gamma} = 0.29$ theory.

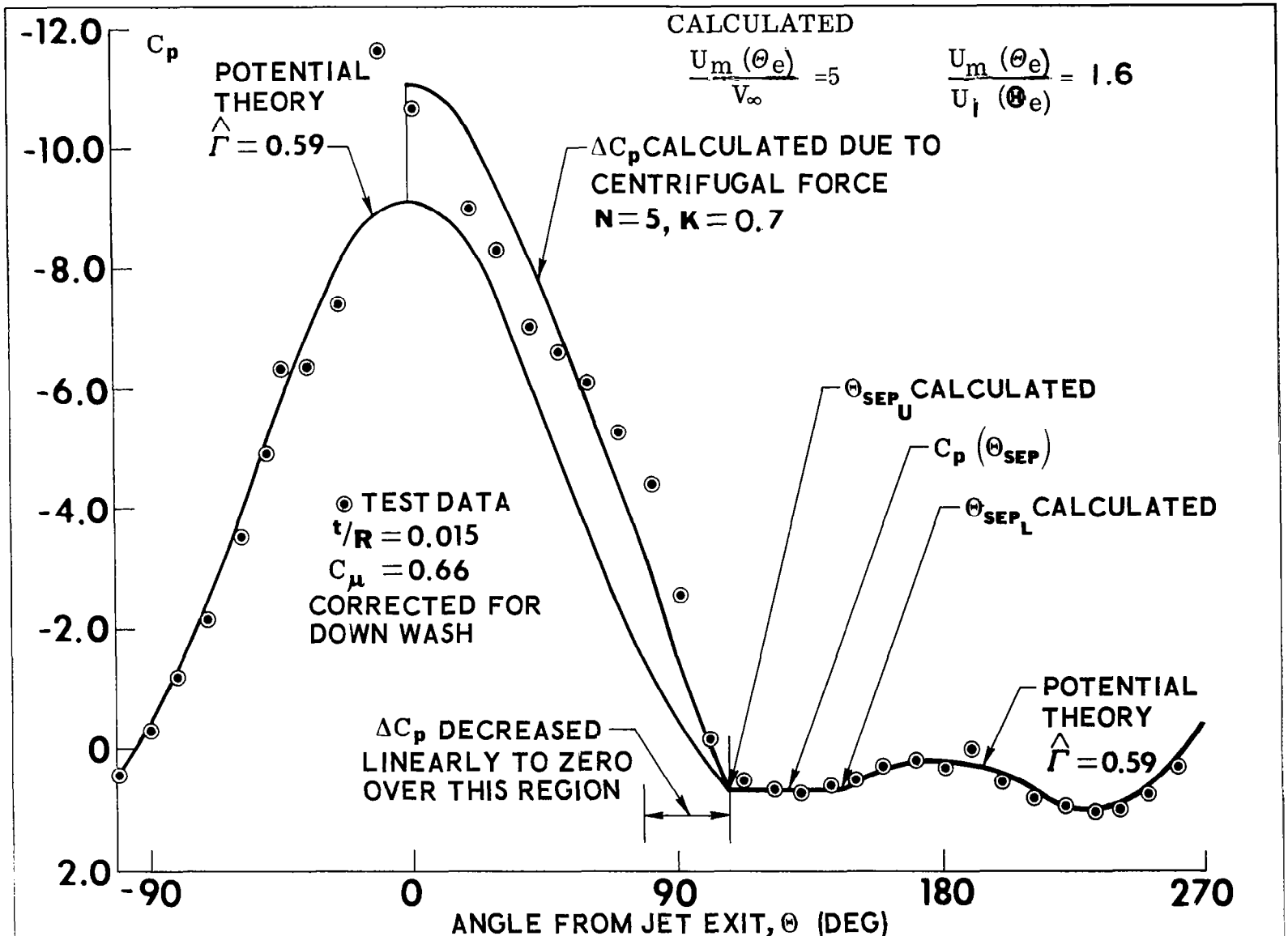

Figure 16.-Effect of tangential blowing on pressure distribution, $t/R = 0.015$, $C_\mu = 0.66$; and comparison with $\hat{\Gamma} = 0.59$ theory.

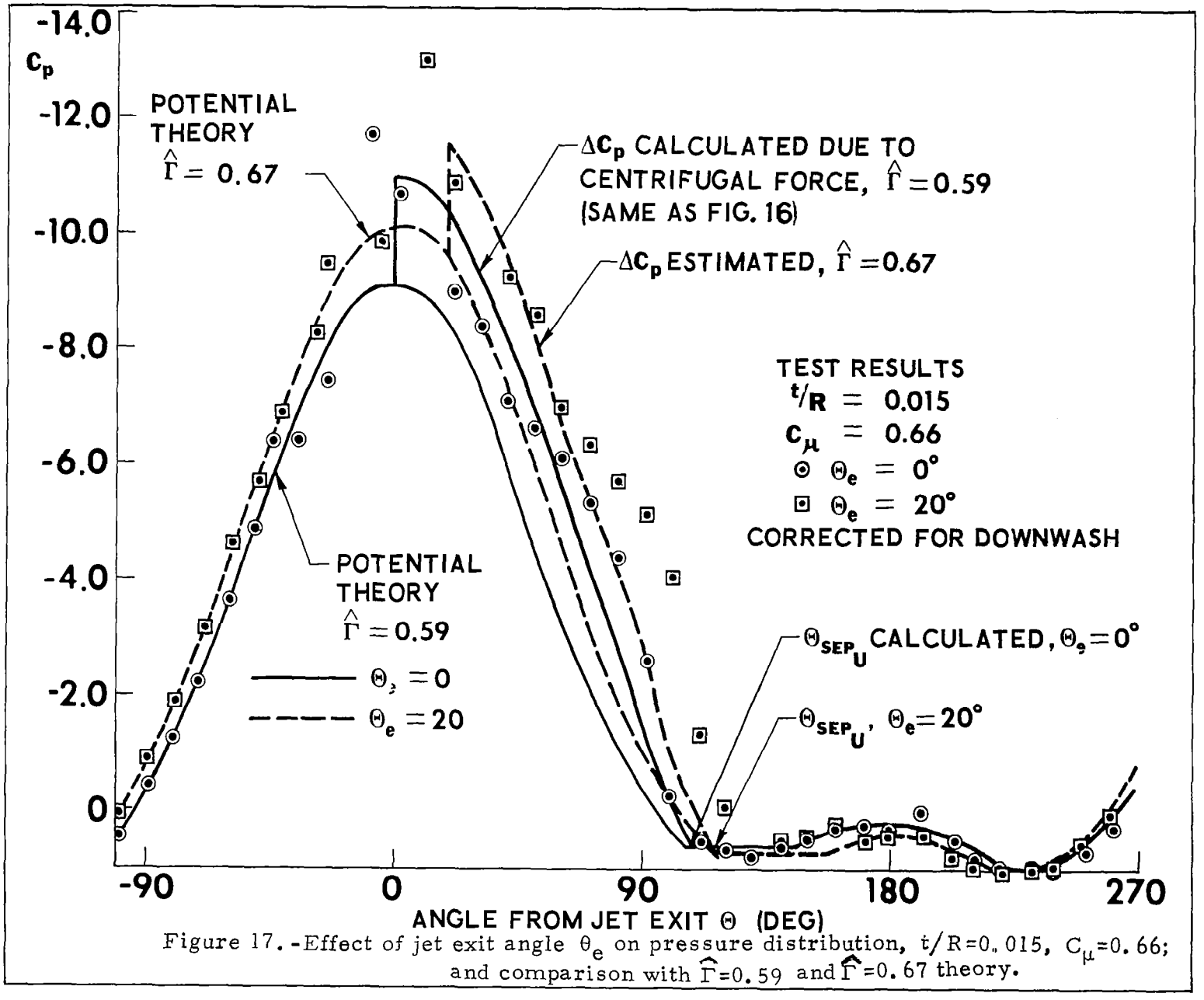

Figure 17.-Effect of jet exit angle θ_e on pressure distribution, $t/R=0.015$, $C_\mu=0.66$; and comparison with $\hat{\Gamma}=0.59$ and $\hat{\Gamma}=0.67$ theory.

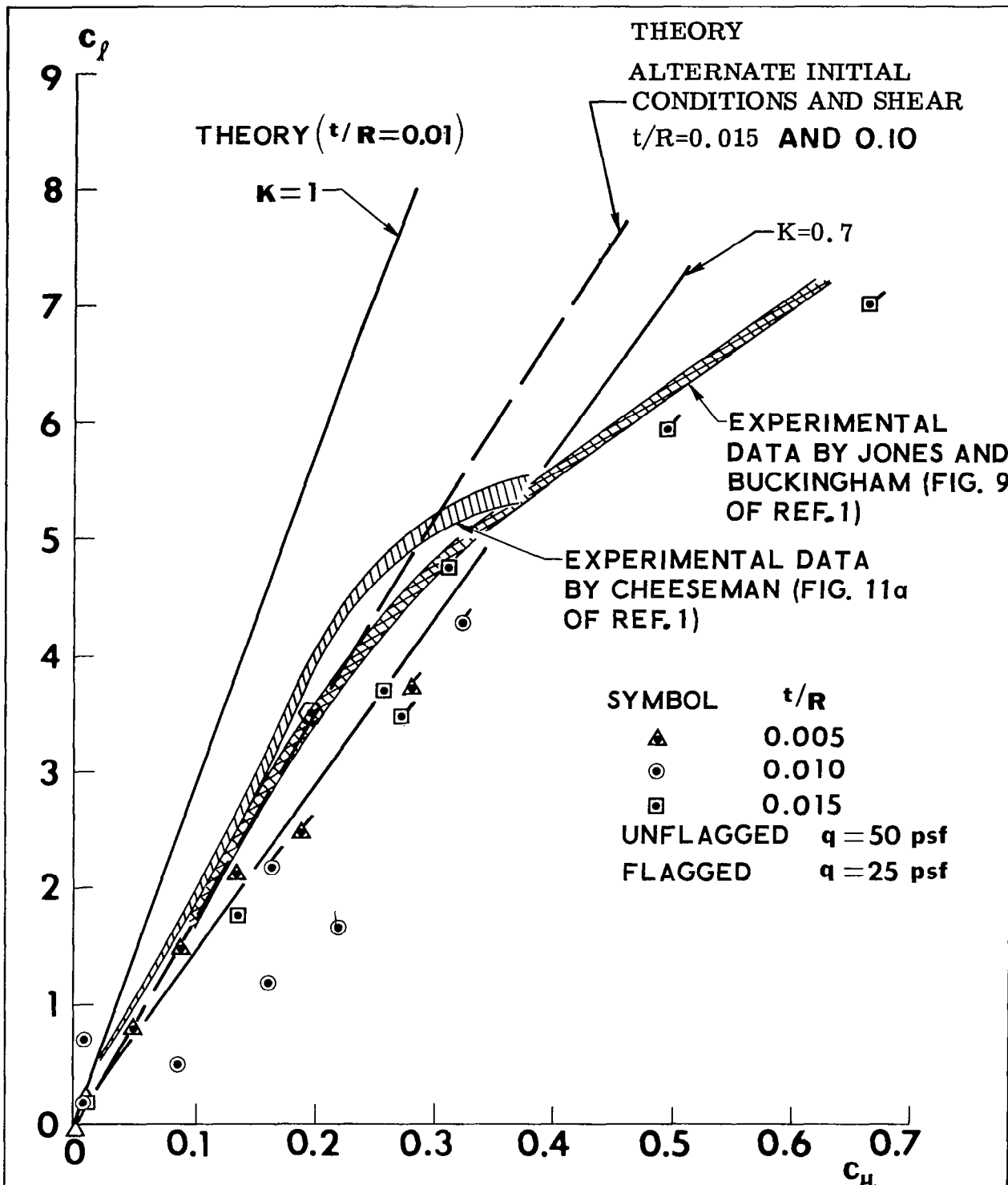

Figure 18.-Comparison of predicted and measured two-dimensional lift coefficient, $\theta_e = 0^\circ$.

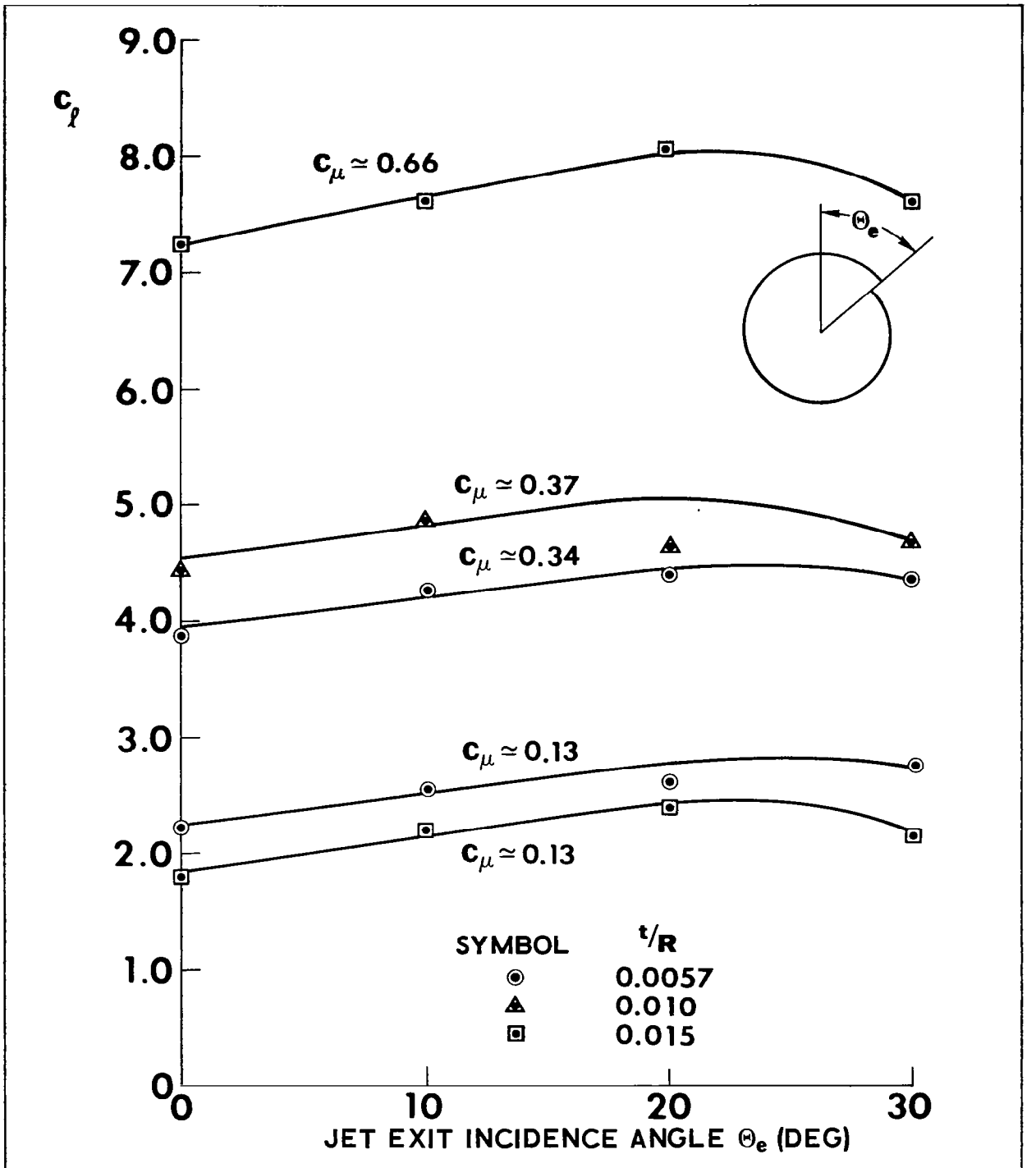

Figure 19. -Effect of jet exit angle θ_e on measured two-dimensional lift coefficient.

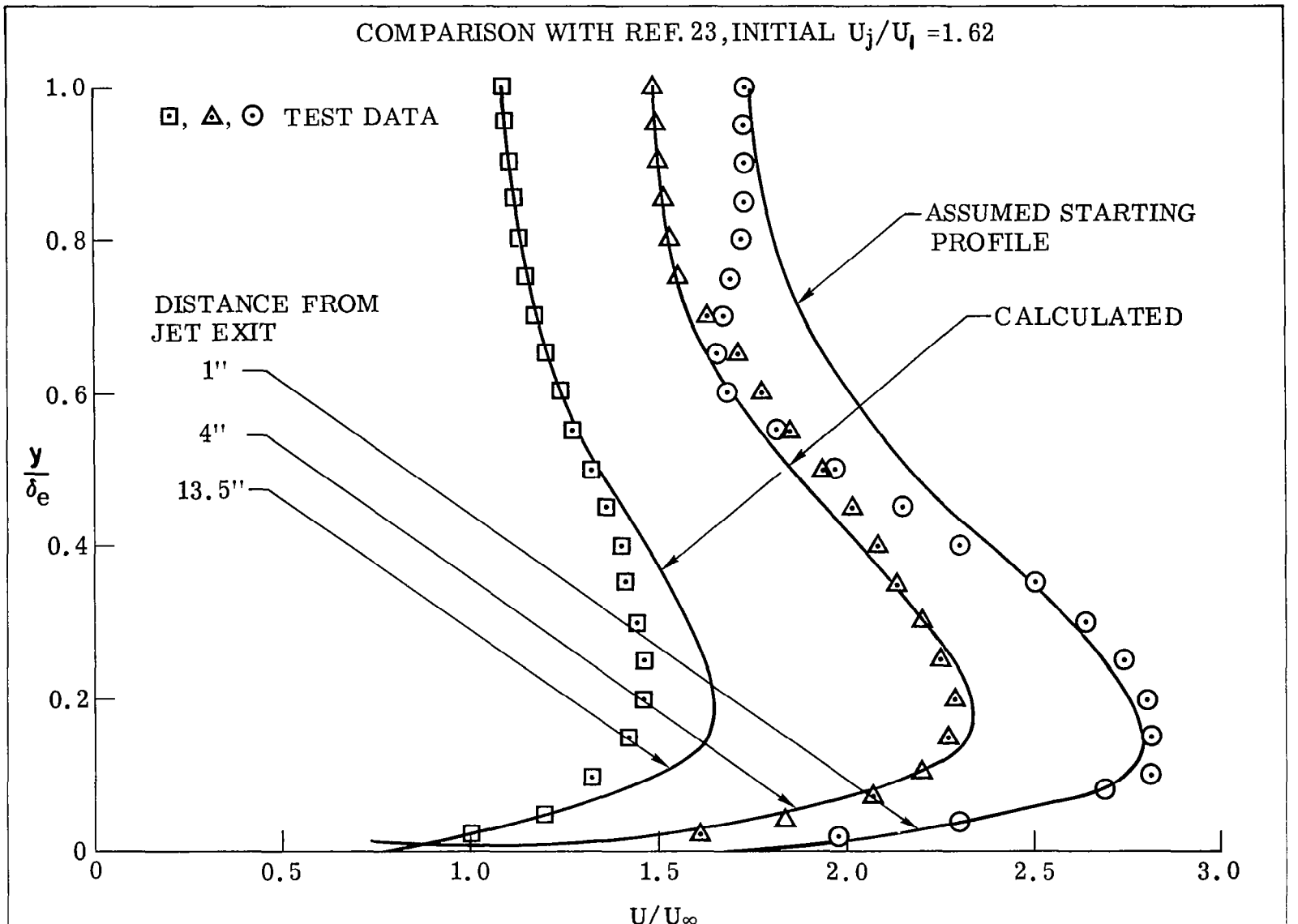

Figure 20. -Comparison of calculated velocity profiles with test data over a flat surface.

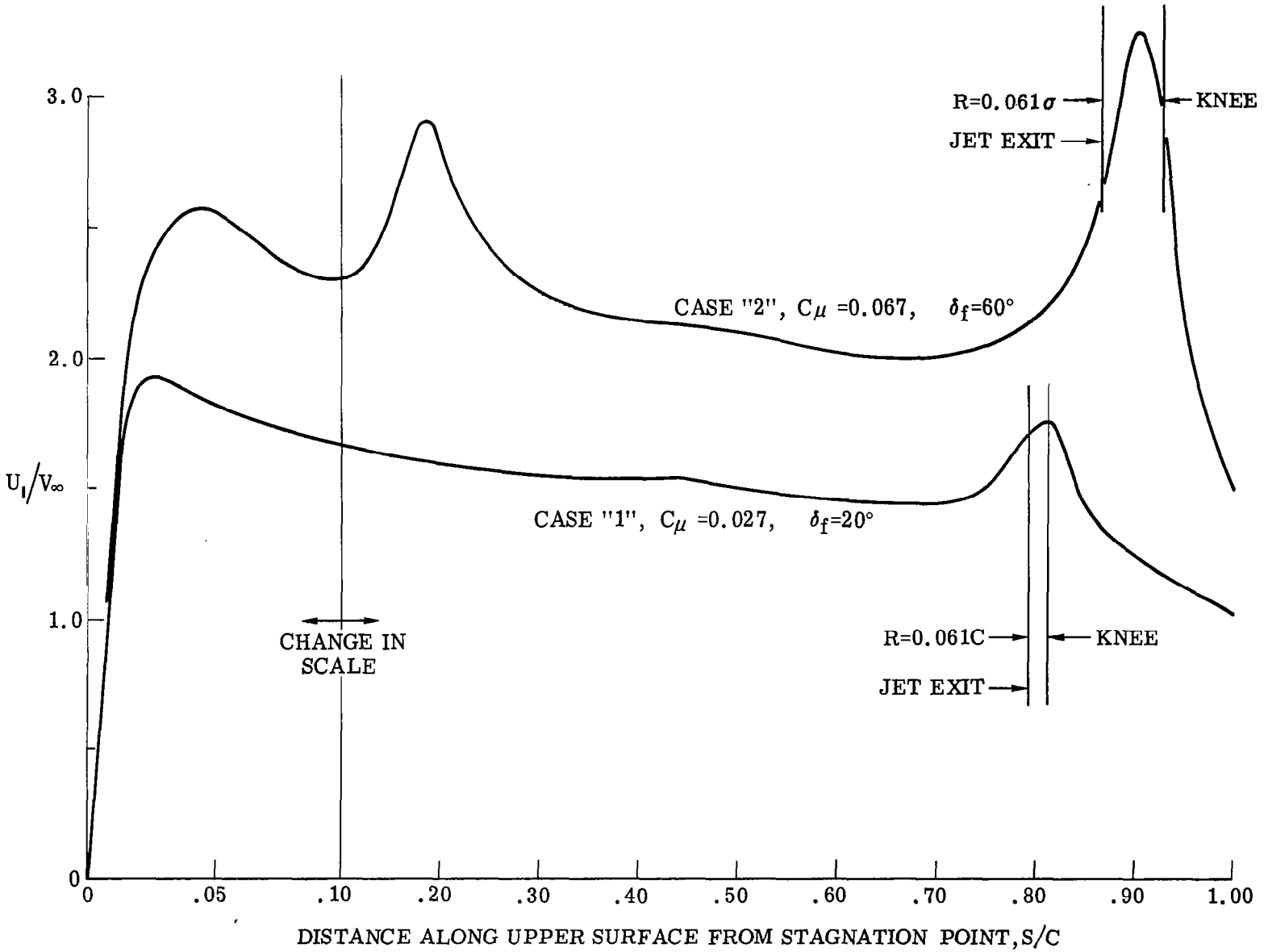

Figure 21. - Velocity distribution from reference 24 for an airfoil with a flap.

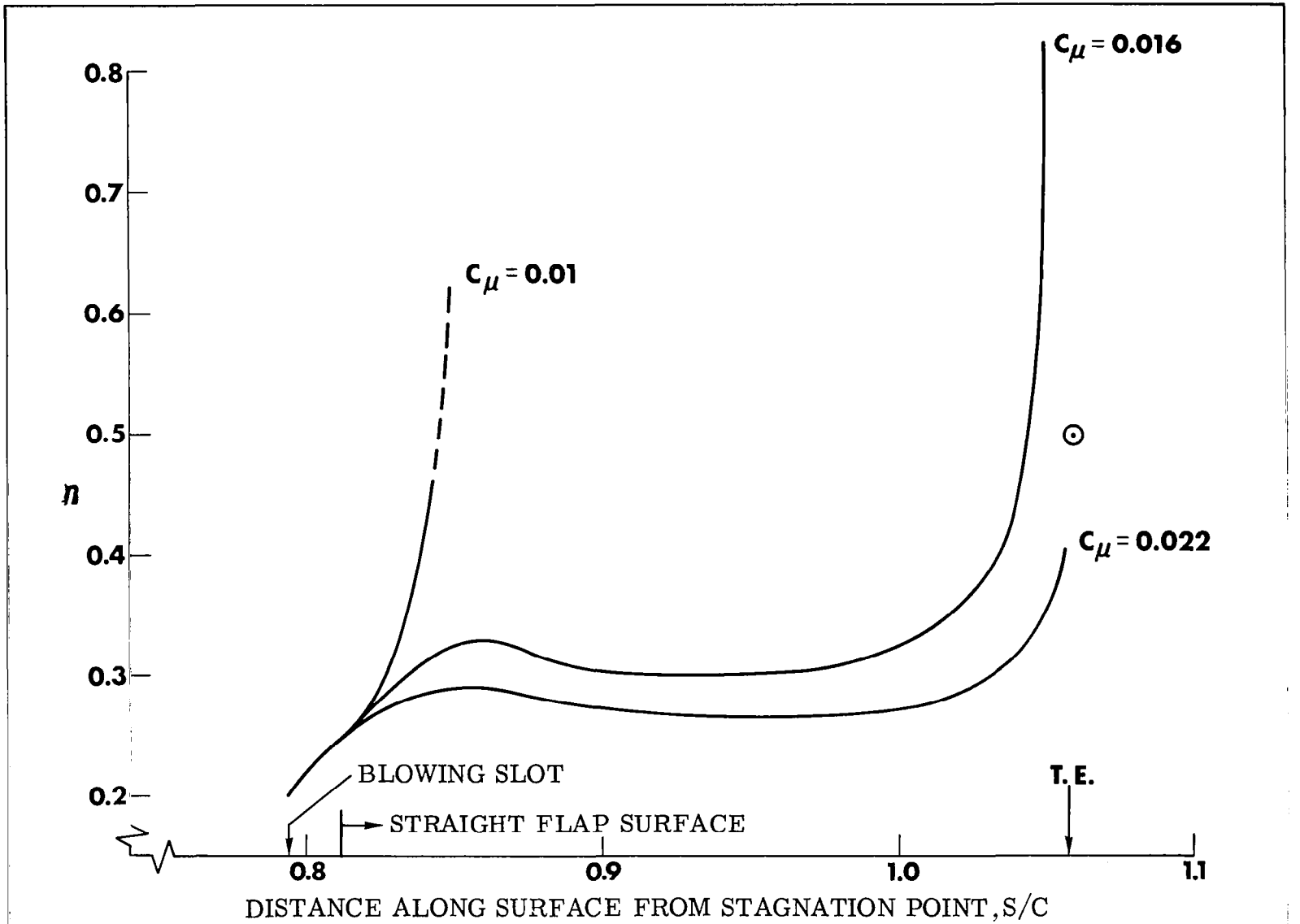

Figure 22.-Separation parameter n versus distance along airfoil surface, $\delta_f = 20^\circ$.

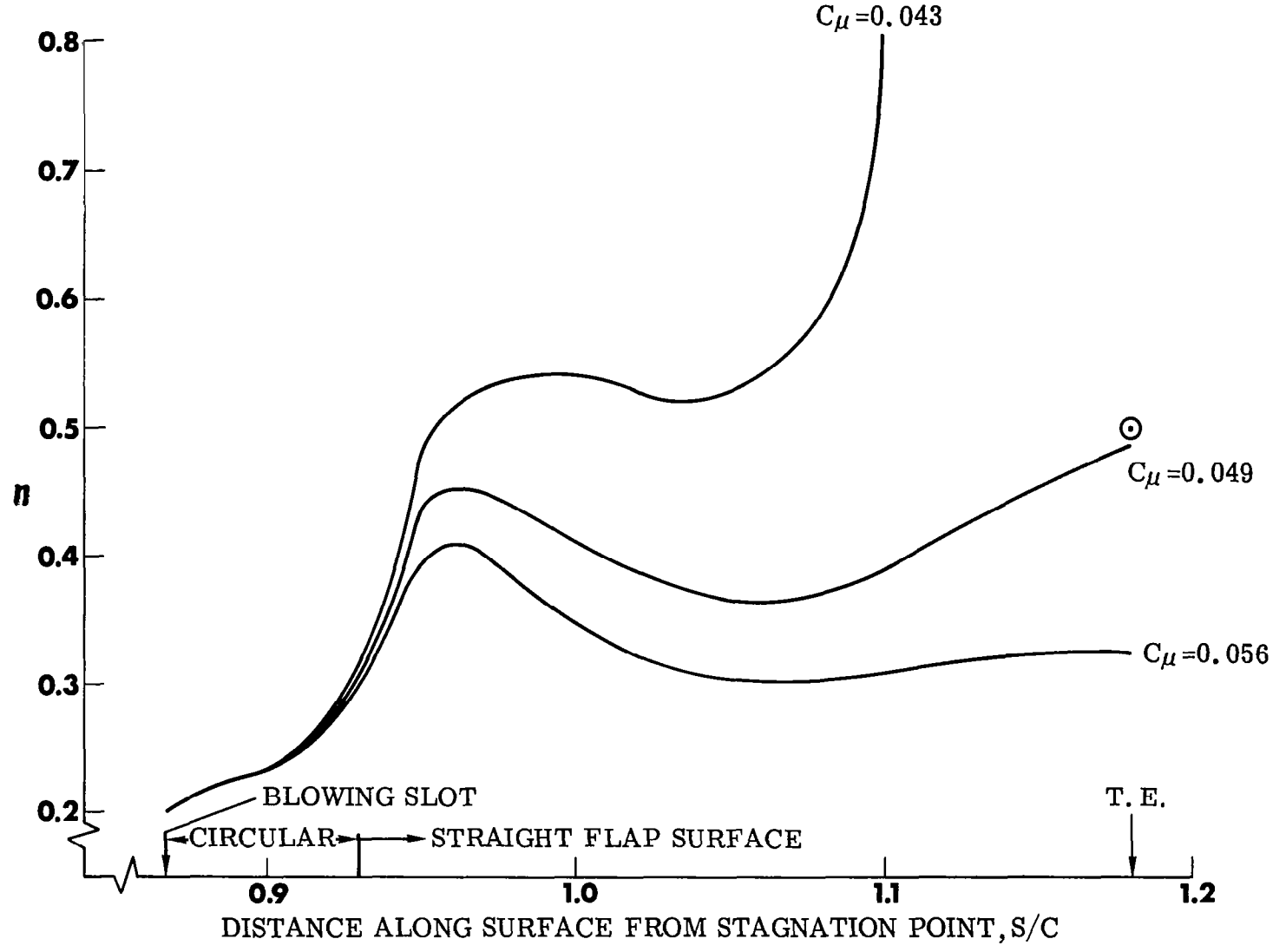

Figure 23. -Separation parameter n versus distance along airfoil surface, $\delta_f = 60^\circ$.

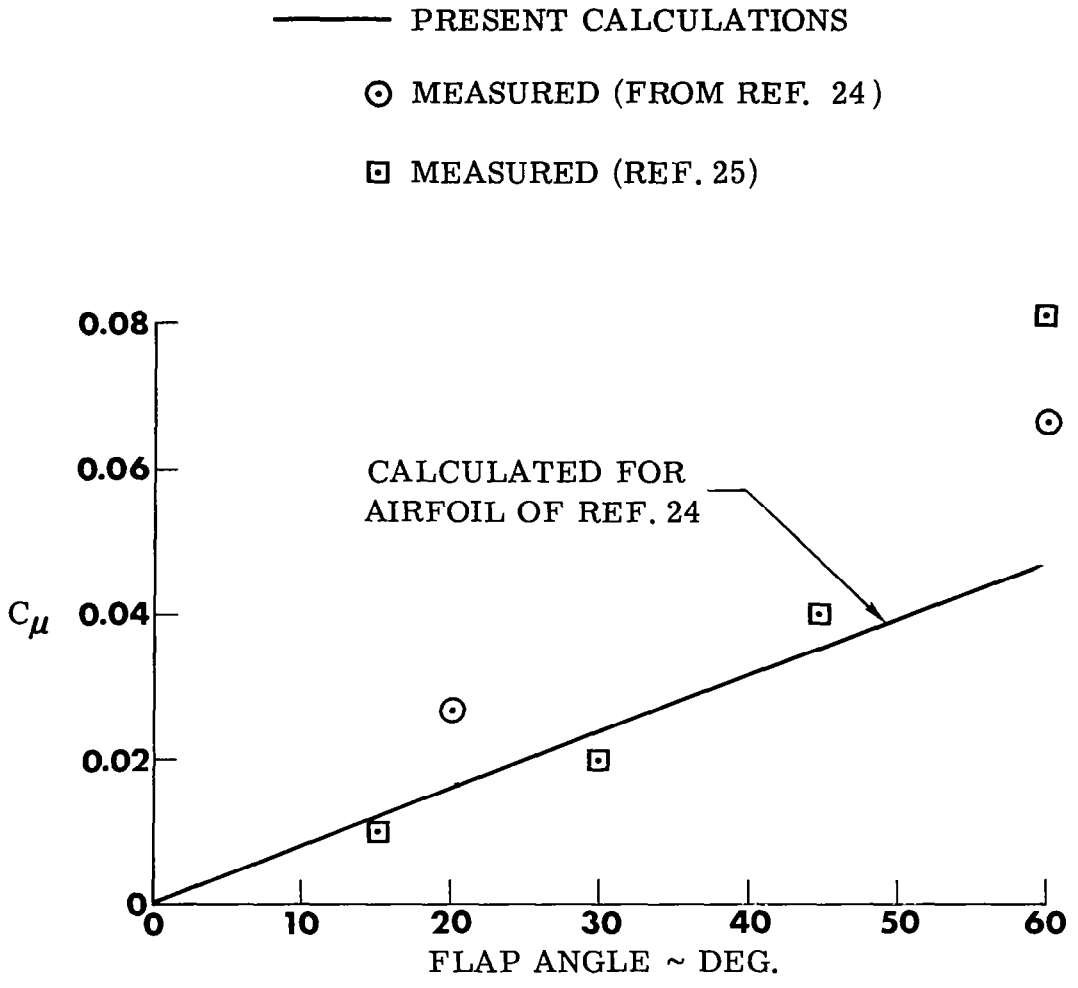

Figure 24. -Blowing coefficient required to move separation point aft to trailing edge.

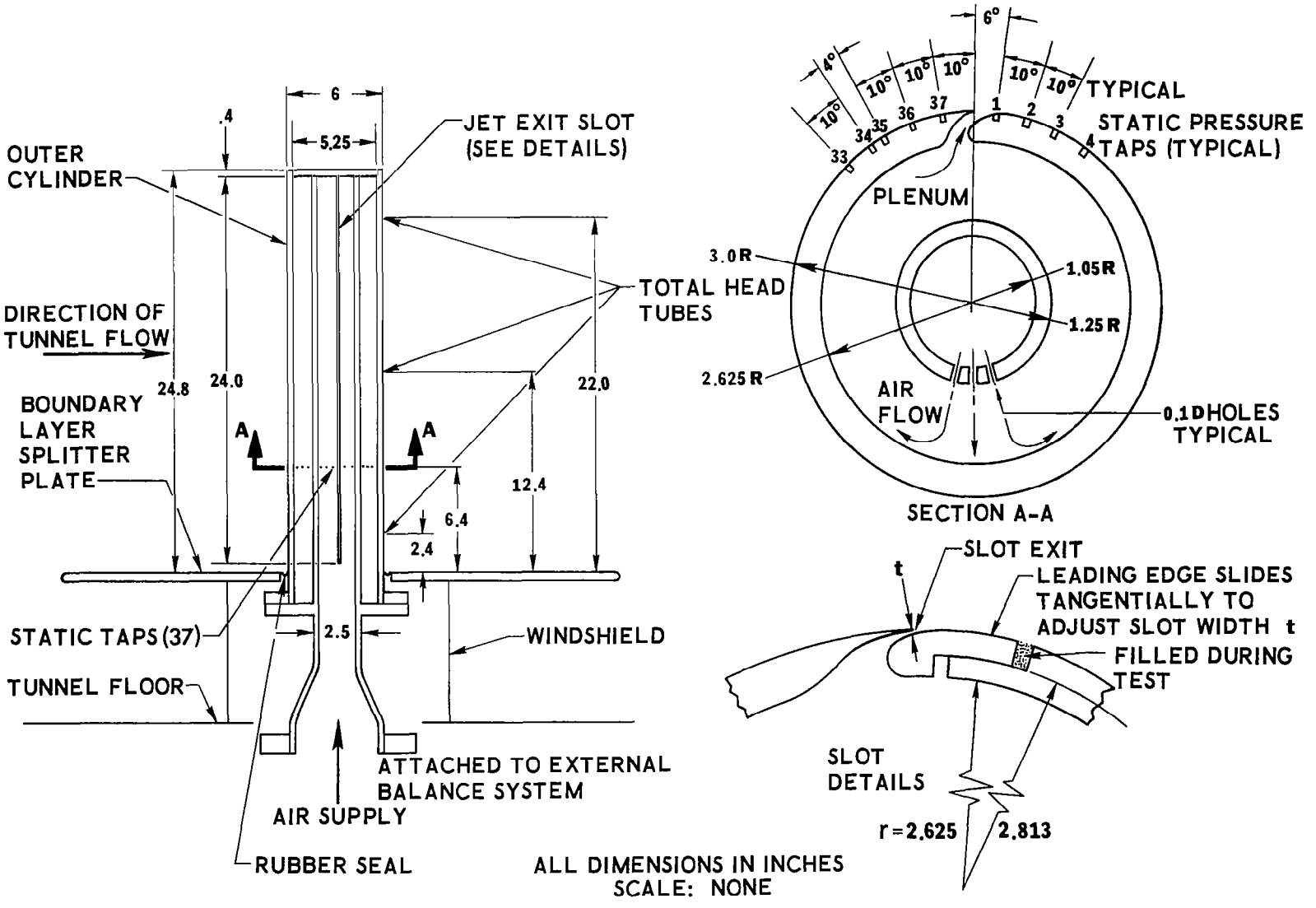

Figure 25.-Semispan tangential blowing wind tunnel model.